MSTO1 Links Cytosolic TRiC Chaperone Activity to Mitochondrial Function

Amy Margaret Bounds

A dissertation

submitted in partial fulfillment of the

requirements for the degree of

Doctor of Philosophy

University of Washington

2026

Reading Committee:

Suzanne Hoppins, Chair

Andrea Wills

Alexey Merz

Program Authorized to Offer Degree:

Biochemistry

University of Washington

Abstract

MSTO1 Links Cytosolic TRiC Chaperone Activity to Mitochondrial Function

Amy Margaret Bounds

Chair of the Supervisory Committee:

Suzanne Hoppins

Department of Biochemistry

Mitochondria are constantly fusing, dividing, and moving on microtubules to maintain structural and functional integrity. Mitochondrial dynamics are regulated by cytosolic factors and signaling pathways, providing critical integration into cellular physiology. In addition, maintenance of mitochondrial DNA (mtDNA) is essential for mitochondrial health, as the genome encodes essential oxidative phosphorylation proteins. Recently, mutations in *MSTO1* have been linked to clinical disease phenotypes typical of mitochondrial dysfunction. MSTO1 is tubulin/FtsZ related protein that localizes to the cytoplasm. MSTO1 mutant patient-derived fibroblasts have short mitochondria and a striking loss of mtDNA. This suggests MSTO1 is a novel regulator of mitochondrial fusion and mtDNA maintenance. Outside of MSTO1 patient studies, virtually nothing is known about the function of MSTO1 in vertebrates. In *Drosophila melanogaster,* the MSTO1 homolog Misato has been shown to stabilize the TCP-1 (TRiC in humans) chaperone. TRiC is a heterooligomer that aids in the folding of about 10% of cytosolic proteins, with an obligate role in folding tubulin and actin. It is not known if this relationship between TRiC and MSTO1 is conserved in humans. To build a system to uncover the molecular details of MSTO1 in humans, I generated cell lines using the auxin-inducible degradation (AID) system to allow temporal control of MSTO1 protein stability. After two hours of auxin treatment, MSTO1-FLAG-AID protein decreased to almost undetectable levels. MSTO1-FLAG-AID cells treated with auxin for six days

possessed shorter mitochondria than controls and MSTO1-FLAG-AID cells treated with auxin for only three days. MSTO1-FLAG-AID also did not interact with either Mfn1 or Mfn2 by co-immunoprecipitation. The extended length of time required for structural changes in the mitochondrial network and absence of mitofusin interaction suggest MSTO1 may indirectly regulate mitochondrial fusion. Furthermore, MSTO1-depleted cells had a significant decrease in TRiC protein expression 2 days before mitochondrial changes were observed. Knockdown of TRiC was sufficient to induce cells with a short mitochondrial network, suggesting the mitochondrial changes in MSTO1-depleted cells may be due to a loss of TRiC rather than MSTO1. Knockdown of TRiC also decreased MSTO1 protein levels, indicating that MSTO1 and TRiC protein levels are dependent on each other. Using co-immunoprecipitation and BN-PAGE, I found that MSTO1 interacts with the fully assembled TRiC. Using co-immunoprecipitation and BN-PAGE, we found that MSTO1 interacts with the fully assembled TRiC chaperone and our data suggests that MSTO1 assists in assembling early TRiC assembly intermediates. Together, these findings identify MSTO1 as a TRiC assembly factor and connect mitochondrial defects caused by MSTO1-depletion to the loss of TRiC.

Table of Contents

Table of Figures

Acknowledgements

I am incredibly thankful to everyone who supported me during graduate school. I would like to thank my thesis advisor, Suzanne Hoppins, for her support and wonderful mentorship over the past 6 years. She provided the space, support, and encouragement for me to chase my professional and personal goals. I would also like to thank the past and current members of the Hoppins Lab for their advice, support, and meaningful discussions. A special thank you to Sophie, who started as a lab mate but became one of my best friends. I would like to thank my thesis committee members Alexey Merz, Andrea Wills, Antonio Bedalov, and Sandra Bajjalieh for their guidance on my research.

I would also like to thank my family and friends for their support on this journey. My parents, Christy Haagsma and Tim Bounds, have always supported me, even when it meant I was moving across the country during a pandemic. My second family, Susan, Ron, Christy, and Dennis, for taking me in and always cheering me on from the sidelines. Lastly, I would like to thank my partner, Jeremy, who, without him, I could not have done this. Thank you for your constant love, support, and encouragement

Chapter 1. Introduction

1.1. Mitochondria and mitochondrial dynamics

Mitochondria are widely recognized as the “powerhouses of the cell.” They make the energy required for most cellular functions by producing the molecular energy carrier adenosine triphosphate (ATP). ATP is made with machinery located within the folds of the mitochondrial inner membrane, called cristae. In addition, mitochondria are responsible for much more than energy production, including calcium buffering, lipid synthesis, apoptosis (cell death), and responding to stressors inside and outside the cell (Lee-Glover *et al.*, 2025). Mitochondrial dysfunction is implicated in a wide variety of diseases, including heart disease, cancer, diabetes, and neurodegenerative diseases like Alzheimer’s and Parkinson’s (Boland *et al.*, 2013; Srivastava, 2017; Forte *et al.*, 2021).

For the mitochondria to perform these diverse functions and adapt to a cell's changing needs, mitochondria constantly change their shape. There are hundreds of mitochondria in a cell, and they move, divide, and fuse to create a dynamic network (Lewis and Lewis, 1915). At steady state, fusion and fission are balanced, creating a partially connected or reticular network (Hoffmann and Avers, 1973; Stevens and White, 1979; Stevens). Changes in mitochondrial structure occur by altering the balance between fusion and fission, which constantly shift in response to the cell’s needs. Cellular stresses, including increased reactive oxygen species (ROS) levels, high-glucose conditions, and physiological stress, cause mitochondrial fragmentation (Fan *et al.*, 2010; Yu *et al.*, 2011). A fragmented mitochondrial network enables repair and quality-control mechanisms to isolate damaged mitochondria or activate cell-death pathways (Karbowski and Youle, 2003; Goyal *et al.*, 2007; Whitworth and Pallanck, 2009; Ni *et al.*, 2015). Conversely, under starvation conditions, when glucose is limited, mitochondria fuse to form a hyperfused network, which remodels the cristae. Hyperfusion creates more physical space in the cristae, allowing more ATP-producing machinery (OXPHOS) to be inserted in the membrane, thereby increasing overall ATP capacity (Gomes *et al.*, 2011; Yu *et al.*, 2025). During cell division, the mitochondrial network also rearranges. During G1-S transition, the mitochondrial network is hyperfused to meet the energetic demands of DNA replication and cell division (Mitra *et al.*, 2009). As the cell enters mitosis, the mitochondria fragment, becoming smaller and more spherical, to ensure an even distribution between the two daughter cells (Gekko *et al.*, 2025). Although there is ample evidence that mitochondria sense and

adapt their network to cellular needs, the molecular details of the signals and regulatory proteins that drive mitochondrial dynamics remain incompletely understood.

1.2. Regulation of mitochondrial dynamics

Mitochondrial fusion and fission are regulated by molecular machines, or proteins, from the dynamin superfamily proteins (DSPs). DSPs are in all cells, where they mediate membrane remodeling of organelles in eukaryotes and the plasma membrane in bacteria (Jimah and Hinshaw, 2019). The structure of DSPs includes a GTPase domain that facilitates GTP hydrolysis and at least one α-helical bundle domain, which is thought to drive self-assembly into higher-order species (Jimah and Hinshaw, 2019). DSPs drive membrane remodeling by hydrolyzing GTP and inducing conformational changes in the α-helical bundle domains (Jimah and Hinshaw, 2019). Regulation of DSPs by effector proteins is a common feature within the family, but not all members have traditional protein-binding domains. For instance, the founding member of this family contains a proline-rich domain (PRD) that binds a wide range of effector proteins, though the mitochondrial fusion proteins, mitofusins (Mfns), lack canonical PRDs (Jimah and Hinshaw, 2019). Accordingly, little is known about how Mfns are regulated.

1.2.1. DSPs and their effector proteins

Dynamin is a cytoplasmic protein that is recruited to the budding vesicle membrane. There it oligomerizes around the bud neck, and facilitates membrane scission to release the vesicle into the cell (Heymann and Hinshaw, 2009; Antonny *et al.*, 2016; Jimah and Hinshaw, 2019). Dynamin has a wide range of effector proteins that bind to the PRD and regulate membrane recruitment, assembly, and coordination of actin dynamics during scission (Kim and Chang, 2006; Ferguson and De Camilli, 2012). Effector proteins include cytosolic proteins that possess SH3 domains, which bind to specific proline-rich sequences commonly found in eukaryotic proteins, including the dynamin PRD domain (Heymann and Hinshaw, 2009; Jimah and Hinshaw, 2019). SH3 proteins that bind dynamin include endophilin and intersection, which recruit and anchor dynamin to sites of endocytosis (Knezevic *et al.*, 2011; Ross *et al.*, 2011). SH3 proteins can also accelerate GTP hydrolysis and mediate interactions between actin and dynamin, thereby coordinating constriction, as with SNX9 and cortactin (Soulet *et al.*, 2005; Yamada *et al.*, 2013).

While the PRD domain is unique to dynamin, other members of the DSPs have effector proteins that regulate their function. Like dynamin, Dynamin-related protein 1 (DRP1), a cytosolic protein that mediates mitochondrial fission, is regulated by effector proteins. During fission, DRP1 is recruited to the membrane, oligomerizes into a ring-like structure around the mitochondria, and then constricts, initiating a scission event(Jimah and Hinshaw, 2019). The recruitment of DRP1 is facilitated by mitochondrial outer membrane proteins Mff, Mid49/51, and Fis1 (Losón *et al.*, 2013; Palmer *et al.*, 2013). Each alone is sufficient to recruit DRP1, but studies suggest different adaptors may be important for specific types of fission events. Knockouts of Mid49/51 lead to apoptotic-resistant cells, suggesting that Mid49/51 recruitment is associated with fission events during cell death (Osellame *et al.*, 2016). Fis1 is thought to recruit DRP1 to mitophagy-related fission sites and to control autophagosome morphology during Parkin-mediated mitophagy (Shen *et al.*, 2014; Yamano *et al.*). Overall, DRP1-dependent fission is regulated by effector proteins that recruit DRP1 to the mitochondrial membrane, thereby enabling distinct fission events tailored to specific cellular functions.

1.2.2. The Mitofusins

Vertebrates have two mitofusin paralogs, Mfn1 and Mfn2, that mediate outer membrane mitochondrial fusion. The mitofusins have a GTPase domain, two helical bundles (HB1 and HB2), and a transmembrane (TM) domain (Rojo *et al.*, 2002). The exact mechanism of outer-membrane mitochondrial fusion is not yet fully understood. At steady state, the mitofusins are dimers, and efficient fusion requires mitofusin to be present on both membranes (Hoppins *et al.*, 2011b). GTP binding to both mitofusin dimers on opposite membranes drives tethering, allosteric regulation, and self- assembly. Tethering occurs when two mitofusin dimers on opposite membranes come into contact (Detmer *et al.*, 2008; Hoppins *et al.*, 2011a; Sloat and Hoppins, 2023). GTP also induces allosteric regulation, or small changes in amino acid orientation, throughout the mitofusins that assist in driving large conformational changes and oligomerization (Ishihara *et al.*, 2004; Engelhart and Hoppins, 2019; Sloat *et al.*, 2019; Hurwitz *et al.*, 2026). Oligomerization occurs within the same membrane (cis) and between opposing membranes (trans). Blue Native PAGE (BN-PAGE), a high-resolution technique that separates protein complexes based on size, indicates that the mitofusins are cis dimers at steady state. In the presence of a non-hydrolysable GTP analogue or a transition-state mimic of GTP hydrolysis, the mitofusins assemble into

higher-order cis oligomers, which are necessary for efficient fusion (Ishihara *et al.*, 2004; Engelhart and Hoppins, 2019; Sloat *et al.*, 2019).

While either Mfn1 or Mfn2 alone is sufficient for fusion, optimal efficiency requires both, suggesting that the paralogs are partially nonredundant in their roles in mitochondrial fusion (Santel and Fuller, 2001; Chen *et al.*, 2003a; Eura *et al.*, 2003; Züchner *et al.*, 2004; Jimah and Hinshaw, 2019; Sloat *et al.*, 2019). Mfn1 and Mfn2 are 77% similar and 62% identical in amino acid sequence, but Mfn1 has a GTPase activity eightfold greater than Mfn2, suggesting Mfn1 and Mfn2 are functionally different (Santel and Fuller, 2001; Chen *et al.*, 2003a; Eura *et al.*, 2003; Sloat *et al.*, 2019). Functional differences between Mfn1 and Mfn2 are also consistent in disease models. Mutations in *Mfn2* lead to a rare peripheral neuropathy, Charcot-Marie-Tooth Syndrome Type 2A (CMT2A) (Züchner *et al.*, 2004; Larrea *et al.*, 2019). No disease reports have been associated with mutations in *Mfn1,* suggesting that loss of Mfn1 is lethal and that mutations are not tolerated. This is also consistent in mice, where knockout of either *Mfn1* or *Mfn2* results in different phenotypes. Both mitofusin knockouts cause embryonic lethality, but *Mfn2*-null mice die during mid-gestation due to placental defects, which have not been observed in *Mfn1*-null mice (Chen *et al.*, 2003b). Mfn1- and Mfn2-null mouse embryonic fibroblasts immortalized from these knockout mice also have different doubling times and mitochondrial morphology. Both Mfn1 and Mfn2-null cells have fragmented mitochondria, but Mfn2-null mitochondria are more spherical. Mfn2-null cells are also more rounded and grow faster than Mfn1-null cells. One study suggests Mfn2-null cells are more rounded due to a peripheral F-actin band that increases cell rigidity and contractility. While Mfn1 and Mfn2 are highly similar, there are unique features in each protein (Wang *et al.*, 2023). Unlike Mfn1, Mfn2 has a proline-rich domain between HB1 and the TM domain, which is likely responsible for specific protein-protein interactions with effector proteins that may regulate specific metabolic processes and mitochondrial fusion itself.

Despite other DSPs having numerous effector proteins that assist with recruitment, oligomerization, and membrane constriction, very few have been identified in mitochondrial fusion. Proteins such as SMAD, MitoPLD, and SLC25A46 have been reported to regulate mitofusins, but only mitochondrial morphology was assessed in these studies, not fusion efficiency (Kumar *et al.*, 2016; Zhang *et al.*, 2016; Obinata *et al.*, 2025). Only one mitofusin interactor is known to directly increase

mitochondrial fusion efficiency: the pro-apoptotic factor Bax. Cytosolic Bax has been identified as a pro-fusion factor in Mfn2 homotypic fusion events and compensates for CMT2A defects using our lab's reconstituted *in vitro* fusion assay (Hoppins *et al.*, 2011b). This assay quantitatively measures mitochondrial fusion and can be used to measure how purified protein or cytosolic-enriched fractions affect fusion efficiency. When purified Bax was reintroduced with isolated mitochondria from Bax null cells, fusion efficiency was restored to levels comparable to those of mitochondria that received cytosolic-enriched extract from wild-type cells, suggesting that Bax is a pro-fusion factor (Hoppins *et al.*, 2011b).

Our lab has found that cytosolic proteins compensate for mitochondrial fusion defects caused by mutations in Mfn1, suggesting that mitofusins have unidentified effector proteins (Engelhart and Hoppins, 2019). Due to the sequence similarity between Mfn1 and Mfn2, Mfn2 disease-associated variants found in CMT2A patients often also cause aberrant mitochondrial morphology when placed at Mfn1-conserved residues. For example, Mfn1^{F202L} appeared to be a hyperactive variant when expressed at endogenous levels in Mfn1-null cells; fusion efficiency was only 40 percent of controls when measured with our lab's reconstituted *in vitro* fusion assay. If the cytosol-enriched fraction was added to the assay, mitochondria with Mfn1^{F202L} displayed a two-fold increase in fusion compared to a 1.3-fold increase with wild-type mitochondria. This indicates that cytosolic components augment mitochondrial fusion and can compensate for fusion defects; however, the identity of these components remains unknown (Engelhart and Hoppins, 2019). Overall, the regulation of mitofusins is poorly understood, highlighting a large gap in our understanding of mitochondrial dynamics.

1.2.3. Cytoskeletal regulation of mitochondrial dynamics

The cytoskeleton is a dynamic network of microtubules, actin, and intermediate filaments that determines cell shape, facilitates movement, and maintains structural integrity. Mitochondria move along microtubules, long filaments composed of two tubulin isoforms, α- and β-tubulin. This motility requires the mitochondrial transport complex. Dynein and kinesin are the molecular motors that carry mitochondria on microtubules. Dynein moves towards the minus end of microtubules (retrograde) and kinesin moves towards the plus end of microtubules (anterograde) (Schwarz, 2013; Melkov and Abdu, 2017; Canty *et al.*, 2023). Cells treated with nocodazole, which disrupts microtubule polymerization by competitively binding to β-tubulin, have fragmented mitochondria that cluster around the perinuclear space (Fernández Casafuz

et al., 2023). Transport of mitochondria is important for maintaining subcellular ATP concentrations and maintaining mitochondrial function (Hung, 2021). In neurons, the largest cells in the body, mitochondria move along the axon in an anterograde direction to provide ATP for high-energy processes such as synaptic vesicle recycling (Li and Sheng, 2022). Consistent with this, in a transgenic mouse model expressing a Mfn2 disease-related variant $Mfn2^{T105M}$ in motor neurons, mitochondria were absent from axons, leading to energy depletion and early axon degeneration (Detmer *et al.*, 2008). Together, these observations highlight that microtubule-based transport is essential not only for mitochondrial positioning but also for maintaining mitochondrial function and cellular energy homeostasis.

Actin, the most abundant protein in human cells, forms dynamic filaments that support cell motility, protrusions, and endocytosis (Dominguez and Holmes, 2011; Mooren *et al.*, 2012; Schaks *et al.*, 2019). These processes are driven by actin's unique ability to generate constriction force when actin-binding proteins move along the filaments (Murrell *et al.*, 2015). Actin filaments contribute directly to the mechanical dynamics of mitochondrial membrane remodeling. Consistent with a need for the constriction activity of actin, the diameter of the mitochondria is larger than the diameter of the DRP1 ring before fission, suggesting other factors help constrict the mitochondria (Hatch *et al.*, 2014). At mitochondrial-ER contact sites, formin protein Inverted Formin 2 (INF2) polymerizes actin around the mitochondria while Myosin-IIa creates a mechanical force responsible for actin cable contraction for constriction before fission (Korobova *et al.*, 2013; Prudent and McBride, 2016; Shi *et al.*, 2025). Recently, actin filaments and the ER have also been identified at mitochondria fusion sites (Gatti *et al.*, 2025). Before mitochondrial fusion, actin has been identified at fusion sites, but its mechanistic role remains unclear (Gatti *et al.*, 2025).

1.3. Mitochondrial DNA

Mitochondrial DNA (mtDNA) maintenance is critical for the health of the mitochondrial network. There are hundreds to thousands of copies of the mitochondrial genome per cell, packaged in structures called nucleoids and spatially organized across the mitochondrial network. Normally, each cell has about 100 - 1000 copies of mtDNA packaged as nucleoids, which contain 1-2 copies of the circular mitochondrial genome and are distributed throughout the network (Kukat *et al.*, 2011; Lee and Han, 2017; Pavluch *et al.*, 2023). MtDNA is critical for aerobic respiration, mitochondrial membrane potential, and the energetic

demands of the cell as it encodes essential subunits of the oxidative phosphorylation (OXPHOS) complexes and the mitochondrial translation machinery(Anderson *et al.*, 1981). Therefore, the maintenance and distribution of this genome are necessary to sustain cellular energy levels and mitochondrial health.

To maintain the mitochondrial genome, mitochondria must balance two processes: mtDNA replication and mtDNA quality control. Replication of mtDNA is not coupled to the cellular division cycle and requires unique enzymes encoded by nuclear genes that make up the mitochondrial replication machinery or replisome (Gustafsson *et al.*, 2016; Chapman *et al.*, 2020). MtDNA and mitochondrial fission are also spatially linked. In U2OS cells, actively replicating mtDNA nucleoids were present at future fission sites - before membrane constriction and DRP1 recruitment (Lewis *et al.*, 2016). During DNA replication, errors in DNA copying are common because, unlike the nuclear genome, mtDNA lacks most of the proofreading proteins present in the nucleus that correct errors. DNA and the mtDNA proofreading enzyme can also be damaged by ROS, which are byproducts of OXPHOS (Hahn and Zuryn, 2019; Anderson *et al.*, 2020). The proximity of OXPHOS machinery and mtDNA in mitochondria increases the likelihood of mtDNA mutations. Therefore, mtDNA must be maintained to ensure a healthy mitochondrial network.

Mitochondria leverage mitochondrial dynamics and mitophagy pathways to ensure functional mtDNA is well distributed throughout the mitochondrial network (Chen *et al.*, 2010; Silva Ramos *et al.*, 2019). After mitochondrial fusion, the contents, including mtDNA nucleoids, are mixed and spread throughout the connected network. Content mixing means the population of mtDNA in a cell is heterogeneous, allowing damaged mtDNA to mix with undamaged mtDNA, thereby offsetting the effects of mutated mtDNA on the mitochondrial network (Aryaman *et al.*, 2019; Hahn and Zuryn, 2019). However, if the number of damaged mtDNA nucleoids exceeds a certain threshold, mtDNA is removed through mitophagy or mitochondrial-derived vesicles (MDVs). During mitophagy, mitochondrial fragments are detached from the mitochondrial network, encapsulated by an autophagosome, and delivered to the lysosome for degradation (Sen *et al.*, 2022; Liu *et al.*). Inducing DNA damage increases the number of mtDNA found in autophagosomes, suggesting mitophagy is one mechanism for dealing with mtDNA damage (Sen *et al.*, 2022). MtDNA has also been observed in MDVs, which are vesicles that contain either the outer or inner mitochondrial membranes, or both, along with mitochondrial contents (Sugiura *et al.*, 2014; Amari and

Germain, 2021; König *et al.*, 2021). One destination for MDVs is the lysosome, where contents are degraded. Interestingly, it remains unclear how mitochondria identify, mark, and sort mtDNA molecules for removal. One study in yeast suggests that the OXPHOS machinery and mtDNA are localized together (Jakubke *et al.*, 2021). Therefore, when the OXPHOS machinery is damaged, the local mtDNA is also damaged. By contrast, another study found that damaged mtDNA nucleoids were in proximity to more vesicle- and lysosome-related proteins than healthy mtDNA, suggesting that changes in the local proteome drive MDV-dependent removal of mtDNA (Kakanj *et al.*, 2025). Taken together, mitochondrial mtDNA maintenance is crucial for maintaining ATP production, because disruption leads to mtDNA loss and disease.

1.4. Mitochondrial and mtDNA disease

1.4.1. Mitochondrial dysfunction in disease

Mitochondria are often more fragmented compared to healthy controls in a wide range of diseases, including heart disease, cancers, and neurodegenerative diseases like Alzheimer's and Parkinsons. These diseases affect tissues or cells with high energy demands. In heart disease, mitochondria in the heart muscle are often fragmented and exhibit OXPHOS defects, inhibiting ATP production (Chen *et al.*, 2011; Papanicolaou *et al.*, 2011; Forte *et al.*, 2021, 2021). In cancer, defects in mitochondrial dynamics can manifest differently depending on cancer type. In some cancers like hepatocellular carcinoma (HCC), the most common primary liver cancer, where Mfn1 or Mfn2 is downregulated, the mitochondrial network is fragmented shifting the energy damage away from OXPHOS toward glycolysis (Sebastián *et al.*, 2016; Zhang *et al.*, 2020). The opposite is true in some non-small cell lung cancers, where Mfn1 is upregulated creating a more fused network that may protect cancer cells from apoptosis (Dutkowska *et al.*, 2024). Lastly, in neurodegenerative diseases, neurons rely heavily on energy at synapses, which requires efficient energy production and mitochondrial transport from the cell body to the axons. In Alzheimer's disease and Parkinson's disease, mitochondria are excessively fragmented, limiting ATP production (Calkins *et al.*, 2011; Feng *et al.*, 2020).

While expression levels of the fusion machinery are altered in common diseases, autosomal dominant mutations in Mfn2 lead to a rare peripheral neuropathy, CMT2A. Patients present with distal weakness, sensory loss, gait impairment, and foot deformation, and often have significant loss of muscle

control in their limbs (Züchner *et al.*, 2004; Larrea *et al.*, 2019). The onset and severity of the disease vary, as do the structural locations of the documented variants. The GTPase domain is most often mutated in disease, but mutations have also been reported in HB1 and near the TM domain (Filadi *et al.*, 2018; Li *et al.*, 2019). Mitochondrial phenotypes vary depending on the specific mutation; some lead to fragmented mitochondrial networks, whereas others cause mitochondrial clustering around the nucleus (Baloh *et al.*, 2007; Sharma *et al.*, 2021; Sloat and Hoppins, 2023). Understanding how CMT2A variants affect mitochondrial fusion has been important for elucidating the function and mechanism of the mitofusins.

1.4.2. MtDNA and disease

Dysregulation of mitochondrial dynamics is a key driver in muscular myopathies and heart disease, while mtDNA depletion syndromes often present with ataxia, peripheral neuropathy, hypotonia, and hepatic dysfunction. MtDNA depletion syndromes are a group of autosomal recessive disorders leading to a significant loss of mtDNA content and impaired energy production. mtDNA depletion is commonly caused by mutations in nuclear genes required for mitochondrial nucleotide synthesis (*TK2, SUCLA2, SUCLG1, RRM2B, DGUOK, and TYMP*) and mtDNA replication (*POLG2* and *TWNK*). Most mtDNA depletion syndromes are severe and early-onset (El-Hattab and Scaglia, 2013; Nogueira *et al.*, 2014). Currently, there is no cure or treatment for these syndromes, highlighting a large gap in the development of mitochondrial disease therapies.

Recently, studies link mtDNA depletion syndromes to mutations in mitochondrial dynamic proteins, including DRP1 and the mitofusins. Patients with mutations in *DRP1* present with similar symptoms to mtDNA depletion syndromes, including ataxia, cognitive impairments, and developmental delays (Sheffer *et al.*, 2016; Wei and Qian, 2021; Lhuissier *et al.*, 2022). *DRP1* patient cells exhibit hyperfused mitochondrial networks, remodeling of cristae, and OXPHOS defects (Sheffer *et al.*, 2016; Lhuissier *et al.*, 2022; Robertson *et al.*, 2023). Knockdown of DRP1 resulted in a few large mtDNA nucleoids, suggesting a defect in the separation of recently replicated nucleoids (Ban-Ishihara *et al.*, 2013; Lewis *et al.*, 2016). Defects in mitochondrial fusion have also been linked to mtDNA dysregulation but only in Mfn1/Mfn2-null cells, where fusion is completely abolished. In conditional heart Mfn1/Mfn2 knockout mice and MEFs, 50-70 percent of mtDNA was depleted, and nucleoids displayed a clustering

phenotype. Although the mechanistic link is unclear, it was suggested that the mtDNA loss was attributable to altered replisome component stoichiometry, a finding also reported in these cells (Silva Ramos *et al.*, 2019). Taken together, these reports suggest mitochondrial dynamics proteins may play a role in mtDNA maintenance.

1.4.3. MSTO1-associated disease

In 2017, the first paper was published describing a rare neuromuscular disorder that leads to mitochondrial fusion and mtDNA maintenance defects in patient cells (Nasca *et al.*, 2017a). Researchers identified mutations in the nuclear gene *MSTO1* as the cause of this disease. MSTO1-related disease is characterized by myopathy-dystrophy, ataxia, cerebellar involvement, and, in some cases, retinopathy and cognitive impairments (Gal *et al.*, 2017; Nasca *et al.*, 2017a; Iwama *et al.*, 2018; Ardicli *et al.*, 2019; Donkervoort *et al.*, 2019; Schultz-Rogers *et al.*, 2019; Li *et al.*, 2020; Nasca *et al.*, 2021a; Liu *et al.*, 2022). MSTO1 patient fibroblasts have short mitochondria and a striking 30-60% loss of mtDNA. In MSTO1 patient fibroblasts, most cells have fragmented mitochondria, whereas control cells possess fused or reticular mitochondria (Nasca *et al.*, 2017b, 2021b; Donkervoort *et al.*, 2019). Consistent with this, photoactivation assays showed decreased mitochondrial fusion activity in patient cells compared with controls (Gal *et al.*, 2017). Despite the drastic loss of mtDNA and mitochondrial fusion defects, only a few MSTO1 patients have reported OXPHOS deficiencies (Gal *et al.*, 2017; Nasca *et al.*, 2017b). This absence of OXPHOS defects could be due to cell-type-specific energy demands. Only patient fibroblasts have been assayed, but in other cell types that require more energy, like neurons and muscle cells, OXPHOS deficiencies may be more apparent. Mitochondrial motility, membrane potential, and calcium uptake were also unaffected by MSTO1 knockdown in HeLa cells, indicating mitochondrial fusion defects in patient fibroblasts are not secondary to bioenergetic or movement impairments (Gal *et al.*, 2017).

Patients have compound heterozygous mutations in *MSTO1*, meaning each patient has a different deleterious mutation in each *MSTO1* allele (Figure 1.1 A). Parents of patients with only one mutated allele do not present with symptoms, suggesting that having one functional copy of *MSTO1* is sufficient to compensate for mutations in the other allele (Nasca *et al.*, 2017a; Donkervoort *et al.*, 2019; Chen *et al.*, 2022; Gerber *et al.*, 2023). All MSTO1 patients tested for MSTO1 protein have reported nearly

undetectable levels, suggesting that the amino acid substitutions destabilize the protein (Nasca *et al.*, 2017a, 2021a; Donkervoort *et al.*, 2019; Chen *et al.*, 2022).

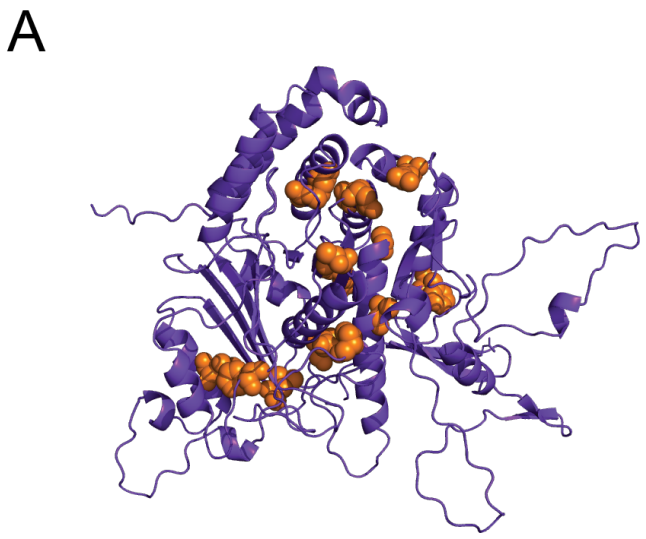

Figure 1.1 Predicted Structure of MSTO1. **(A)** Predicted structure of MSTO1, adapted from the AlphaFold Protein Structure Database (UniProt ID: Q9BUK6-2; AlphaFold DB ID: AF-Q9BUK6-2-F1-v6). Reported MSTO1 variants are predominantly located within the interior of the predicted protein structure and are highlighted in orange.

1.5. MSTO1

1.5.1. MSTO1 genetics and evolution

In humans, *MSTO1* is located on chromosome 1q22. About 37 million years ago, around the period when New World monkeys diverged from Old World monkeys, a large segmental duplication occurred on the human 1q22 chromosome. The *MSTO1* ortholog, *MSTO,* was duplicated, creating two transcriptionally active genes, *MSTO1* and *MSTO2P* (Kuryshev *et al.*, 2006). Both *MSTO1* and *MSTO2P* are present in New World monkeys and humans, but *MSTO2P* is absent in other model organisms, including mice, flies, yeast, or frogs. In humans, *MSTO1* and *MSTO2P* have 99% DNA sequence identity. *MSTO2P* appears to be a pseudogene that encodes for a long noncoding RNA (lncRNA) but no protein (Kuryshev *et al.*, 2006). Little is known about *MSTO2P*. Only nine papers reference *MSTO2P,* and all assess cancer prognosis based on RNA expression changes (Li *et al.*, 2017; Wei *et al.*, 2017; Wang *et al.*, 2019; Shi *et al.*, 2020; Yan *et al.*, 2020; Gu and Wang, 2022; Guo and Zhang, 2022; Gál *et al.*, 2023a; Chen *et al.*, 2025). In gastric, lung, and colorectal cancer, increased expression of *MSTO2P* long noncoding RNA (lncRNA) has been linked to rapid tumor cell proliferation and poor prognosis (Li *et al.*, 2017; Wei *et al.*, 2017; Wang *et al.*, 2019; Shi *et al.*, 2020; Yan *et al.*, 2020; Gu and Wang, 2022; Guo and Zhang, 2022; Chen *et al.*, 2025). *MSTO2P* lncRNA has been predicted to regulate gene expression of mTOR-related proteins, PD-L1, EZH2, and CDKN1A (Wang *et al.*, 2019; Shi *et al.*, 2020; Yan *et al.*,

2020; Guo and Zhang, 2022). While *MSTO2P* lncRNA is contingently linked to gastric and lung cancers, the biological function of MSTO1 is unknown.

Based on sequence similarity, MSTO1 is most closely related to tubulin and a bacterial cell division protein, Ftsz. Both FtsZ and tubulin are GTPases that form long filaments to facilitate cell division, but MSTO1 GTP binding and oligomerization have not been tested (Nogales *et al.*, 1998; Gal *et al.*, 2017). The MSTO1 protein structure has not been solved; therefore, information about MSTO1 protein structure relies on AlphaFold predictions. MSTO1 has two tubulin-like domains and a predicted secondary structure similar to tubulin and FtsZ. MSTO1 is larger than both tubulin and FtsZ due to extra amino acid sequences predicted to be structurally disordered regions (Miklos *et al.*, 1997a; Palumbo *et al.*, 2015). Despite these similarities in secondary structure, the functional relationship between MSTO1 and FtsZ/tubulin remains unclear and warrants further investigation.

The structural relationship between MSTO1 and FtsZ presents an evolutionary conundrum: both plants and animals inherited FtsZ from ancestral bacteria during endosymbiosis, yet only chloroplasts retained FtsZ as their primary fission machinery (Kiefel *et al.*, 2004; TerBush *et al.*, 2013a). FtsZ, a bacterial cell division protein present in the last common ancestor of bacteria and archaea, was retained in the chloroplast lineage following the endosymbiosis of cyanobacteria and transferred to the nuclear genome, where it now functions in chloroplast division in plants (TerBush *et al.*, 2013b). In contrast, despite mitochondria arising from an α-proteobacterial ancestor, fungi, higher plants, and metazoans lack FtsZ homologs and instead rely on DSP proteins to regulate mitochondrial dynamics (Margolin, 2005). It is not known how metazoans lost FtsZ and evolved DSPs to fuse and divide mitochondria. Instead, this conundrum opens an interesting question about the evolution of MSTO1 and its relationship to FtsZ and mitochondrial DSPs.

Overall, the molecular details of MSTO1 function remains unknown, and its role in mitochondrial fusion is not evident from evolutionary and structural predictions.

1.5.2. MSTO1 in other organisms

Outside of patients with mutations, MSTO1 has been understudied in vertebrate systems, creating a substantial knowledge gap. The Mouse Genome Database reports a mouse with an *MSTO1* endonuclease-mediated double knockout resulting in embryonic lethality before organogenesis. Mice with

one *MSTO1* wild-type allele survive past gastrulation and present with a decreased body length, smaller spleen, enlarged kidney, increased circulating triglyceride level, and abnormal seminal vesicle morphology (Msto1 Endonuclease-mediated Allele Detail MGI Mouse (MGI:6257438)). Overall, these data suggest that *MSTO1* is an essential gene for early development.

The *MSTO1 Saccharomyces cerevisiae* or budding yeast homolog, *DML1*, is essential for meiosis. Meiosis with heterozygous Dml1+/- strains gives rise to only two viable spores - those that inherited the wild-type *DML1* allele. However, both viable spores are sporadically petite and lack mtDNA, suggesting *DML1* is also important for mtDNA inheritance in meiosis. When wild type *DML1* was transformed back into *DML1* mutants, mtDNA inheritance defects were reversed, suggesting that loss of *DML1* is the cause of the mtDNA defects in yeast (Gurvitz *et al.*, 2002).

Most research on an MSTO1 homolog has been done in *Drosophila,* otherwise known as fruit flies. *Misato* null flies exhibit a metaphase arrest phenotype, resulting in lethality in the third-instar larval stage. These larvae are unable to undergo morphogenesis because their imaginal discs are underdeveloped due to defects in mitotic spindle formation (Miklos *et al.*, 1997b; Palumbo *et al.*, 2015). In brain tissue from fly embryos with conditional knockdowns of *misato*, each subunit in the TCP-1 tubulin chaperone complex (TCP-1 complex) was decreased (Palumbo *et al.*, 2015). The TCP-1 complex is a 16-subunit chaperone that folds approximately 10% of cytosolic proteins in the cell, including essential cell division proteins like tubulin (Ghozlan *et al.*, 2022; Kim *et al.*, 2024).

In *Drosophila*, the downstream effects of TCP-1 complex loss in *Misato* null cells are cell-type specific. In *Misato* null embryos, the loss of the TCP-1 complex leads to decreased tubulin protein levels and monopolar spindle formation. In the *Misato* null brain tissue, no changes in tubulin protein levels were observed (Palumbo *et al.*, 2015). Interestingly, in *Misato* conditional knockdowns in visceral muscle, which is important for contractile movement during digestion, flies lacking Misato showed reduced tubulin and actin protein levels when visualized by immunofluorescence (Min *et al.*, 2017). This indicates a tissue-specific phenotype: embryos require tubulin for cell division, whereas visceral muscle requires actin for contractility. Overall, the loss of *Misato* leads to a decrease in the TCP-1 complex and a tissue-specific decrease in tubulin and actin.

In *Drosophila*, mitochondrial changes due to the loss of *Misato* have been poorly characterized. In *Misato* visceral muscle knockdowns, mitochondria were more fragmented than in controls. The mitochondria also showed an increase in the apoptosis using a TUNEL assay, suggesting that loss of *Misato* increases the response to apoptosis in visceral muscle (Min *et al.*, 2017). In *Misato*-null brain cells, mitochondrial distribution was similar to that in controls. This study also immunostained for Misato in *Drosophila* spermatids, and Misato was not localized to the mitochondria. Consistent with this, Misato was absent in the mitochondrial fractions extracted from *Drosophila* brain cells (Mottier-Pavie *et al.*, 2011). While Mottier-Pavie et al., concludes that Misato is not involved in mitochondrial behavior, a study of an MSTO1 patient assessed the MSTO1 localization using immunofluorescence and strategic membrane permeabilization to determine which detergent released MSTO1 from the cell (Gal *et al.*, 2017). These assays suggested MSTO1 is a cytoplasmic protein that can be loosely bound to the outer mitochondrial membrane, suggesting that the techniques used in *Drosophila* brains may have missed this transient interaction.

1.6. The TRiC chaperone

In mammals, the homolog of the *Drosophila* TCP-1 complex is the T-complex protein Ring Complex (TRiC), which is also a 16-subunit chaperone (Figure 1.2). TRiC is required to fold a large range of obligate substrates, including tubulin, actin, CDC20, eIF3i, and the active form of cyclin E (Ghozlan *et al.*, 2022; Kim *et al.*, 2024). The literature has also speculated that TRiC is not only involved in protein folding but also regulates various cellular processes and sequesters proteins to prevent their activation (Cuéllar *et al.*, 2022; Zeng *et al.*, 2024). Overall, TRiC folds a wide diversity of substrates and is an active participant in a wide range of cellular pathways, including autophagy, transcription, translation, and the cell cycle (Ghozlan *et al.*, 2022; Zeng *et al.*, 2024).

The diversity of folding substrates and cellular functions is thought to arise from differences in subunits and their arrangement within the chaperone. TRiC is a 1 MDa hetero-oligomeric chaperone composed of two rings with 8 ATPase subunits (Cong *et al.*, 2010; Leitner *et al.*, 2012). Each subunit is thought to have arisen through gene duplication early in evolution, and then independently diverged to acquire a unique function present in almost all eukaryotes (Archibald *et al.*, 2001; Zeng *et al.*, 2024). Each TRiC subunit has an equatorial domain, intermediate domain, and apical domain. TRiC subunits are

highly conserved in the ATPase domain and diverge in the substrate-binding domain (Cong *et al.*, 2010). The subunits are arranged in groups of high and low ATPase activity and net charge within the chamber (Reissmann *et al.*, 2012). The specific arrangement of TRiC has prompted investigation into how TRiC assembles into the exact orientation.

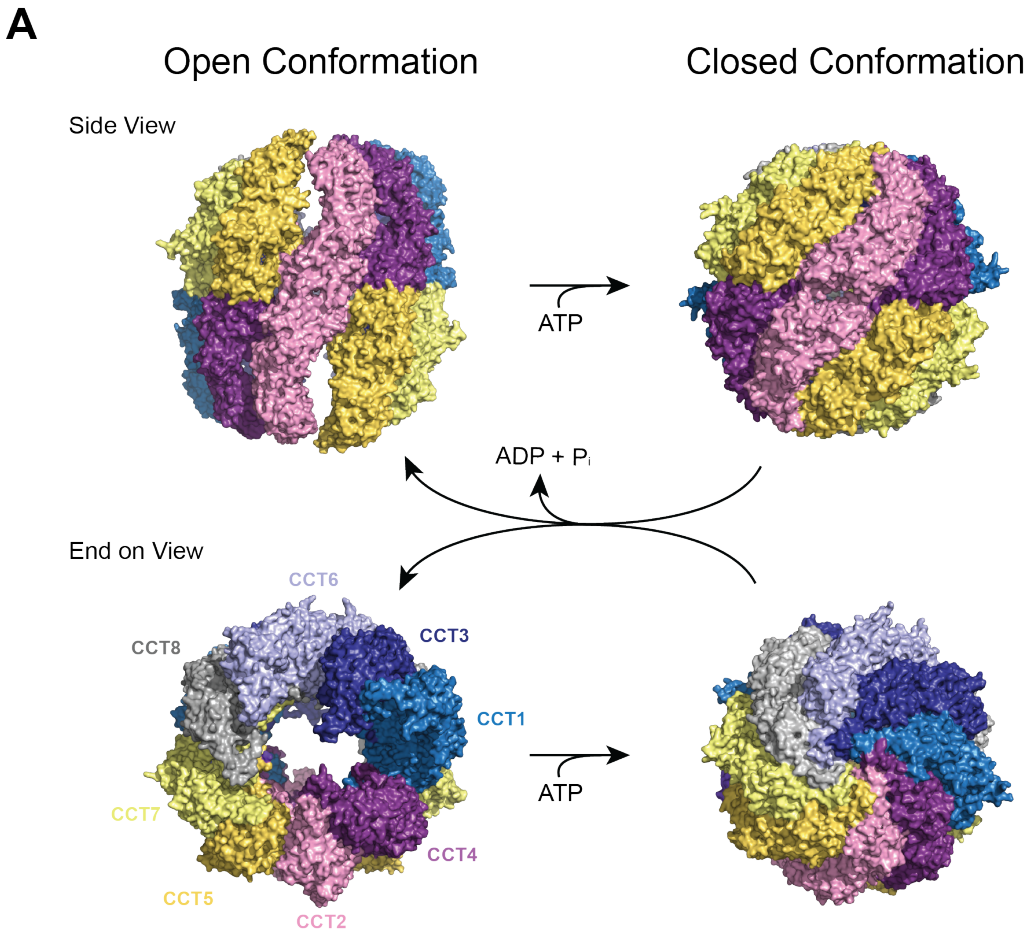

Figure 1.2. Structure of TRiC and duty cycle. (A) Side and end-on views of human TRiC in the open and closed conformations (adapted from PDB entries 7X3J and 7LUM, respectively), highlighting the eight CCT subunits arranged in each ring. ATP hydrolysis occurs cooperatively across the complex and drives large-scale conformational changes that transition TRiC between open and closed states. Adapted from Smith and Willardson (2022).

TRiC does not assemble spontaneously, but the molecular details of TRiC assembly in cells are unknown. One of the challenges in studying TRiC assembly is that altering the stoichiometric expression of each subunit by overexpression leads to aberrant complex formation (Betancourt Moreira *et al.*, 2023). A recent paper outlined a hierarchical pathway for subunit assembly in mammalian cells, suggesting assembly occurs through intermediate scaffolds that are rapidly degraded when not in use. This study

also suggests that TRiC assembly is not thermodynamically favorable; therefore, unknown external regulators are driving TRiC assembly in mammalian cells (Betancourt Moreira *et al.*, 2023). This is consistent with work done in *E coli*, where expressing each TRiC subunit leads to the formation of aberrant complexes (Sergeeva *et al.*, 2019). TRiC assembly has also never been seen using pure protein. Studies have purified functional TRiC subunits with ATPase activity, but they do not assemble by themselves (Collier *et al.*, 2021; Betancourt Moreira *et al.*, 2023). Overall, this data suggests TRiC assembly requires unidentified factors.

1.7. TRiC chaperone and mitochondria

MSTO1 has not been systematically analyzed in any system, leaving open fundamental questions about its function. Although the *Drosophila* homolog Misato has been linked to defects in cell division and TRiC stability, no cell division defects have been documented in MSTO1 patients. It is unknown whether the function of vertebrate MSTO1 is consistent with that of its *Drosophila* homolog's role in TRiC stability. Consistent with this, MSTO1 is not highly conserved across model organisms; human MSTO1 has only 29 percent amino acid sequence conservation with *Drosophila* Misato, suggesting vertebrate MSTO1 may have species-specific functions (The UniProt Consortium, 2025).

Currently, there is little direct evidence connecting TRiC to the mitochondria. Most mitochondrial proteins are encoded in the nucleus, translated in the cytoplasm, and then imported into the mitochondria through outer and/or inner mitochondrial membrane translocase complexes (Kizmaz *et al.*, 2024). These proteins are generally thought to remain at least partially unfolded during import and thus are not predicted to require chaperone-mediated folding before mitochondrial entry. This has contributed to the current view that TRiC does not fold mitochondrial proteins. However, known TRiC substrates are involved in a wide range of processes, including the cell cycle, translation, transcription, and autophagy, all of which could potentially affect mitochondria (Ghozlan *et al.*, 2022; Zeng *et al.*, 2024). Interestingly, in cells missing functional TRiC, some mitochondrial proteins are highly downregulated. In TRiC patients and TCP-1 knockdown cells, proteome and transcriptomic analysis indicated that some of the largest changes occurred in mitochondrial metabolism proteins (Kraft *et al.*, 2024). Strikingly, mitochondrial inner membrane proteins, such as TFAM, which is associated with mitochondrial DNA nucleoids, are also affected (Kraft *et al.*, 2024; Wu *et al.*, 2025). This is unexpected, as these proteins typically have limited

interaction with cytosolic machinery once localized to mitochondria. Together, these observations highlight a gap in current understanding of the relationship between TRiC and the mitochondria. In this context, MSTO1 represents an intriguing but still poorly characterized factor that may link TRiC protein folding and mitochondrial function.

Chapter 2. MSTO1 promotes assembly of TRiC to maintain mitochondrial function

This chapter is closely adapted from the paper in preparation.

2.1. Abstract

Mitochondria are constantly fusing, dividing, and moving on microtubules to maintain structural and functional integrity. In addition, maintenance of mitochondrial DNA (mtDNA) is essential for mitochondrial health, as the genome encodes essential oxidative phosphorylation proteins. Recently, mutations in *MSTO1* have been linked to clinical disease phenotypes typical of mitochondrial dysfunction. MSTO1 patient-derived fibroblasts have short mitochondria and a striking loss of mtDNA, leading to a model that MSTO1 regulates mitochondrial fusion. However, the molecular function of MSTO1 in vertebrate cells remains poorly understood. Here we use the auxin-inducible degradation (AID) system to temporally control MSTO1 protein stability. MSTO1-FLAG-AID protein is rapidly depleted, decreased to almost undetectable levels and these cells recapitulate the short mitochondrial phenotype observed in patients. We find that prior to any changes in mitochondria, MSTO1-depleted cells had a significant decrease in TRiC, an essential cytosolic ATP-dependent chaperone. Reciprocally, knockdown of TRiC led to a decrease in MSTO1 protein levels and was sufficient to induce a short mitochondrial phenotype. This reveals a previously unrecognized connection between TRiC and the mitochondria that was independent of changes in tubulin or actin, well-known obligate substrates of TRiC. Using co-immunoprecipitation and BN-PAGE, we found that MSTO1 interacts with the fully assembled TRiC chaperone, and our data suggests that MSTO1 assists in assembling early TRiC assembly intermediates. Together, these findings identify MSTO1 as a TRiC assembly factor and connect mitochondrial defects caused by MSTO1-depletion to the loss of TRiC.

2.2. Introduction

To maintain mitochondrial health, mitochondria constantly fuse, divide, and move along microtubules to maintain an interconnected network. The dynamic mitochondrial network is important for

cellular physiology, including responses to cell stress, cell cycle progression, and cell death. Regulation of mitochondrial dynamics is also integral for ATP production, especially in neuronal and muscle cells, which have high energy demands. Altered mitochondrial dynamics is common in muscular myopathies, heart disease, and neurodegenerative diseases (Boland *et al.*, 2013; Srivastava, 2017; Forte *et al.*, 2021).

Recently, patients have been documented with a neuromuscular disease caused by compound heterozygous mutations in the nuclear gene, *MSTO1*. MSTO1 patients present with myopathy-dystrophy, ataxia, cerebellar involvement, and sometimes retinopathy and cognitive impairments. MSTO1 patients have almost undetectable MSTO1 protein levels, suggesting that reported amino acid substitutions or deletions reduce protein stability (Nasca *et al.*, 2017a, 2021a; Donkervoort *et al.*, 2019; Chen *et al.*, 2022). Patient-derived fibroblasts have reduced mitochondrial fusion activity and a 30-60% decrease in mitochondrial DNA (mtDNA) (Gal *et al.*, 2017; Nasca *et al.*, 2017a, 2021a; Iwama *et al.*, 2018; Ardicli *et al.*, 2019; Donkervoort *et al.*, 2019; Schultz-Rogers *et al.*, 2019; Li *et al.*, 2020; Liu *et al.*, 2022). MtDNA is critical for fulfilling the energetic demands of the cell as it encodes essential subunits of the oxidative phosphorylation (OXPHOS) complexes, mitochondrial tRNA, and rRNA. In MSTO1 patients, studies have implicated defects in mitochondrial fusion as the primary defect. Consistent with this, MSTO1 patient fibroblasts have short and fragmented mitochondria compared to control cells (Nasca *et al.*, 2017b, 2021b; Donkervoort *et al.*, 2019). In MSTO1 knockdown HeLa cells, mitochondrial motility, membrane potential, and calcium uptake were unaffected, indicating mitochondrial fusion defects are not secondary to bioenergetic or movement impairments (Gal *et al.*, 2017). The molecular functions of MSTO1 are unknown, and it remains unclear how the loss of MSTO1 leads to defects in mitochondrial fusion.

While vertebrate MSTO1 function has only been connected to mitochondria, only one study has reported mitochondrial changes upon depletion of the *Drosophila* homolog, Misato (Min *et al.*, 2017). Specifically, conditional knockdown of misato in visceral muscle resulted in mitochondrial fragmentation, similar to MSTO1 patient fibroblasts. Misato was first characterized as a factor required for stability of the tubulin chaperone complex (TCP-1 or TRiC in vertebrates). The TCP-1 complex is a cytosolic chaperone predicted to fold approximately 10% of cytosolic proteins, including its obligate substrates tubulin and actin. Larvae with *misato* conditional knockouts have decreased TCP-1 complex and α-tubulin protein levels. The decrease in tubulin causes metaphase arrest arising from mitotic spindle defects in misato-null

larvae (Miklos *et al.*, 1997b; Palumbo *et al.*, 2015). In these conditional brain-specific *misato* knockouts, the mitochondrial network was reported to be similar to controls (Mottier-Pavie *et al.*, 2011). A functional connection with the vertebrate TRiC has not been tested in patients and cell division defects are neither noted in patient studies nor would be consistent with ataxia and myopathy.

In vertebrates, TRiC is a 1 MDa hetero-oligomeric chaperone composed of two rings with 8 ATPase subunits (CCT1-CCT8). The relative arrangement of the subunits in TRiC are conserved across species and is critical for TRiC function. How TRiC assembles, especially given that subunits that share such a high degree of structural similarity, is not known. Assembly is also critical for stability of the subunits and complex. Any excess subunits are degraded, and depletion/loss of any one subunit compromises the stability of the entire complex, resulting in depletion of the entire TRiC complex. While each CCT subunit can be purified and possess ATPase activity, they do not assemble into a functional TRiC complex. Rather, some subunits form homooligomers and others interact promiscuously with non-cognate neighbors (Sergeeva *et al.*, 2013, 2019; Collier *et al.*, 2021). This suggests that TRiC is assembled in cells by an active mechanism. A recent paper outlined a hierarchical pathway for TRiC assembly in mammalian cells where assembly occurs through intermediate scaffolds, and these are rapidly degraded when not in use. This study also found that the assembly of TRiC by these specific intermediates is not thermodynamically favorable, suggesting that there is an unknown external regulation driving proper assembly in mammalian cells (Betancourt Moreira *et al.*, 2023). Candidate assembly factors have not been identified.

To date, there is no definitive connection between TRiC and mitochondria. Although, no mitochondrial proteins have yet been identified as TRiC substrates, it is unlikely that all substrates are known. Known substrates are involved in a wide range of processes, including cell cycle, translation, transcription, and autophagy, each of which could potentially all impact mitochondrial function. In this study, we find that MSTO1 links TRiC and mitochondria. Using an auxin-degradation system in HCT116 cells, we find that MSTO1-depleted cells have shorter mitochondria, like in MSTO1 patient cells. In these cells, we demonstrate that TRiC steady-state protein levels are decreased days before observing changes in mitochondrial morphology. This is consistent with a functional connection between TRiC and mitochondria that is mediated by MSTO1. We establish that knockdown of TRiC is sufficient to alter

mitochondrial morphology and that MSTO1 and TRiC protein stability are reliant on each other. Consistent with this, using co-immunoprecipitations, we found that MSTO1 interacts with TRiC and loss of MSTO1 leads to changes in steady-state protein-levels of TRiC intermediate scaffolds. Overall, our data suggest MSTO1 is a novel TRiC assembly factor that acts as a chaperone for free TCP1 subunits before they are assembled into the complex.

2.3. Results

2.3.1. MSTO1-depleted cells have short mitochondria

To capture the cellular consequences of depletion of MSTO1 with temporal information, we built HCTT16 cells expressing an auxin-inducible degradation (AID) system to control the expression of MSTO1. First, OsTir1-F74G-V5, the ubiquitin ligase required to identify the AID degron, was integrated into HCT116 WT cells. Subsequently, the C-terminus of the endogenous *MSTO1* was engineered to express a FLAG-tag, for detection and downstream biochemical experiments, followed by the mAID-tag (Figure 2.1 A-B). Expression of MSTO1-FLAG-AID was confirmed by Western blot analysis, and knock-in at both alleles was confirmed by PCR. Of note, duplication of a discrete region on chromosome 1q22 in human cells, created *MSTO2P*, a pseudogene of MSTO1 that produces a long noncoding RNA (lncRNA). Due to the very high sequence identity between *MSTO1* and *MSTO2P,* integration of the FLAG-AID sequence also occurred at the 3-prime end of *MSTO2P*. *MSTO2P* is transcriptionally active and is predicted to make long noncoding RNA (lncRNA). *MSTO2P* is not predicted to make functional protein, as *MSTO2P* has a frame shift mutation that leads to a premature stop codon before the last exon; therefore, the FLAG-AID insertion in *MSTO2P* is not expected to affect our results (Figure 6.1) (Timmis *et al.*, 2004).

MSTO1-FLAG-AID was rapidly degraded after addition of the auxin analog, 5-Ph-IAA (hereafter auxin) (Figure 1.1 C). Immunoblotting for FLAG revealed that the MSTO1 protein level is 25% of vehicle (DMSO) treated controls after 2 hours of auxin treatment (Figure 2.1 D). This was consistent across three different clonal populations of cells with MSTO1-FLAG-AID (Figure 6.2). Our MSTO1-FLAG-AID cells offer an unprecedented opportunity to establish the consequences of MSTO1 depletion with temporal resolution unavailable with other approaches. Therefore, we have generated an advantageous model for studying the molecular mechanism of an understudied protein, MSTO1.

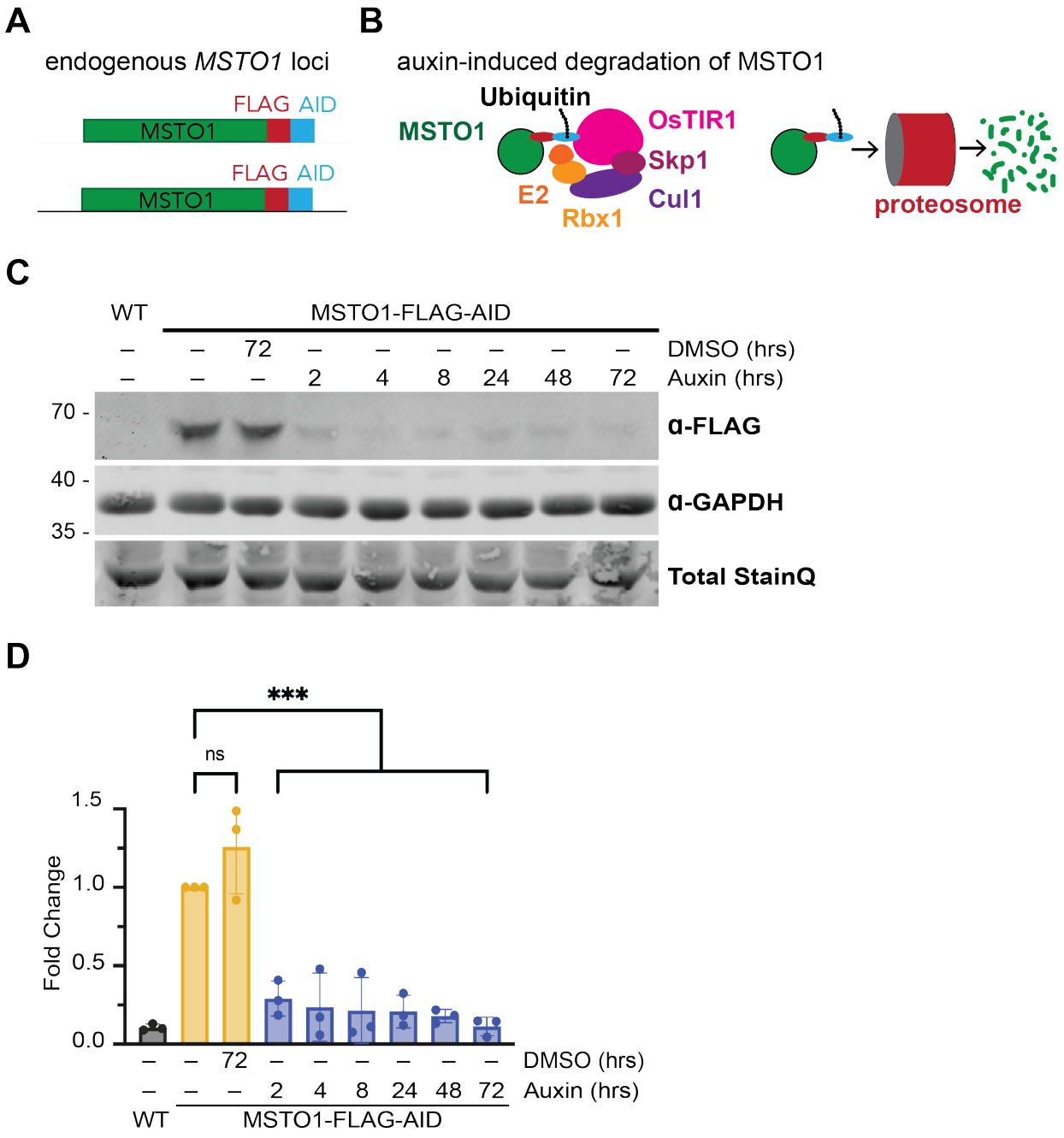

Figure 2.1. MSTO1 is depleted after 2 hours of auxin treatment. (A) Sequence encoding FLAG and AID tags were integrated at endogenous MSTO1 loci using CRISPR-Cas9-mediated homology-based repair in HCT116 cells. **(B)** Upon the addition of the small molecule auxin, OsTIR1 will bind the AID tag and mediate recruitment of ubiquitination protein complex, leading to the degradation of MSTO1. **(C)** MSTO1-FLAG-AID cells were treated with 20 μM auxin for the indicated time. Whole-cell lysates prepared from MSTO1-FLAG-AID cell lines subject to SDS–PAGE and immunoblotting with anti-FLAG and anti-GADPH. Staining of total protein with Total StainQ was used as loading control. **(D)** Quantification of Western blot from (C). Average fold change of MSTO1-FLAG-AID protein expression relative to WT HCT116 cells from three independent experiments are shown. The graph shows mean and standard deviation from 3 independent experiments, ns: not significant, ***P < 0.001, ordinary one-way Anova with multiple comparisons.

We first examined mitochondrial morphology following depletion of MSTO1. We expected to observe an increase in short and/or fragmented mitochondria, as reported in patient-derived fibroblasts (Gal *et al.*, 2017; Nasca *et al.*, 2017a, 2021a; Iwama *et al.*, 2018; Ardicli *et al.*, 2019; Donkervoort *et al.*, 2019; Schultz-Rogers *et al.*, 2019; Li *et al.*, 2020; Liu *et al.*, 2022). Mitochondrial morphology was scored in blinded experiments. The mitochondrial network of wild type HCT116 cells is a mixture of reticular and short, with most mitochondria having a length that is greater than 5 μm, and few mitochondria in the network are between 2.5 and 5 μm in length. Quantification of mitochondrial morphology in HCT116 cells expressing OsTir1-F74G-V5 yielded comparable results to wild type cells. We treated MSTO1-FLAG-AID cells with either vehicle or 20 micromolar auxin and then imaged cells treated after either 24 hours or 72 hours. No changes in mitochondrial morphology were observed (data not shown). We extended the time with auxin and found that after 6 days, MSTO1-FLAG-AID cells had a higher percentage of short and fragmented mitochondria compared to earlier timepoints (Figure 2.2 A-B). In contrast, the mitochondrial network in MSTO1-FLAG-AID cells treated with vehicle were like wild type HCT116 cells when quantified (Figure 2.2 A-B). This phenotype was also consistent across three MSTO1-FLAG-AID isolates (Figure 6.3 A-B). MSTO1 was previously knocked down in HeLa cells, where they observed mitochondrial morphology changes by 72 hours after transduction (Kimura and Okano, 2007; Gal *et al.*, 2017). Of note, HeLa cells have multiple copies of chromosome 1 resulting in high expression levels of MSTO1 protein. This unique context may underlie the differences in our data.

Another common observation in MSTO1 patient-derived fibroblasts was a decrease in mtDNA copy number compared to controls. We assessed mtDNA content in our cells in two ways: first by visualizing nucleoids with PicoGreen staining and second with qPCR. We assessed mtDNA following 6 days of auxin treatment, when we observed changes in mitochondrial connectivity. The MSTO1-AID cells stained with Picogreen had no obvious changes in mtDNA nucleoid number, size, or distribution compared to wild type or MSTO1-AID cells treated with DMSO (Figure 2.2 A). The relative mtDNA copy number quantified by qPCR was also comparable to DMSO controls (Figure 2.2 D). Therefore, in this timeframe, we do not observe a decrease in mtDNA following depletion of MSTO1.

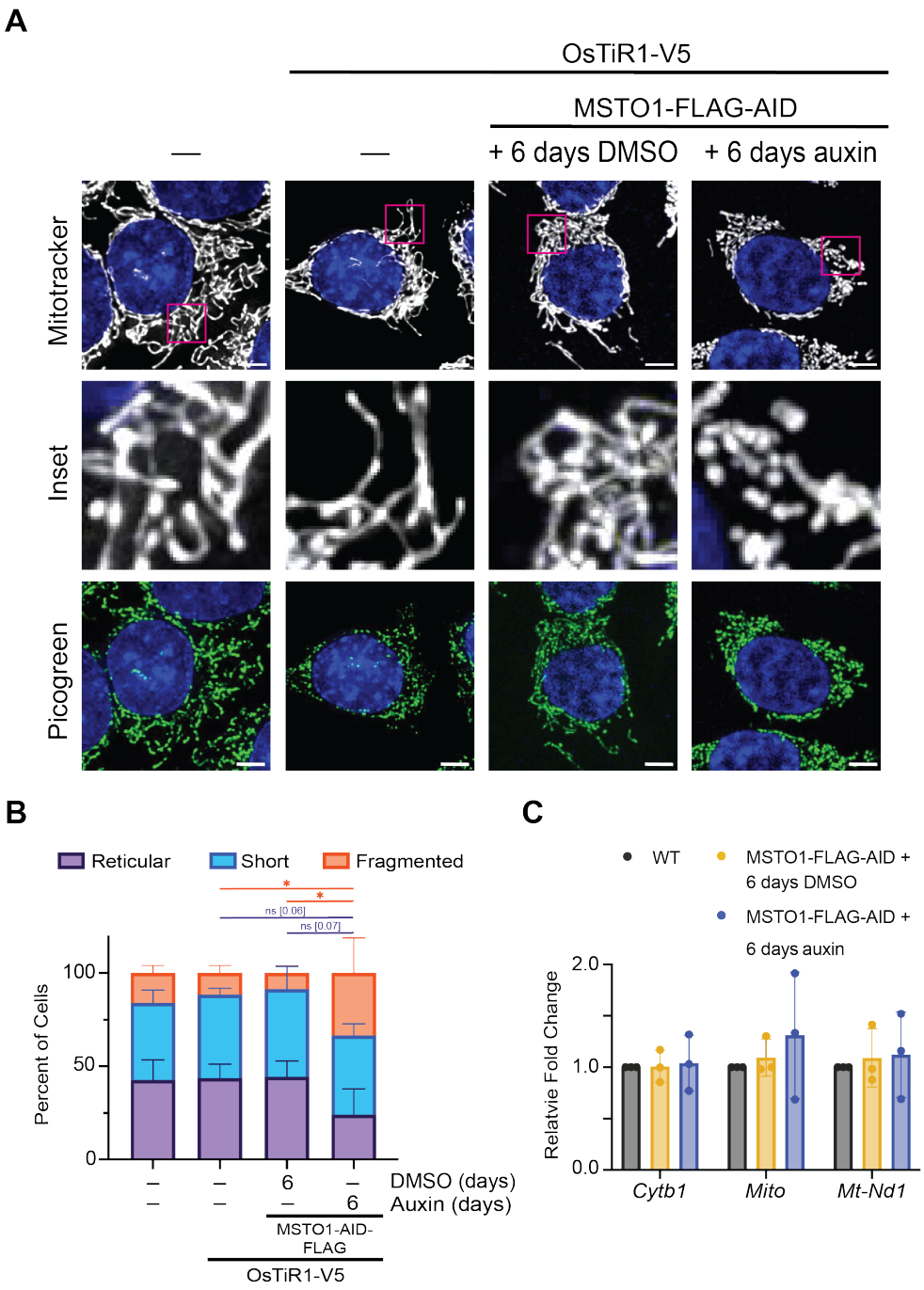

Figure 2.2. MSTO1-depleted cells have short mitochondria. (A) Representative live cell images of WT, WT+OsTiR1-V5, and MSTO1-FLAG-AID treated with auxin or vehicle for 6 days. Mitochondria were labeled with Mitotracker Red CMXRos, mtDNA were labeled with Quant-iT™ PicoGreen® dsDNA Reagent, and nuclei were labeled with NucBlue. All were visualized by fluorescence microscopy. Scale bar is 5 μM **(B)** Quantification of mitochondrial morphology for cell lines described in (A). The graph shows mean and standard deviation from 3 independent experiments, ns [p-value]: not significant, *P < 0.05, ordinary two-way Anova with multiple comparisons. **(C)** Genomic DNA samples were prepared from MSTO1-AID-FLAG cells treated with auxin or vehicle for 6 days. MtDNA was quantified relative to *GAPDH*, a nuclear housekeeping gene, by qPCR.

2.3.2. TRIC levels are significantly reduced before mitochondrial morphology changes

One important step forward in understanding the cellular roles of MSTO1 is to determine if vertebrate MSTO1 is also functionally connected to TRiC, as reported for Misato and TCP-1. Each TRiC subunit has independently evolved to have a unique function that is highly conserved in almost all eukaryotes. The specific arrangement of each subunit in the complex is critical for TRiC activity, especially to allow a diversity of folding substrates (Joachimiak *et al.*, 2014). Knockdowns of any individual subunit lead to the collapse of the entire complex and degradation of remaining subunits by the proteasome or autophagy (Palumbo *et al.*, 2015; Betancourt Moreira *et al.*, 2023). Hence, we chose the most frequently used antibody to detect TRiC, CCT1, to test TRiC steady-state protein levels following depletion of MSTO1-FLAG-AID. Using the same protocol as in Figure 2.1 C-D, we probed with anti-CCT1 and observed that after 48 hours of auxin treatment, CCT1 protein level was significantly decreased compared to DMSO controls (Figure 2.3 A-B). Similar losses of CCT1 occurred in all three MSTO1-AID isolates (Figure 6.4 A-D). To confirm CCT1 protein levels were still decreased at 3 and 6 days, where mitochondrial morphology changes were observed, we quantified CCT1 protein abundance. Indeed, CCT1 protein levels decreased to 40% versus controls at these timepoints (Figure 6.4 E-F). This decrease suggests that either MSTO1 only stabilizes a subset of TRiC or the small amount of MSTO1-FLAG-AID present after auxin treatment is sufficient to partially fulfill its functional role.

MSTO1 patients have never been assessed for TRiC expression. We wanted to determine if the loss of TRiC observed in our MSTO1-FLAG-AID system was also a feature of MSTO1 patient-derived fibroblasts. We obtained MSTO1 patient fibroblasts from Nasca et al., which have a drastic reduction in MSTO1 protein levels (Nasca *et al.*, 2017b). CCT1 steady-state protein levels were quantified in MSTO1 patient fibroblasts as a proxy for the TRiC complex. The MSTO1 patient-derived cells have a significant decrease in CCT1 protein level compared to control fibroblasts (Figure 2.3 C-D). This decrease is similar to what we observed in MSTO1-depleted cells, suggesting the MSTO1-AID-FLAG cells are a valid model to understand the relationship between MSTO1, TRiC, and mitochondrial morphology.

TRiC is most well-characterized for its obligate role in folding tubulin and actin. Both cytoskeletal elements contribute to mitochondrial morphology and dynamics. Mitochondria move along both microtubules and actin filaments, and this movement is important for mitochondrial positioning. Actin is

also present at mitochondrial fission sites and constricts the mitochondria before DRP1-mediated fission. Actin has also been visualized at mitochondrial fusion sites, but its mechanistic role remains unclear (Gatti *et al.*, 2025). Therefore, we hypothesized that if tubulin and/or actin steady-state protein levels were decreased due to the loss of TRiC, this could impact mitochondrial connectivity.

Therefore, we quantified α-, β-, and γ-tubulin, and β-actin protein steady-state levels after 3 and 6 days of auxin treatment to capture the consequence of the depletion of TRiC, which is decreased at 3 days. Despite the significant decrease of TRiC, no changes in steady-state levels of any of these cytoskeleton components were observed at either of these timepoints (Figure 2.3 E-F). This was also consistent across 2 MSTO1-AID-FLAG isolates (Figure 6.5 A-B). Accordant with this, no changes in the microtubule or actin network were observed at steady-state when MSTO1-depleted cells were imaged by immunofluorescence for α-tubulin, or Phalloidin for actin (Figure 6.5 C). Taken together, the decrease in CCT1, and therefore TRiC, in both MSTO1-depleted cells and MSTO1 patient fibroblasts suggests MSTO1 and TRiC are functionally connected, and this is conserved between *Drosophila* and humans.

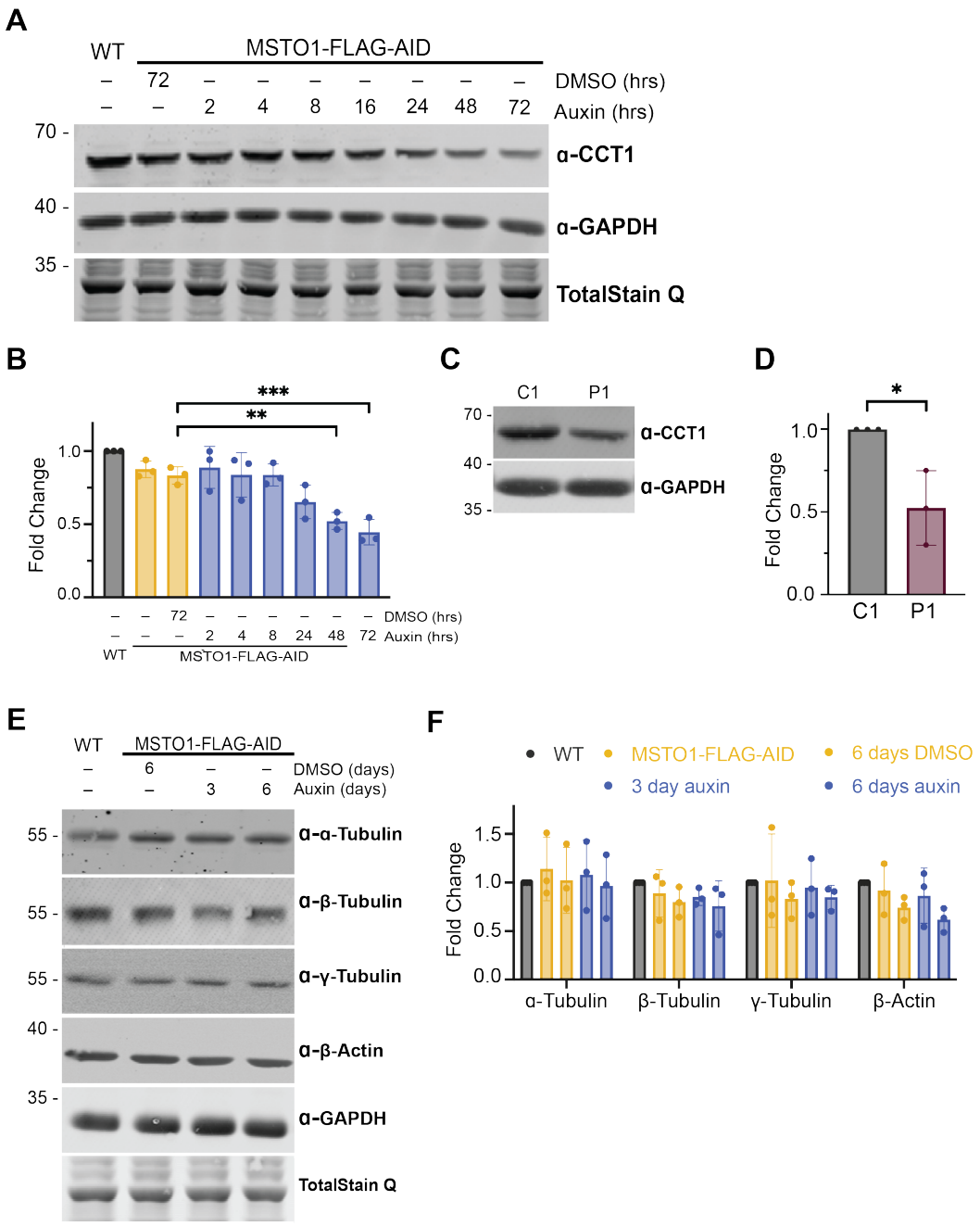

Figure 2.3. TRiC levels are significantly reduced before mitochondrial morphology changes. (A) MSTO1-FLAG-AID cells were treated with 20 μM auxin for indicated times. Whole-cell lysates prepared from MSTO1-FLAG-AID cell lines subject to SDS–PAGE and immunoblotting with anti-CCT1, and anti-GADPH. Staining of total protein with Total StainQ was used as loading control. **(B)** Quantification of Western blot from (A). Average fold change of CCT1 protein expression relative to WT HCT116 cells from three independent experiments are shown. The graph shows mean and standard deviation from 3 independent experiments, **P < 0.01, ***P < 0.001, ordinary one-way Anova with multiple comparisons. **(C)** Whole-cell lysates prepared from MSTO1 patient fibroblasts subject to SDS–PAGE and immunoblotting with anti-CCT1 and anti-GADPH. **(D)** Quantification of Western blot from (C). Average fold change of CCT1 protein expression relative to WT patient fibroblasts from three independent experiments are shown. The graph shows mean and standard deviation from 3 independent experiments,

*P < 0.05, Welch's unpaired T-test. **(E)** MSTO1-FLAG-AID cells were treated with 20 μM auxin for 3 or 6 days. Whole-cell lysates prepared from MSTO1-FLAG-AID cell lines subject to SDS–PAGE and immunoblotting with anti-α-tubulin, anti-β-tubulin, anti-γ-tubulin, anti-β-actin, and anti-GADPH. Staining of total protein with Total StainQ was used as loading control. **(F)** Quantification of Western blot from (E). Average fold change of -tubulin, β-tubulin, γ-tubulin, β-actin protein expression relative to WT HCT116 cells from three independent experiments are shown. The graph shows mean and standard deviation from 3 independent experiments.

2.3.3. TRiC is required to maintain MSTO1 steady state protein levels and mitochondrial morphology

To date, there is no evidence in vertebrates directly linking TRiC chaperone function with mitochondrial morphology. To determine if loss of TRiC leads to changes in mitochondrial morphology, CCT1 expression was reduced by expression of short hairpin RNA (shRNA) targeting CCT1 transcripts in MSTO1-AID cells. As discussed earlier, loss of CCT1 has been shown to reduce the amount of assembled TRiC. Consistent with data identifying CCT1 as an essential protein, knockdown of CCT1 led to a decrease in cell proliferation and an increase in cell death (Ursic and Culbertson, 1991; Liu *et al.*, 2005). Compared to the control shRNA to RFP, cells expressing shCCT1 A or shCCT1 C had reduced CCT1 protein levels (~40% and ~60% respectively) (Figure 2.4 A-B). Cells expressing either shRNA also have an increased portion of the population with fragmented and short mitochondria compared to controls (Figure 2.4 B). No changes in mtDNA nucleoid number or distribution were observed (Figure 2.4 C). Therefore, loss of TRiC leads to altered mitochondrial morphology and the change is strikingly similar to what has been observed in MSTO1 patients and our MSTO1-depleted cells.

As shown above, MSTO1 is required to maintain TRiC protein levels. To determine if TRiC in turn regulates the steady state levels of MSTO1, we assessed MSTO1-FLAG protein levels following CCT1 knockdown. In both knockdowns of CCT1, we observe significant decreases in MSTO1-FLAG-AID protein (Figure 2.4 A and E, 30% and 43% of controls, respectively). Therefore, in humans, MSTO1 stability depends on TRiC and vice versa. It is important to note that since MSTO1 protein levels are reduced in TRiC-depleted cells, it is difficult to deconvolve whether the change in mitochondrial morphology is due to the loss of MSTO1, TRiC, or both.

We next sought to determine if steady state levels of either tubulin or actin are affected by the reduced expression of CCT1 in our shRNA conditions. We quantified α-tubulin and β-actin in cells expressing either shCCT1 A or shCCT1 C (Figure 2.4 A and F). Consistent with the greater reduction in

CCT1 levels with shCCT1 C, α-tubulin levels decreased in these cells, but not the cells expressing shCCT1 A. The level of β-actin did not detectably change under either condition (Figure 2.4 A and G).

Together, our data highlight similarities and differences between cells specifically depleted of MSTO1 and cells with reduced expression of CCT1. Patients with disease-associated variants of MSTO1 and TRiC also present with notable differences. Impairment of TRiC function caused by mutations in TRiC subunits was recently coined TRiCopathy. Heterozygous variant alleles of most CCT subunits have been reported (not CCT2). Patients present with severe global developmental disorders, brain malformations, microcephaly, muscle hypotonia, ataxia, and intellectual disability (Kraft *et al.*, 2024). Cells expressing shCCT1 A and C have cell proliferation defects compared to shRFP controls, requiring twice as many cells to be plated at the start of each experiment. We never observed a growth difference in MSTO1-FLAG-AID cells treated with auxin. Taken together, the decrease in tubulin and cell proliferation in shCCT1 cells suggests loss of CCT1 and loss of MSTO1 are not entirely redundant. Therefore, both should be studied.

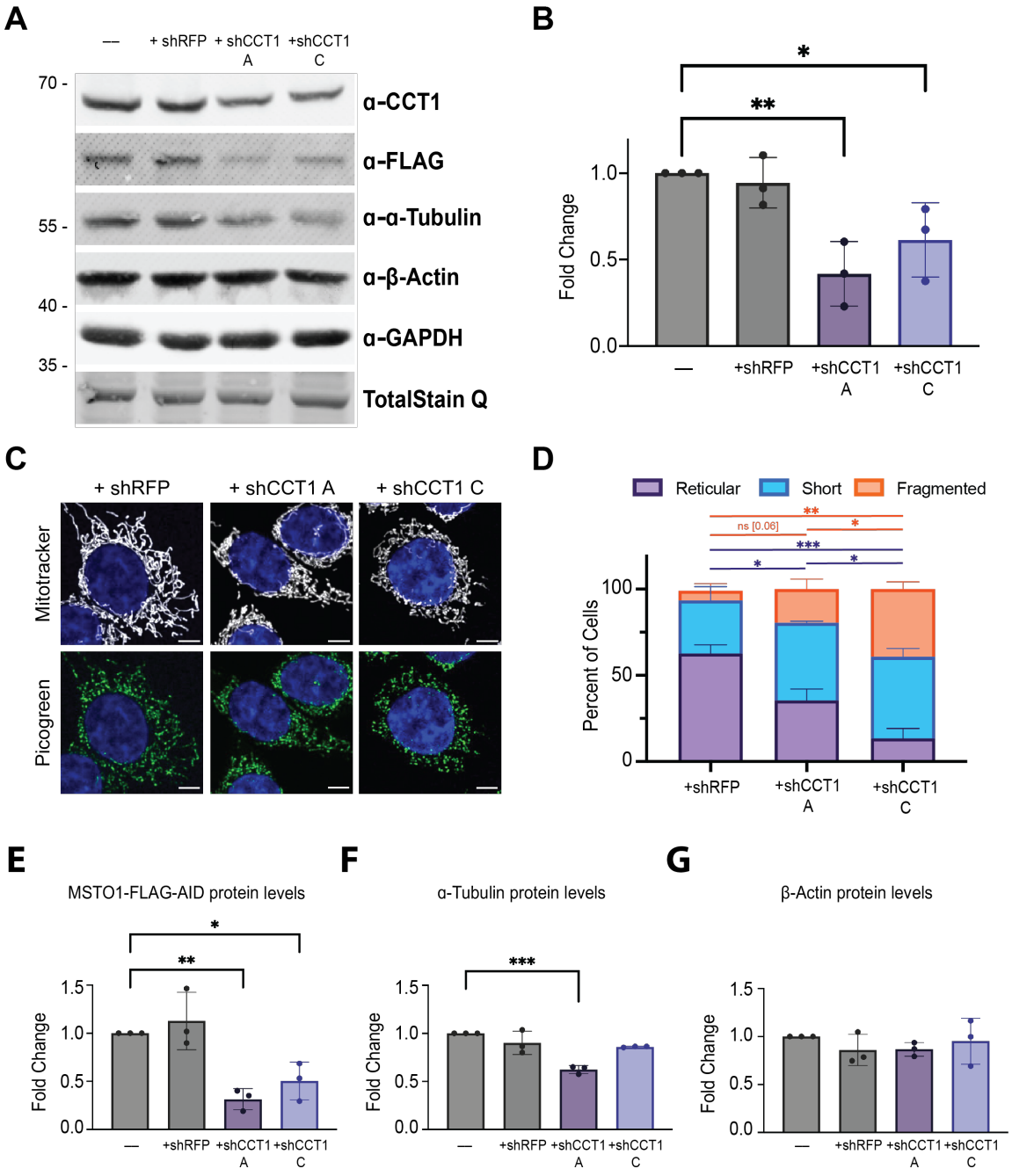

Figure 2.4. TRiC is required to maintain MSTO1 steady state protein levels and mitochondrial morphology. MSTO1-FLAG-AID cells transduced with either shRFP or shRNAs targeting MSTO1 (shCCT1 A or C) 10 days prior to live cell imaging and collection of whole-cell lysates. **(A)** Whole-cell lysates prepared from shRFP, shCCT1 A, and shCCT1 C subject to SDS–PAGE and immunoblotting with anti-CCT1, anti-FLAG, anti-α-tubulin, anti-β-actin, and anti-GADPH. Staining of total protein with Total StainQ was used as loading control. **(B)** Average fold change of CCT1 protein expression relative to WT HCT116 cells from three independent experiments are shown. The graph shows mean and standard deviation from 3 independent experiments, *P < 0.05, **P < 0.01, ordinary one-way Anova with multiple comparisons. **(C)** Representative live cell images of MSTO1-FLAG-AID + shRFP, +shCCT1 A, or +CCT1 C. Mitochondria were labeled with Mitotracker Red CMXRos, mtDNA were labeled with Quant-iT™ PicoGreen® dsDNA Reagent, and nuclei were labeled with NucBlue. All were visualized by fluorescence microscopy. Scale bar is 5 μM. **(D)** Quantification of mitochondrial morphology for cell lines described in

(C). The graph shows the mean and standard deviation from 3 independent experiments. **(E-G)** Quantification of (E) FLAG, (F) α-tubulin, (G) β-actin protein levels from Western blot in (A). Average fold change of protein expression relative to WT HCT116 cells from three independent experiments are shown. The graph shows mean and standard deviation from 3 independent experiments *P<0.05, **P < 0.01, ***P < 0.001, ordinary one-way Anova with multiple comparisons.

2.3.4. MSTO1 interacts with TRiC

MSTO1 has been established as a cytosolic factor that regulates mitochondrial fusion. Our data have revealed that MSTO1 is required for TRiC stability and *vice versa*. These functions suggest that MSTO1 may physically interact with the outer mitochondrial membrane fusion machine or TRiC. To test this, we immunoprecipitated MSTO1-FLAG-AID or mcherry-FLAG from wild type HCT116 cells as a negative control (Figure 2.5 A). The immunoprecipitation of MSTO1-FLAG-AID was efficient and none of the proteins of interest were found in the elution following immunoprecipitation of mCherry-FLAG. While neither Mfn1 nor Mfn2 interacted with MSTO1 in this assay, we found that endogenous MSTO1 does interact with CCT1. The results were consistent across two clonal populations of MSTO1-FLAG-AID (Figure 2.5 A).

We were curious if MSTO1 interacts with the TRiC holocomplex or TRiC assembly intermediates. Betancourt Moreira et al. 2023, found that TRiC assembly occurs through pre-assembly of intermediate scaffolds containing two to three subunits. Specifically, their data are consistent with a model where CCT2 and CCT4 dimers assemble with CCT5 and CCT7, followed by CCT8, and the last intermediate includes CCT1-CCT3-CCT6. To determine if MSTO1 interacts with intermediate scaffolds at specific steps in assembly, we chose one subunit from each distinct group of intermediate scaffolds. CCT8 was not chosen because it did not consistently assemble alone; sometimes, CCT8 assembled with CCT5 and CCT7 (Betancourt Moreira *et al.*, 2023). We find that MSTO1 interacts with CCT2, CCT7, and CCT3, representing each intermediate assembly unit (Figure 2.5 A-B) The results were consistent across two clonal populations of MSTO1-FLAG-AID cells (Figure 6.6 A-B).

Interestingly, MSTO1 and TRiC subunits are estimated to have drastically different cellular concentrations or protein copy number. These relative concentrations were estimated by quantitative mass spectrometry analysis of endogenously tagged genes in HEK293T cells (Cho *et al.*, 2022). TRiC subunits are present at ~ 6000 nM in human cells, while MSTO1 was about 20-fold less abundant at ~170 nm. Thus, it is unlikely MSTO1 is a stoichiometric interaction partner with TRiC.

2.3.5. MSTO1 is a novel TRiC assembly factor

Assembled TRiC and its assembly intermediates or subcomplexes can be visualized by native gel electrophoresis (Betancourt Moreira *et al.*, 2023). Betancourt Moreira et al., 2023, demonstrated that intermediate subcomplexes accumulate in cells where TRiC assembly is compromised (Betancourt Moreira *et al.*, 2023). To determine if changes occur in TRiC assembly intermediates when MSTO1 is depleted, MSTO1-FLAG-AID cells were treated with auxin for 3 days. To capture all assembly intermediates, cell lysates were then subjected to Blue Native-PAGE, and immunoblotting against CCT3, CCT7, and CCT2 (Schägger and von Jagow, 1991). CCT1 intermediate scaffolds could not be detected by Betancourt Moreira et al. Therefore, we used anti-CCT3 to detect the last intermediate scaffold. Consistent with what we observed through western blotting, by 3 days of auxin treatment, fully assembled TRiC was decreased in all cases (Figure 2.5 C). Along with the fully assembled TRiC, we observe assembly intermediates at a smaller molecular weights, consistent with intermediates previously identified by Betancourt Moreira et al., CCT2-CCT4 is predicted to assemble with CCT5-CCT7, and MSTO1-depleted cells had more CCT2 and CCT7 intermediate assemblies compared to vehicle-treated controls (Figure 2.5 C). CCT1-CCT3-CCT6 is the last assembly intermediate to join the complex. In MSTO1-depleted cells, CCT3 intermediate scaffolds were unchanged compared to controls (Figure 2.5 C). These data were consistent across two clonal populations of MSTO1-FLAG-AID (Figure 6.6 C).

Together, our data implicate MSTO1 in efficient TRiC assembly. When MSTO1 is depleted, the holocomplex is less abundant and assembly intermediates accumulate. We therefore propose that MSTO1 facilitates the assembly of CCT2-CCT4 with CCT5-CCT7.

To determine if MSTO1 interacts with TRiC intermediate assemblies, the fully assembled complex, or both, we assessed the migration of MSTO1-FLAG-AID by BN-PAGE. Lysates from MSTO1-FLAG-AID cells treated with vehicle were separated by BN-PAGE and immunoblotted for anti-FLAG. All detectable MSTO1-FLAG-AID migrates at the same molecular weight as the TRiC holo complex (Figure 2.5 C, Figure 6.6 C). We cannot rule out that small amounts of MSTO1 interact with assembly intermediates and are not detected by western blot, but our data clearly indicate that a significant portion of MSTO1 interacts with the fully assembled chaperone.

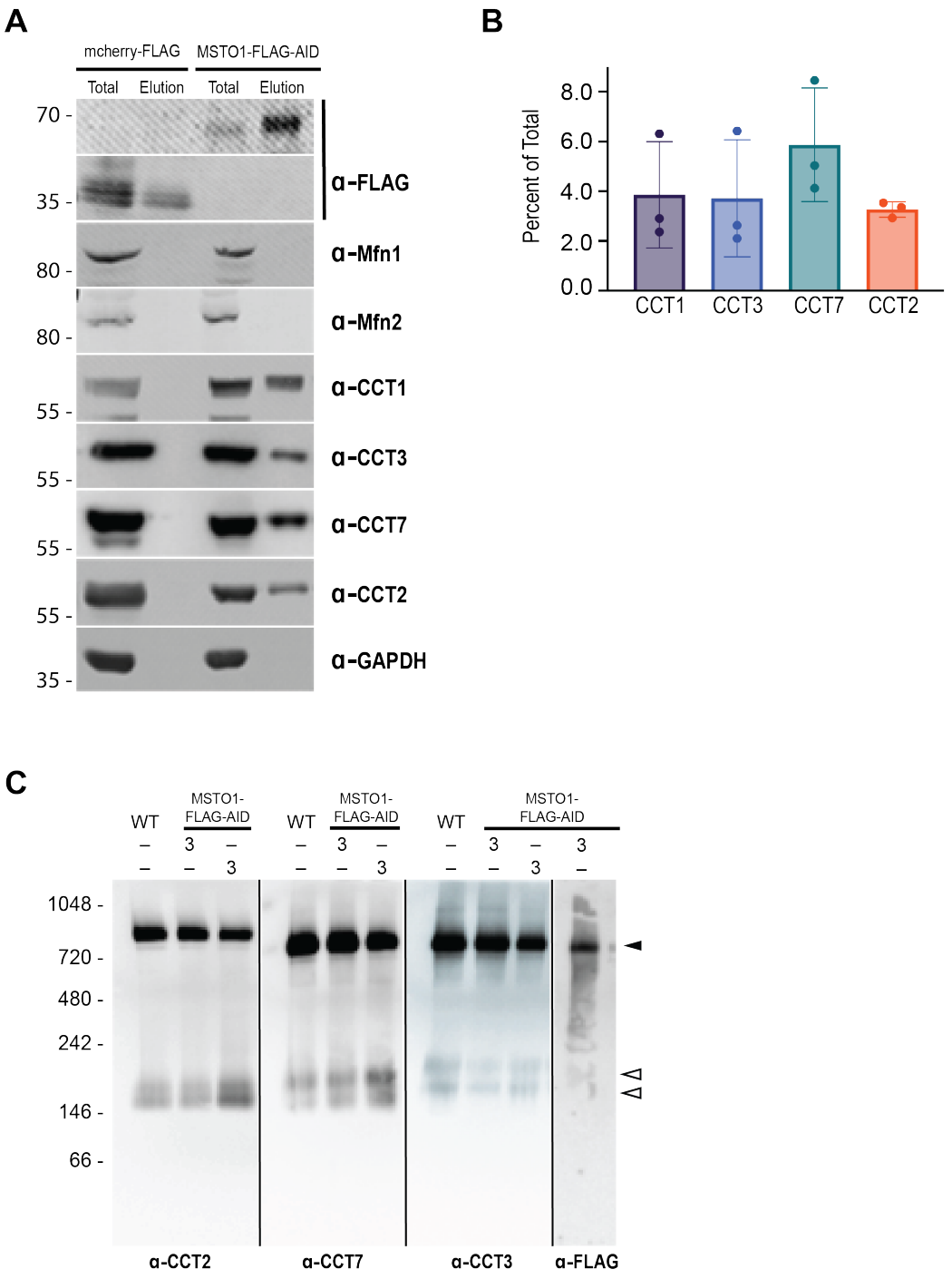

Figure 2.5. MSTO1 interacts with TRiC and is a novel assembly factor. (A) Co-immunoprecipitation (Co-IP) pulling on mcherry-FLAG or MSTO1-FLAG-AID with FLAG-coated magnetic beads. Co-IP Total (0.66%) and Elution (6.6%) subject to SDS–PAGE and immunoblotting with anti-FLAG, anti-Mfn1, anti-Mfn2, anti-CCT1, anti-CCT3, anti-CCT7, anti-CCT2, or anti-GADPH. **(B)** Quantification of fraction of CCT1, CCT3, CCT7, and CCT2 protein levels pulled down in elution compared to total protein levels from Co-IP from (A). **(C)** Whole-cell lysates prepared from MSTO1-FLAG-AID cells treated with auxin or vehicle for 3 days were subject to separation by BN-PAGE followed by immunoblotting with anti-CCT1, anti-CCT3, anti-CCT7, anti-CCT2, or anti-FLAG. Open arrowhead indicates ~146 kDa intermediate scaffolds and closed arrowhead indicate fully assemble TRiC at ~720 kDa.

2.4. Discussion

Bi-allelic variants of MSTO1 result in congenital or early onset mitochondrial myopathy and ataxia. The characterization of MSTO1 patient-derived fibroblasts and HeLa cells with reduced MSTO1 expression have led to the model that MSTO1 is a regulator of mitochondrial fusion. However, the molecular functions of MSTO1 are not fully understood. In this study we used an AID system to determine the cellular and molecular consequences of MSTO1-depletion. We found that depletion of MSTO1 leads to shorter mitochondria compared to controls, which is consistent the phenotypes of MSTO1 patient fibroblasts. The mitochondrial phenotype was evident 6 days after auxin treatment, well after MSTO1 was depleted. We also found that MSTO1 does not interact with the mitofusins, Mfn1 and Mfn2. These results imply that MSTO1 does not directly regulate mitochondrial fusion.

MSTO1 patients-derived cells also have a striking decrease in mtDNA that was not observed in our MSTO1-depleted cells. These findings are in agreement with a MSTO1 patient study, where reintroduction of MSTO1 in patient fibroblast rescued mitochondrial morphology but not mtDNA depletion in after 48 hours (Donkervoort *et al.*, 2019). This may indicate that mtDNA loss is not a direct result of MSTO1 depletion or that mtDNA loss is gradual and not evident after six days of MSTO1 depletion. Another plausible explanation is these cells do not fully recapitulate a physiological or developmental state that strictly requires MSTO1 for mtDNA maintenance.

TRiC is best known for its obligate role in folding tubulin and actin. Our experiments reveal for the first time that TRiC function is required to maintain mitochondrial structure, and this relationship is independent of tubulin and actin. In MSTO1-depleted cells, TRiC levels decrease 4 days before cells have short mitochondria, suggesting mitochondrial morphology changes are due to loss of TRiC. Consistent with this, we demonstrate that cells with CCT1-targed knockdown, and therefore depletion of TRiC, also have short mitochondria. Thus, loss of TRiC is sufficient to induce mitochondrial morphology defects. The molecular basis of this functional connection is not yet clear. The simplest model is that TRiC substrates are required to maintain mitochondrial function. The relevant TRiC substrate could be a protein localized to the cytoplasm, or to the mitochondrial outer membrane. While the vast majority of mitochondrial proteins are encoded by nuclear genes and translated in the cytoplasm, mitochondrial protein import and sorting requires that the nascent proteins are in a mostly unfolded state. Therefore, it is

unlikely that TRiC substrates must cross the outer membrane. Nevertheless, the substrate could be associated with the mitochondrial outer membrane, either integrated or peripherally. While most TRiC substrates are small enough to fit inside the folding chamber, there are some reports of non-canonical open-state folding substrates that are much larger than tubulin or actin (Rüßmann *et al.*, 2012; Zhao *et al.*, 2026).

MSTO1 and TRiC depend on one another for stability. When we knocked down CCT1 to deplete TRiC, MSTOP1 protein levels decreased. Auxin-dependent depletion of MSTO1 decreased CCT1 levels and TRiC complexes. This kind of interdependence is commonly found in a stoichiometric complex but based on to protein abundance measurements and our experiments, MSTO1 only interacts with a small fraction (~4%) of total TRiC in the cell. Assembly of TRiC is known to require an elusive cellular component and an assembly factor would not be expected to exist at stoichiometric levels. In the absence of MSTO1, the TRiC intermediate scaffolds (CCT2-CCT4 and CCT5-CCT7) accumulate in the cell, consistent with altered assembly kinetics. Of note, when TRiC is depleted by knocking down CCT subunits, CCT2 and CCT7 assembly intermediates also accumulate. Given our data demonstrating that knockdown of CCT1 results in depletion of MSTO1, it seems likely that MSTO1 levels are also reduced when the other CCT subunits are knocked down. Therefore, we speculate that MSTO1 promotes assembly of the CCT2-CCT4 and CCT5-CCT7 intermediate scaffolds into the fully assembled TRiC. In the absence of MSTO1, these intermediate scaffolds are either assembling too slow or cannot be assembled without MSTO1, leading to intermediate scaffold accumulation.

MSTO1 cannot be an essential component of all TRiC functions. Other proteins that TRiC interacts with include substrates and co-chaperones. While MSTO1 has homology to tubulin, a key TRiC substrate, the C-terminal FLAG tag on MSTO1 would not be expected to be accessible from the inside of the TRiC folding chamber. It is conceivable that MSTO1 is a co-chaperone with clients that impact mitochondrial function; however, to our knowledge, depletion of other TRiC co-chaperones does not affect the stability of TRiC.

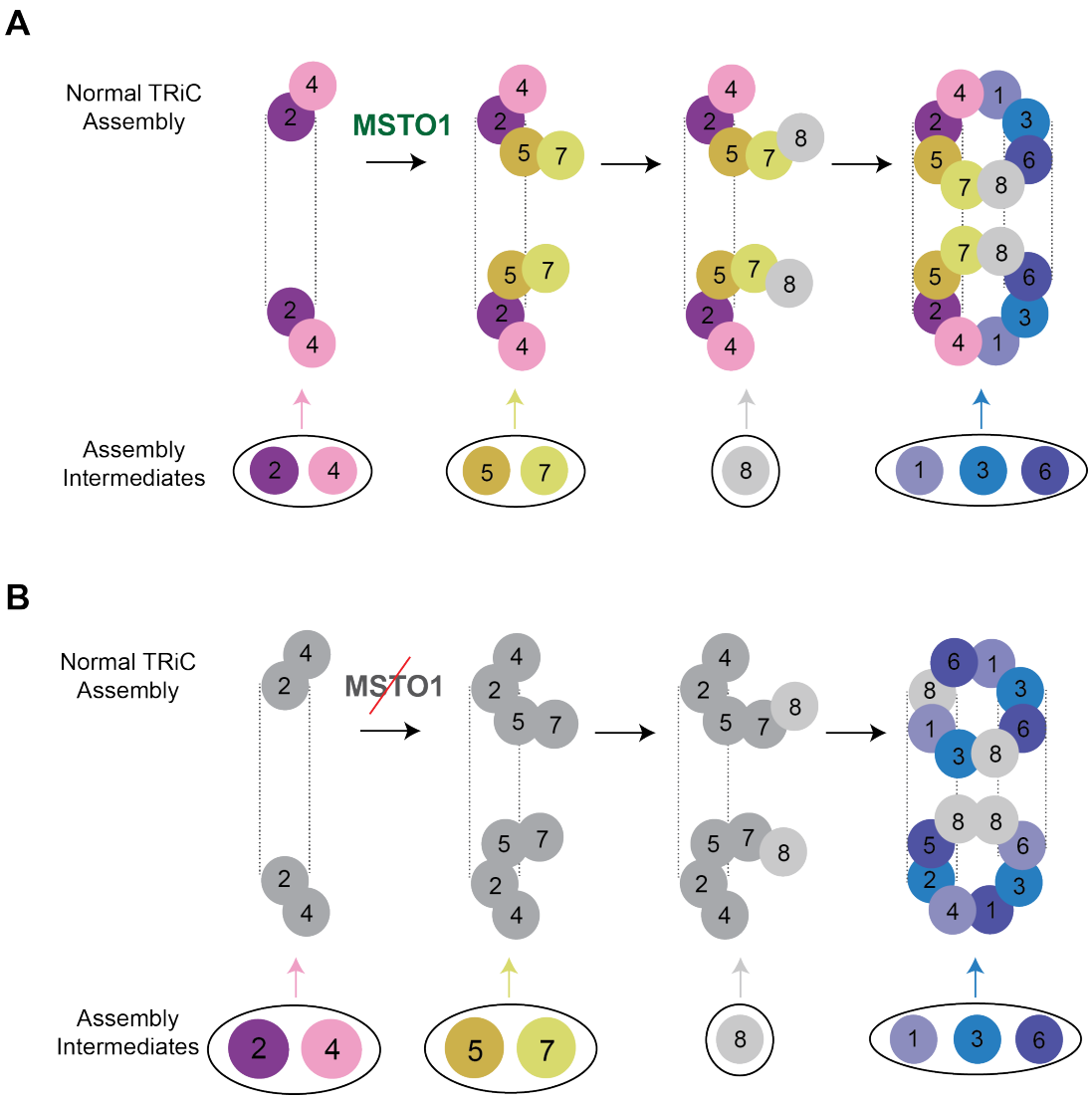

Figure 2.6. Working model for MSTO1-assisted TRiC assembly. (A) MSTO1 brings together CCT2-CCT4 and CCT5-CCT7 assembly intermediates to begin the assembly of each TRiC ring. **(B)** In the absence of MSTO1, CCT2-CCT4 and CCT5-CCT7 assembly intermediates do not assemble into the larger TRiC complex but instead accumulate as assembly intermediates. This potentially leads to formation of aberrant TRiC complexes lacking CCT2, CCT4, CCT5, and CCT7 that are degraded.

2.5. Materials and Methods

2.5.1. Cell Culture

HCT116 cells were cultured in McCoy's 5A medium supplemented with 10% FBS (Seradigm), 2 mM L-glutamine, at 37°C with 5% CO_2. For inducing the degradation of MSTO1-FLAG-mAID, 5-Ph-IAA (Cayman Chemical, 38161) was added to the culture medium at 20 μM. MSTO1 patient cells from the Cell line and DNA bank of Genetic Movement Disorders and Mitochondrial Diseases (GMD-MDbank).

MSTO1 patient cells were grown in DMEM supplemented with 20% FBS (Seradigm) and Glutamax (Invitrogen).

2.5.2. Cell Line Generation

The original HCT116 cell line was obtained from Jodi Nunnari, University of California Davis. To generate OsTir1(F74G) stably expressing cell lines HCT116 cells were transfected with SpCas9-2A-GFP (#79888; Addgene) and the pAAVS1-puro (#80490; Addgene) encoding OsTRI1(F74G)-V5 and the puromycin resistance gene flanked by homology sequence targeting the AAVS1 safe harbor locus using JetPrime Polyplus (VWR Scientific). Cells were incubated in transfection reagents for 48 hrs and then grown for six days in normal media before selection in the presence of Puromycin (1 mg/mL) for 72 hours. Clonal populations were generated by plating cells at very low density, and clones were collected onto sterile filter paper dots soaked in trypsin. In clonal populations, the biallelic insertion of OsTir1(F74G) was confirmed by genomic PCR and the expression of OsTir1(F74G)-V5 was confirmed by Western blotting. This clonal population was used to modify the endogenous MSTO1 gene. An optimal gRNA target sequence closes to the genomic target site was chosen using CHOPCHOP and validated with Synthego CRISPR Design Tool. Individual gRNAs targeting the C-terminus of MSTO1 were cloned into SpCas9-2A-GFP. For knock-in of FLAG-AID, gBlock designs were ordered from IDT that included a homology arm corresponding to the 3-prime end of the MSTO1 coding sequence, the FLAG-AID sequence, the blasticidin resistance coding sequence, and a homology arm corresponding to the beginning of the 3-prime UTR of the MSTO1 gene. These plasmids were transfected into the OsTir1(F74G)-V5 clonal population using JetPrime PolyPlus. Cells were incubated with the transfection reagent for ~48 hrs, grown in normal media for six days and then subject to selection with blasticidin (10 mg/mL) for ~72 hrs. Clonal populations were generated by plating cells at very low density and clones were collected onto sterile filter paper dots soaked in trypsin. Clones were evaluated for the biallelic insertion by genomic PCR. Subsequently, the expression of the MSTO1-FLAG-mAID protein was confirmed by western blotting.

2.5.3. SDS-PAGE, Western Blot analysis, and quantification

Cells were grown to 40 to 80% confluency, and were washed with PBS (Thermo Fisher Scientific, 20012050) before lysis with radioimmunoprecipitation assay (RIPA) buffer (25 mm Tris (pH 7.4)[Millipore Sigma], 150 mm NaCl [Fisher S2711], 1% NP-40 [Thomas Scientific 492018-50ML], 1% sodium

deoxycholate [Thermo Scientific FER89904], 0.1% SDS [Fisher Scientific BP166100], 1× Halt protease inhibitor mixture [Thermo Scientific 78439]. Samples were incubated on ice for 15 min and then spun at 21,000 × *g* for 15 min at 4°C. Supernatant was transferred to a clean tube, and protein concentration was measured by BCA assay (Thermo Scientific). Following separation of 7.5 mg of whole cell lysate [or 25 mg to detect MSTO1] by SDS–PAGE, proteins were transferred to methanol activated Polyvinylidene Fluoride (PVDF) membranes. Membranes were washed in H_2O for 10 min and then incubated in PVDF 1x TotalStain Q staining solution (#AC227; AzureBiosysetms). After decanting the staining solution, the membrane was washed in 1x TotalStain Q Wash Buffer three times for 3 minutes per wash, then visualized in the Cy3 channel. Membranes were then incubated with 4% w/v milk in tris-buffered saline (TBS) with 1% (v/v) Tween 20 (Fisher Scientific BP337-100) at room temperature for 1 to 4 hours. The indicated proteins were detected using primary rabbit or mouse antibodies incubated in 4% milk in TBST overnight at 4°C and visualized with appropriate secondary antibodies conjugated to IRDye also incubated with 4% milk in TBST for 30 minutes at room temperature (Thermo Fisher Scientific). Quantification was performed with Azure Analysis software (Azure Biosystems) and fold change calculated relative to TotalQStain (Azure Biosystems) for all figures except Figure 2.3 D where GAPDH was used. The data were analyzed using Welch's unpaired T-test. The following antibodies were used in this study: mouse monoclonal anti-FLAG (Sigma; 1:1000); rabbit polyclonal anti-TCP1 (ThermoFisher PA5-80100; 1:1000); mouse monoclonal anti-tubulin (ThermoFisher Scientific clone DM1A; 1:5000); mouse monoclonal anti-B-tubulin (ThermoFisher Scientific 32-2600; 1:1000); mouse monoclonal anti-gamma-tubulin (ThermoFisher Scientific MA1-850-A555; 1:1000); rabbit polyclonal anti-B-Actin (Cell Signaling 4967S; 1:1000); rabbit monoclonal anti-GAPDH (Cell Signaling (14C10); 1:500); mouse monoclonal anti-V5 (ThermoFisher R960-25; 1:1000); mouse monoclonal anti-Mfn2 (Sigma clone 4H8; 1:1000); and rabbit polyclonal anti-Mfn1 (gift from Jodi Nunnari, University of California, Davis; 1:500). Briefly, Mfn1 antiserum was raised against His6-tagged fusion proteins comprised of full-length mouse dihydrofolate reductase and an internal region of Mfn1 (residues 350–580). Fusion proteins were purified on nickel nitrilotriacetic acid columns (Thermo Fisher Scientific) in 8 M urea and eluted with 0.1% SDS and 10 mM Tris-Cl, pH 7.4. 7.5 ug whole cell lysates for changes in TCP1, tubulin, and Actin. 25 ug to see changes in MSTO1-FLAG.

2.5.4. Microscopy

All cells were plated in no. 1.5 glass-bottomed dishes (MatTek) treated with 10 mg/mL fibronectin for 4 – 24 hrs at 37°C. HCT116 cells were incubated with 0.1 µg/ml Mitotracker Red CMX Ros, 1 µL/mL of picogreen, and 2 drops of NucBlue (Molecular Probes) for 10 min at 37°C with 5% CO_2, then washed and incubated with complete media pre-incubated at 37°C with 5% CO_2 for at least 4 hours before imaging. A Z-series with a step size of 0.3 µm was collected with a Nikon Ti2E confocal microscope with a 60 × NA (numerical aperture) 1.4 oil objective (Nikon), a cicero spinning disk, a 5-channel Celesta light source (Nikon), and an sCMOS camera (Prime BSI Express). Each cell line was imaged on at least three separate occasions by a blinded experimenter (n > 100 cells per experiment).

2.5.5. Image analysis

Images were deconvolved using 15 iterations of 3D Landweber deconvolution. Deconvolved images were then analyzed using Nikon Elements software. Maximum intensity projections were created using Nikon Elements software and cropped in Fiji software (National Institutes of Health [NIH]). Mitochondrial morphology in mammalian cells was scored as follows: reticular indicates that fewer than 30% of the mitochondria in the cell were fragments (fragments defined as mitochondria less than or equal to 2.5 µm in length); short indicates mitochondria that were between 2.5 and 5 µm in length; fragmented indicates that most of the mitochondria in the cell were less than or equal to 2.5 µm in length. All quantifications were performed by a blinded experimenter. Data was analyzed using ordinary two-way Anova with multiple comparisons.

2.5.6. Coimmunoprecipitation

Whole-cell lysates were prepared from HCT116 cells expressing MSTO1-FLAG-AID or mcherry-FLAG by incubating in lysis buffer (50 mM HEPES-KOH, pH 6.8, 300 mM NaCl, 1 mM $MgCl_2$, 10% glycerol) with 0.5% NP-40 (MilliporeSigma) and 1× Halt Protease Inhibitor (Thermo Fisher Scientific) on a rocker at 4°C for 1 hour. Lysates were cleared at 21,000 × g for 30 min at 4°C and supernatant was transferred to a new tube. When testing for coimmunoprecipitation of A-tubulin or B-actin with MSTO1-FLAG, supernatant was incubated with 5 mM Latrunculin B for 1 hour at 30°C. Supernatant was incubated with 50 µl magnetic mMACS anti-DYKDDDDK microbeads (Miltenyi Biotec) for 4 hours on a rocker at 4°C. The sample was applied to a MACS column (Miltenyi Biotec) and washed twice with lysis

buffer and four times with wash buffer (50 mM HEPES-KOH, pH 6.8, 300 mM NaCl, 1 mM $MgCl_2$, 10% glycerol, 0.1% NP-40 (MilliporeSigma) and 1× Halt Protease Inhibitor). One column volume (25 µl) elution buffer 50 mM HEPES-KOH, pH 6.8, 300 mM NaCl, 1 mM $MgCl_2$, 10% glycerol, 0.1% NP-40 (MilliporeSigma), 6M urea, and 1× Halt Protease Inhibitor) was added and incubated for 15 min at room temperature, then proteins were eluted twice with 50 µl elution buffer. Most protein eluted in the first 50 µl elution. Samples were run on an SDS–PAGE gel and transferred onto PVDF membranes. Membranes were blocked with 4% milk in TBST for at least 45 min and were incubated with the indicated primary antibody at 4°C overnight - anti-Mfn2, anti-Mfn1, anti-FLAG, anti-TCP1, anti-A-tubulin, anti-B-Actin, anti-CCT2 (Abcam, ab92746, 1:1000), anti-CCT3 (Santa Cruz Biotechnology, sc-271336, 1:100), anti-CCT7 (Santa Cruz Biotechnology, sc-271951, 1:143), and anti-GAPDH (Cell Signaling (14C10); 1:500). The next day membranes were incubated with DyLight secondary antibody (Invitrogen) for ~ 40 min at room temperature; anti-CCT3 and anti-CCT7 membranes were incubated with horseradish peroxidase linked secondary antibody (Cell Signaling Technology) for 40 min at room temperature. Membranes were imaged on Azure Biosystems Sapphire Imager (Azure Biosystems).

2.5.7. Genomic DNA qPCR

Total genomic DNA (gDNA) (nuclear and mitochondrial DNA) was extracted from unedited HCT116 and MSTO1-FLAG-AID cells treated with either DMSO or 20 mM 5-Ph-IAA using the DNeasy Blood and Tissue Kits for DNA Isolation (Qiagen, 69504) according to manufacturer's instructions. Relative mtDNA copy number was analyzed by real-time quantitative PCR (qPCR) using the QuantStudio 6 Flex Real-Time PCR system (Thermo Fisher Scientific). Primer sequences specific to mtDNA and the nuclear-encoded housekeeping gene GAPDH were used (see Primer Table).

QPCR reactions were prepared to a total of 5 uL per reaction containing 8 uL PowerUp SYBR Green Master Mix (Thermo Fisher Scientific, A25742), 100 ng gDNA and 250 nM each forward and reverse primers. MtDNA copy number relative to GAPDH was analyzed using the delta delta Ct ($\Delta\Delta$Ct) method and is represented as fold change of control. Relative mtDNA copy number is presented as mean ± SD from at least three independent biological replicates and 2-way ANOVA with multiple comparisons were used to determine statistical significance. *Cytb:* 5' TCTCCGATCCGTCCCTAACA 3' and 5' TGATTGGCTTAGTGGGCGAA 3'. Homo sapiens Mitochondrial gene: 5' ACA CCC TCC TAG CCT TAC

TAC 3’ and 5’ GAT ATA GGG TCG AAG CCG C 3’. *MT-ND1*: 5’ TACGGGCTACTACAACCCTTC 3’ and 5’ ATGGTAGATGTGGCGGGTTT 3’. *GAPDH*: 5’ GGCATTGCCCTCAACGACC 3’and 5’ AAAGAGTTGTCAGGGCCCTTTTTC 3’.

2.5.8. shTCP1

shRNA target sequences were obtained using the RNAi Consortium (TRC; Broad Institute). The sequences of TCP1 short hairpin RNA (shRNA) were as follows: TCP1-shRNA/F: 5’ CCGGGGTGTACAGGTGGTCATTATTCAAGAGATAATGACCACCTGTACACCTTTTTTG 3’; and TCP1-shRNA/R: 5’ AATTCAAAAAAGGTGTACAGGTGGTCATTATCTCTTGAATAATGACCACCTGTACACC 3’. Each TCP1 shRNA and the RFP shRNA control were inserted into the pKLO.1 lentiviral vector. HEK293T cells (Cell Biolabs) were maintained in DMEM complete media supplemented and plated at ~80% confluency the day before transfection. HEK293T cells were transfected with pKLO.1 lentiviral vector expressing CCT shRNA or RFP shRNA using FuGENE HD (Promega). Viral supernatants were collected 48 hrs post transfection and frozen in -80 C overnight. Viral supernatants were incubated with HCT116 and HCT116 + MSTO1-FLAG-AID cells in the presence of 8 mg/mL polybrene. Approximately 48 hrs after viral transduction, HCT116 and HCT116 + MSTO1-FLAG-AID cells were split, and 1 µg/ml of neomycin selection was added for 4-5 days. Cells were either seeded onto no. 1.5 glass-bottomed dishes (MatTek) coated with 10 µg/ml fibronectin (Sigma-Aldrich) for imaging 3 days later or one well of a six-well dish for whole cell lysate preparation 3 days later (described above).

2.5.9. BN-PAGE

Either untreated HCT116-WT or MSTO1-AID-FLAG cells treated with DMSO or auxin were lysed in 0.5% NP-40 (MilliporeSigma), 25 mM HEPES pH 7.5, 150 mM KCl, 10% glycerol, 1.5 mM $MgCl_2$, 1 mM DTT, 1× Halt Protease Inhibitor (Thermo Fisher Scientific) for 10 min in 4°C. Lysates were centrifuged at 19,0000 × *g* at 4°C for 10 min. The cleared lysate was mixed with Invitrogen NativePAGE 5% G-250 sample additive to a final concentration of 0.25%. Samples were separated on a Novex NativePAGE 4–16% Bis-Tris Protein Gels (Invitrogen) at 4°C. Gels were run at 40 V for 30 min and then 100 V for 30 min with dark cathode buffer (1× NativePAGE Running Buffer [Invitrogen], 0.02% [wt/vol] Coomassie G-250). Dark cathode buffer was replaced with light cathode buffer (1× NativePAGE Running Buffer [Invitrogen], 0.002% [wt/vol] Coomassie G-250) and the gel was run at 250 V for 60–75 min until the dye front ran off

the gel. After electrophoresis was complete, gels were transferred to polyvinylidene fluoride membrane (PVDF) (Bio-Rad Laboratories) at 30 V for 16 h in transfer buffer (25 mM Tris, 192 mM glycine, 20% methanol). Membranes were subsequently incubated with 8% acetic acid for 15 min and washed with dH_2O for 5 min. Membranes were dried at 25°C for 60 min and then rehydrated in 100% methanol and washed in dH_2O. Membranes were blocked with 4% milk in TBST for 20 min at room temperature and were incubated with anti-FLAG, anti-TCP1, anti-CCT2, anti-CCT3, and anti-CCT7 in 4% milk/TBST for 4 hr at room temperature or overnight at 4°C. Membranes were incubated with horseradish peroxidase linked secondary antibody in 4% milk/TBST (Cell Signaling Technology) at room temperature for 1 hr. Membranes were developed in SuperSignal Femto ECL reagent (Thermo Fisher Scientific) for 5 min and imaged on Azure Biosystems Sapphire Imager (Azure Biosystems). NativeMark Unstained Protein Standard (Life Technologies) was used to estimate molecular weights of TRiC and MSTO1 protein complexes.

Chapter 3. More pieces to the MSTO1 puzzle

Very little was known about MSTO1 before I embarked on the challenge of uncovering the function of MSTO1. This chapter includes things we learned along the way, pieces of information that we still don't fully understand, and details about experiments that could be helpful during future studies of MSTO1.

3.1. Creating MSTO1 loss-of-function cell lines

In mice, heterozygous knockouts of *MSTO1* are sufficient to cause severe developmental defects, while homozygous knockouts cause late embryonic lethality, suggesting MSTO1 has potent dosage effects during mouse development. In MSTO1 patients, MSTO1 protein levels are almost undetectable but not completely depleted (Donkervoort *et al.*, 2019). Based on the differences between homozygous and heterozygous *MSTO1* knockouts in mice, the small amount of MSTO1 remaining in patients may be important for preventing the embryonic lethality observed in homozygous *MSTO1* knockouts.

3.1.1. MSTO1 knockdown cells

Since MSTO1 protein expression is almost undetectable in MSTO1 patients, we hypothesized

that knocking down MSTO1 in a cell model would be sufficient to recreate cellular phenotypes mimicking disease. We first attempted to reduce MSTO1 protein levels by expression of short hairpin RNA (shRNA) targeting MSTO1 transcripts in wild type mouse embryonic fibroblasts (MEFs) cells using two different shRNA targeting sequences (MSTO1-321 and MSTO1-996) expressed from a lentiviral vector. All cells treated with lentivirus-containing media between 50 and 200 µL survived puromycin selection, consistent with successful viral transduction. Due to the poor commercially available MSTO1 antibodies, endogenous MSTO1 was undetectable in MEFs, and therefore, the knockdown could not be confirmed. Both GeneTex (GTX105110) and Proteintech (28400-1-AP) MSTO1 antibodies were tested at different concentrations, but the antibodies either did not detect anything or bound numerous off-target bands, making it difficult to identify an MSTO1 band.

3.1.2. MSTO1 CRISPR-Cas9 Knockouts

I aimed to build *MSTO1* null cell lines harboring insertions/deletions (indels) that result in frameshift mutations using *MSTO1* Exon 2 or Exon 11 targeted CRISPR-Cas9 gRNAs. Our first cell line of choice was U2OS cells human osteosarcoma cells, as they are amenable to both biochemical and cell biology approaches. U2OS were transfected via nucleofection, a transfection method that uses electrical pulses to transfer DNA directly into the nucleus. Transfected cells were then selected for CRISPR-Cas9 expression by puromycin resistance for 48 hours. Cells were then plated at low density for clonal expansion in 15 cm plates with 50% conditioned media and 20% fetal bovine serum. Isolates from the clonal expansion were screened via TOPO-TA cloning of PCR products amplified from gDNA to identify indels by sequence analysis. We found 6 heterozygous indels in 75 isolates screened, and no clonal population with mutations in both alleles. Consistent with the fact that all patients have bi-allelic mutations, the heterozygous *MSTO1* indel cell lines did not possess a mitochondrial fusion or mtDNA maintenance defect. The inability to obtain homozygous knockouts of *MSTO1* suggests that MSTO1 may be an essential gene. We did not realize at the time of that work was that the human genome contains *MSTO2P*, an *MSTO1* pseudogene (see section 1.5.1). *MSTO2P* is 99% identical to *MSTO1*. Consequently, the CRISPR Cas9 gRNA sequences used to target *MSTO1* also targeted *MSTO2P,* most likely leading to pairs of double-stranded breaks and cell death. In the future, MSTO1 knockout cells must be done in non-human cells or using different technical approaches.

3.1.3 *Xenopus tropicalis* knockdown of MSTO1

To determine if *MSTO1* is an essential gene, we aimed to knockdown MSTO1 in a model organism. In collaboration with Andrea Wills, we knocked down MSTO1 in *Xenopus tropicalis* embryos. *Xenopus tropicalis* are ideal due to its rapid development, well-characterized early development pathways, a reliable developmental cell fate map, and rapid gain- and loss-of-function assays that can be conducted in specific tissues. To knockdown MSTO1, Morpholino oligonucleotides were ordered from Gene Tools to target MSTO1 mRNA and decrease translation. Morpholino oligo (MO) knockdown is robust in *Xenopus tropicalis* with minimal off-target effects (Paraiso *et al.*, 2019). 2-cell stage *Xenopus tropicalis* embryos were injected with increasing amounts of morpholino oligos targeting MSTO1 in each cell, with 1.25, 2.5, 5.0, and 10 ng of MO per embryo. We first sought to determine if depletion of *Xenopus tropicalis* MSTO1 would result in cell division defects, as reported in *Drosophila*. To do this, embryos were monitored between the maternal to zygotic transition (MTZ) (stage 8) and gastrulation (stage 10-12.5). The MTZ occurs about 4-5 hours after fertilization, when most maternal proteins have turned over and been replaced by proteins translated from the zygote genome. Therefore, embryos injected with MSTO1 MOs would be depleted of MSTO1 between 4 and 5-hours post-fertilization. Following the MTZ, if depletion of MSTO1 leads to cell division defects, then embryos would either stop dividing or present with evidence of incomplete cell division. At all doses, MSTO1-MO-injected embryos did not display cell division defects before gastrulation, suggesting the loss of MSTO1 does not inhibit cell division in *Xenopus tropicalis*.

Despite the absence of cell division defects, we found that MSTO1 knockdown embryos developed developmental defects consistent with MSTO1 patient phenotypes. After 2 days, the embryos have developed into actively swimming tadpoles with developed gills, tail fins, and functional pigmentation. MSTO1 knockdown tadpoles presented with dose-dependent defects in body length, tail, and mobility (Figure 3.1). With as little as 1.25 ng of MSTO1 morpholino, 40% of tadpoles displayed twitching movements that inhibited swimming. This progressed to the point where almost all tadpoles injected with 10 ng of MSTO1 MOs had little or no response when gently tapped with a pipette tip (Figure 3.1 A). The movement defect is notable, resembling the phenotypes of MSTO1 patients who present with ataxia and lack of voluntary muscle coordination. MSTO1-MO-injected tadpoles also had decreased body

length when measured in a straight line from head to end of the tail (Figure 3.1 D). This is most likely a result of tadpole tail defects, where the tail was curved back towards the head, shortening the overall body length (Figure 3.1 B-C). Overall, these results suggest MSTO1 plays a role in development in *Xenopus tropicalis*.

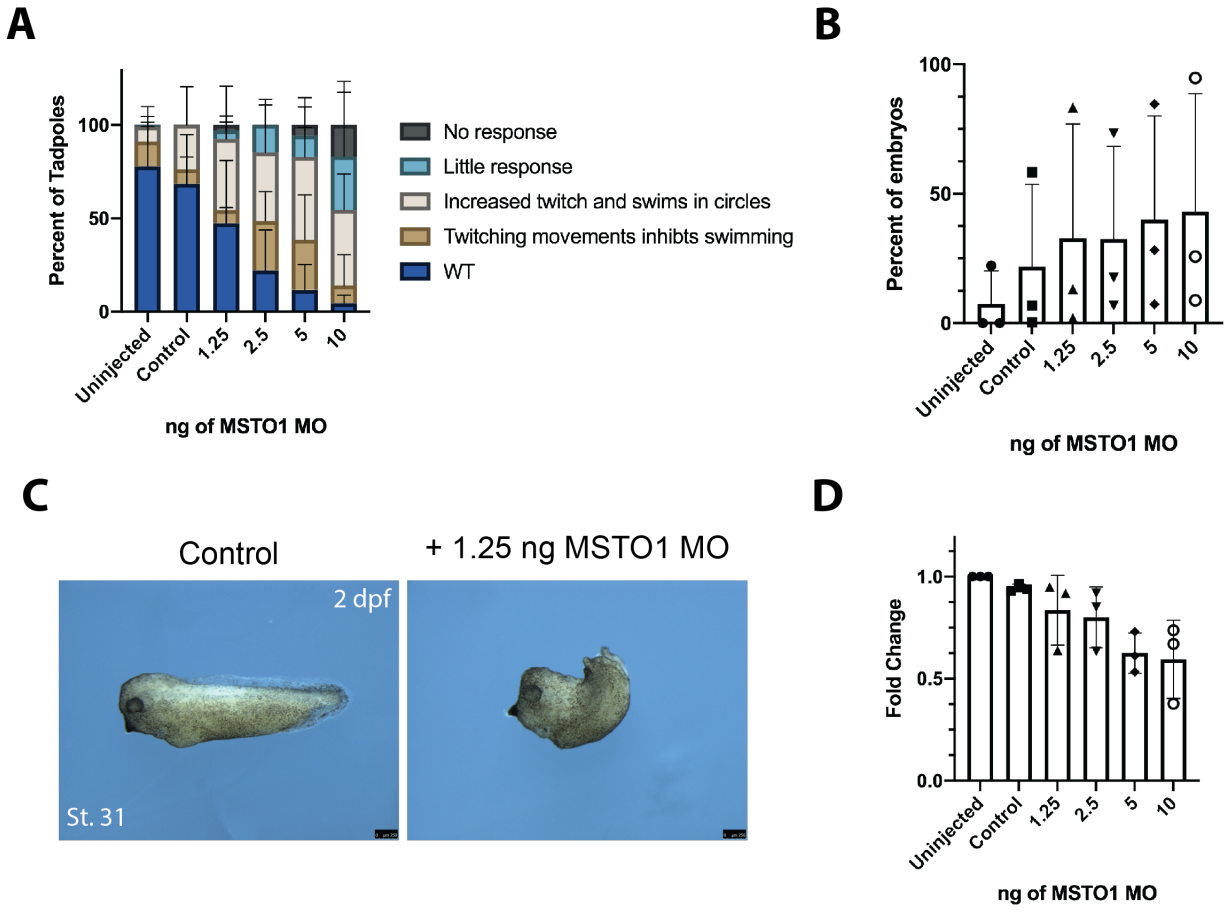

Figure 3.1. MSTO1 knockdown in *Xenopus tropicalis* pilot experiment. (A) Quantification of motor control and movement of MSTO1 MO injected tadpoles at 48 hours post fertilization. The graph shows mean and standard deviation from 3 independent experiments. **(B)** Quantification of percent of tadpole with tail defects. The graph shows mean and standard deviation from 3 independent experiments. **(C)** Representative images of MSTO1 MO injected tadpoles. All were visualized by light field microscopy. **(D)** Average fold change of MSTO1 MO injected tadpole tail length. The graph shows mean and standard deviation from 3 independent experiments.

3.2. MSTO1-V8M

All MSTO1 patients to date have bi-allelic *MSTO1* variants and almost undetectable levels of MSTO1, clearly implicating loss of MSTO1 function in disease. However, a dominant-negative variant was reported in an MSTO1 patient in 2017. In this variant, an amino acid in the N-terminus of MSTO1 was

putatively changed from valine to methionine (V8M) (Gal *et al.*, 2017). This putative dominant-negative variant provided an opportunity to build cells overexpressing MSTO1-V8M to gain insight into the molecular functions of MSTO1. Therefore, I began building these cells in parallel with my efforts to create MSTO1-null alleles. In 2023, Gerber et al. found 16 patients who initially appeared to have MSTO1-V8M variants. However, but after reevaluating the primers used for DNA sequencing, they found the primers were amplifying both *MSTO1* and *MSTO2P*. After amplifying *MSTO1* and *MSTO2P* in individual patients using specific primers, they found that their patients had a mutation in *MSTO2P,* not *MSTO1* (Gerber *et al.*, 2023). Following the publication of this article, Gal et al. used the same specific primers and confirmed that the MSTO1-V8M mutation was actually in the *MSTO2P* gene (Gál *et al.*, 2023b). The work implicating MSTO1-V8M in disease has since been retracted. However, it is not known why patients with *MSTO2P* mutations present with disease phenotypes similar to MSTO1 patients, especially since *MSTO2P* is predicted to be a lncRNA that does not encode protein.

Despite MSTO1-V8M not being a bona fide dominant-negative variant, cells expressing MSTO1-V8M possessed mitochondrial phenotypes (Figure 3.2 C-D). To create these cells, wild type MEFs were transduced with retroviral particles encoding MSTO1-WT or MSTO1-V8M with a C-terminal FLAG tag. Cells expressing MSTO1 were selected with puromycin and plated at low density for clonal expansion. Clonal populations were screened for MSTO1-FLAG expression by western blot analysis, probing for the FLAG tag. Cells expressing low, medium, and high levels of MSTO1-V8M or MSTO1-WT were selected for further analysis (Figure 3.2 A-B). Mitochondria and mtDNA were visualized by live-cell imaging using mitotracker Red (Figure 3.2 C) and pico green (not shown), respectively. Low and medium-expressing MSTO1-WT cells had more cells with reticular and hyperfused mitochondria than wild type controls, suggesting that overexpression of MSTO1 leads to increased mitochondrial fusion (Figure 3.2 D). Interestingly, cells expressing high levels of MSTO1-WT exhibited a mix of reticular and fragmented mitochondria, suggesting that excessive MSTO1 might induce mitochondrial stress. In cells with all levels of MSTO1-V8M expression, the mitochondria were short and fragmented compared to wild type controls, suggesting MSTO1-V8M is a gain-of-function mutation. No obvious changes in mtDNA number or distribution were observed. It is unclear how MSTO1-V8M is disrupting mitochondrial fusion. My research suggests the loss of TRiC in MSTO1-depleted cells may drive mitochondrial changes; therefore, MSTO1-

V8M may disrupt the normal MSTO1-TRiC relationship. Additionally, no obvious changes in mtDNA number or distribution were observed.

Interestingly, some MSTO1-V8M cells also appeared to have plasma membrane blebbing, which was almost absent in WT and MSTO1-WT controls. Blebbing is the formation of irregular bulges in the plasma membrane that often occur when the plasma membrane detaches from the cytoskeleton. This can occur during apoptosis, cell division, cell migration, and as a response to stress. All three MSTO1-V8M isolates with similar expression levels had between 20 and 40% of cells with blebbing (Figure 3.2 E). This suggests that cells expressing MSTO1-V8M may have an increase in cellular stress and/or changes in the cytoskeleton. It is important to note that the blebbing was observed due to the off-target effects of mitotracker which often faintly marks entire MEF cells. To confirm that blebbing is occurring, cells would need to be stained with plasma membrane and cytoskeleton markers.

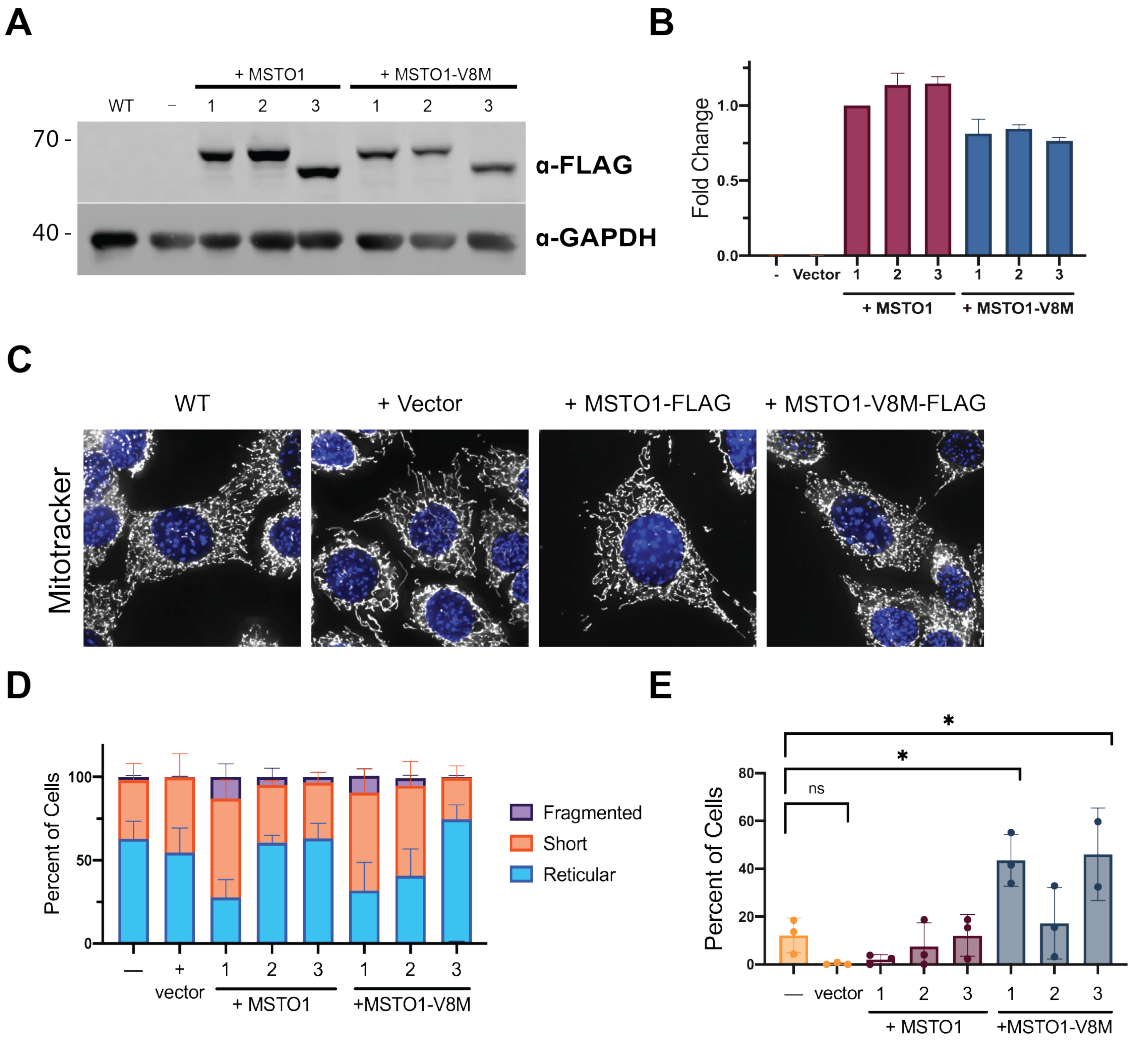

Figure 3.2. MSTO1-V8M cells have short mitochondria and a blebbing phenotype. (A) Whole cell lysates prepared from wild type, vector, MSTO1-FLAG, and MSTO1-V8M-FLAG cell lines subject to SDS-PAGE and immunoblotting with anti-FLAG and anti-GAPDH. **(B)** Quantification of Western blot from (A) Average fold change of protein expression relative to WT HCT116 cells from three independent experiments are shown. **(C)** Representative live cell images of wild type, vector, MSTO1-FLAG, and MSTO1-V8M-FLAG. Mitochondria were labeled with Mitotracker Red CMXRos and and nuclei were labeled with NucBlue. All were visualized by fluorescence microscopy. **(D)** Quantification of mitochondrial morphology for cell lines described in (C). The graph shows the mean and standard deviation from 3 independent experiments. **(E)** Quantification of blebbing phenotype in wild type, vector, MSTO1-FLAG, and MSTO1-V8M-FLAG cell lines. The graph shows mean and standard deviation from 3 independent experiments ns: not significant, *P<0.05, ordinary one-way Anova with multiple comparisons.

3.3. Cytoskeleton Dynamics

MSTO1-AID cells depleted of MSTO1 have reduced TCP1 and short mitochondria but no changes in tubulin steady-state protein levels. MSTO1-depleted cells also have no obvious changes in the microtubule and actin network when visualized using immunofluorescence for α-tubulin and phalloidin. We hypothesized that even though the microtubule network was unaltered at steady-state, MSTO1-depleted cells could have altered microtubule assembly or disassembly. To test microtubule assembly in MSTO1-depleted cells, MSTO1-AID cells were treated with either DMSO or auxin for 3 days and then treated with nocodazole for 75 minutes to completely depolymerize the microtubule network. After nocodazole treatment, cells were rinsed twice with McCoys media and then incubated at 37°C in fresh McCoys media for 0, 1.5, 2.5, 5, 7.5, and 10 minutes. Immediately after incubation, cells were fixed with 4% paraformaldehyde and microtubules were visualized by immunofluorescence using α-tubulin antibody. The Microtubule Organizing Center (MTOC) is present in some cells at the earliest time point, and by 2.5 minutes, microtubule regrowth is rapidly occurring, with the entire network almost reestablished by the final time point. The results from this experiment were inconsistent. Compared to DMSO-treated controls, MSTO1-depleted cells regrew the microtubule network both faster and slower in different biological replicates (data not shown). This may have been due to the toxicity of a long-term nocodazole treatment, which can affect more than just microtubules. In future experiments, ice treatments may be an effective way to depolymerize microtubules with fewer off-target effects. Microtubule dynamics could also be tracked via expression of the End Binding protein 1 (EB1) tagged with a GFP. EB1 is a plus-end microtubule protein that localizes to growing tip microtubules. Previous studies have tracked microtubule polymerization and depolymerization in cells expressing EB1-GFP using live cell imaging (Drum *et al.*, 2016).

3.4. Assessing MSTO1 cellular localization with MSTO1-NeonGreen cell lines

Endogenous MSTO1 has never been visualized in cells. Information regarding MSTO1 localization comes from overexpression systems where MSTO1 is tagged with a fluorescent marker and transiently expressed in HeLa cells. Overexpressed MSTO1 localizes to the cytoplasm, but it is not diffuse; it dots the cytoplasm. We aimed to build cells endogenously expressing a NeonGreen fluorescent marker at the C terminus of *MSTO1* to detect MSTO1 localization and whether it changes under different physiological and developmental contexts. We used CRISPR-Cas9 to engineer HCT116 cells expressing MSTO1-mNeonGreen-FLAG-AID. Expression of MSTO1-mNeonGreen in a mixed population was confirmed by Western blot analysis. Live cell imaging of mixed populations of MSTO1-mNeonGreen revealed some cells with very faint signal that could not be distinguished from background noise (data not shown). Therefore, we were unable to visualize endogenous MSTO1 with conventional approaches. In the future, we propose using a SNAP-tag, which is brighter and more photostable than mNeonGreen.

3.5. MSTO1 interacts with actin but not tubulin

When I first saw our co-immunoprecipitation data suggesting that MSTO1 interacts with only about 4 percent of TRiC, I wondered whether MSTO1 was interacting with TRiC only while it is folding specific substrates. Cochaperones of TRiC, like prefoldin, phosducin-like proteins (PhLPs), and PDCD5, only interact with TRiC to facilitate the folding of specific substrates. Some TRiC cochaperones are found in the chamber with the substrate, like phosducin-like proteins (PhLPs) and PDCD5, when actin is folded, while prefoldin brings many different nascent polypeptides from the ribosome to TRiC for folding (Kelly *et al.*, 2022; Xing *et al.*, 2025). I hypothesized that MSTO1 might be interacting with other TRiC substrates. To test this, I performed a co-immunoprecipitation on full cell lysates treated with Latrunculin B from MSTO1-FLAG-AID or wild type HCT116 cells + mcherry-FLAG cells. We treated lysates with Latrunculin B to depolymerize actin and inhibit non-specific binding of actin filaments to the FLAG-coated beads. The latrunculin B treatment did not disrupt MSTO1-FLAG and CCT1 interactions. We found that MSTO1 interacts with β-Actin but not α-tubulin (Figure 3.3 A). Interestingly, the amount of β-Actin was significantly greater than that of the CCT1 pulled down, suggesting that the MSTO1-actin interaction is not in the TRiC

chamber. Instead, my data suggests MSTO1 is interacting with β-Actin, but whether this is facilitated by TRiC or another protein cannot be determined from this assay.

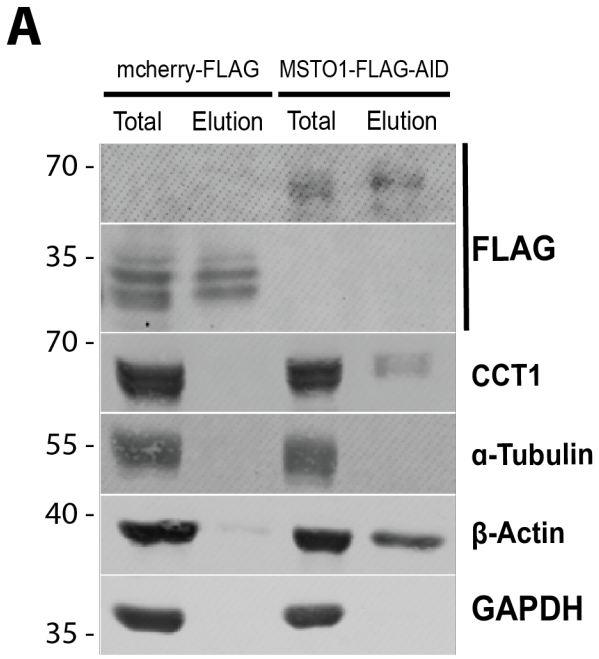

Figure 3.3. MSTO1 interacts with β-Actin but not α-tubulin. (A) Co-immunoprecipitation (Co-IP) pulling on mcherry-FLAG or MSTO1-FLAG-AID with FLAG-coated magnetic beads. Lysates prior to bead incubation treated with latrunculin B for 1 hr at 30C. Co-IP Total (0.66%) and Elution (6.6%) subject to SDS–PAGE and immunoblotting with anti-FLAG, anti-CCT1, anti- α-tubulin, anti-β-Actin, or anti-GADPH.

Chapter 4. Conclusions

In this dissertation, I have used biochemical and molecular biology techniques to establish MSTO1 as the link between TRiC and mitochondrial fusion. Before my studies, there was a lack of consensus in the literature describing MSTO1 function. Patient papers focused on mitochondrial fusion, while the *Drosophila* homolog was primarily implicated in stabilizing the TCP-1 chaperone (TRiC in humans). My work bridges the gap between the two fields, establishing that MSTO1 connects mitochondria and TRiC in humans.

4.1. MSTO1 is not a direct regulator of mitochondrial fusion

In this study, I used an auxin-inducible degradation (AID) system to determine the molecular consequences and their timing after MSTO1-depletion. I found that MSTO1-depletion led to a change in the mitochondrial network consistent with decreased fusion activity. After 6 days of auxin treatment MSTO1-FLAG-AID cells had shorter mitochondria than controls. I also found that MSTO1 does not interact with the mitochondrial outer membrane fusion machinery. The MSTO1 patient papers hinted that MSTO1 was a direct regulator of mitochondrial fusion implying Mfn1 and/or Mfn2 were the targets of this regulation; my results suggest this is not the case. Also, knockdown of either Mfn1 or Mfn2 by shRNA

results in fragmented mitochondria as early as 48 hours after viral transduction, suggesting that if MSTO1 were directly regulating fusion, I would have observed the effects before 6 days (Ding *et al.*, 2015; Yu *et al.*, 2021). Taken together, my data indicate that MSTO1 is not a direct regulator of mitochondrial fusion, despite MSTO1 patients presenting with a mitochondrial disease.

4.2. Absence of mtDNA depletion in MSTO1-depleted cells

The MSTO1-FLAG-AID cell lines did not recapitulate the mtDNA depletion phenotype observed in MSTO1 patients. MtDNA in MSTO1-FLAG-AID cells treated with auxin for 6 days had no change in mtDNA nucleoids or copy number when analyzed by imaging with picogreen and qPCR, respectively. MSTO1-FLAG-AID cells were also imaged for mtDNA as far out as 20 days on auxin, but changes in mtDNA were still not apparent. The absence of changes in mtDNA nucleoids or copy number in MSTO1-depleted cells may indicate that these cells do not recapitulate the physiological or developmental state that requires MSTO1 for mtDNA maintenance.

MSTO1 may be required to maintain mitochondrial DNA during development, as its depletion *in Xenopus tropicalis* causes dose-dependent neurological and motor defects consistent with ataxia. Ataxia is commonly caused by mtDNA depletion (El-Hattab and Scaglia, 2013; Nogueira *et al.*, 2014). In patients with ataxia, part of the brain called the cerebellum is impaired, inhibiting neuronal signals to the rest of the body, leading to a lack of voluntary muscle coordination (Radmard *et al.*, 2023). In *Xenopus tropicalis*, even the smallest dose of MSTO1 MO led to dose-dependent twitching phenotypes that inhibited proper swimming. At the highest dose of MSTO1 MO, some tadpoles lost the ability to respond to stimuli at all. Taken together, my data suggest MSTO1 may be important for mtDNA maintenance during development, but further investigation is required.

4.3. Novel relationship between TRiC and mitochondria

My research establishes that loss of TRiC occurs before mitochondrial morphology changes in MSTO1-depleted cells, suggesting the short mitochondrial phenotype may be a result of decreased TRiC rather than loss of MSTO1. Currently, there is no definitive connection between TRiC and mitochondria in the literature. My research is the first to suggest a link between TRiC and mitochondrial structure, but the exact molecular details are still not known.

4.3.1. MSTO1-depletion may alter TRiC substrates that alter mitochondrial dynamics

One possible link between TRiC and mitochondria is through TRiC substrates. The most obvious link between TRiC and mitochondrial dynamics would be through tubulin and actin, but neither tubulin nor actin protein levels nor their respective networks are altered in MSTO1-depleted cells. Tubulin and actin were most likely not affected in MSTO1-depleted cells since they are abundant in the cell and may outcompete less abundant proteins for occupancy in the limited amount of TRiC chaperone. Therefore, other less abundant proteins may be more heavily impacted by the loss of TRiC and these changes could affect mitochondria-related processes. TRiC folds proteins involved in a wide range of cellular processes, including transcription, translation, cell cycle, and autophagy; therefore, changes in TRiC could alter specific protein levels in any of these processes that potentially affect the mitochondrial network.

4.3.2. An outer mitochondrial membrane protein may be an TRiC substrate

The relationship between TRiC and the mitochondrion could also suggest that TRiC folds an outer mitochondrial membrane protein. Currently, no mitochondrial proteins have been identified as TRiC substrates. Most proteins in the mitochondria are encoded in the nuclear genome, translated in the cytoplasm, and then translocated and sorted into the right mitochondrial functional compartment. Mitochondrial proteins are not folded after translation to facilitate translocation across membranes via the mitochondrial import machinery. This implies that mitochondrial proteins do not require TRiC. This does not rule out the possibility that outer mitochondrial membrane proteins, which are not translocated across mitochondrial membrane, could require chaperones. These pathways of targeting are less well-defined, and it is not known if outer mitochondrial membrane proteins are fully folded before insertion into the membrane. Therefore, TRiC may assist in folding and or trafficking one or more outer mitochondrial membrane or peripherally associated proteins, which are altered after the loss of TRiC in MSTO1-depleted cells.

4.3.3. TRiC may have a novel mitochondrial-related function

TRiC may have a novel mitochondrial function. TRiC has been studied almost exclusively in its role as an obligate chaperone to complete the folding of tubulin and actin, but my data indicate that this does not explain the mitochondrial defect following loss of MSTO1. There have been hints in the literature that TRiC has functions outside of protein folding. For example, TRiC sequesters Gelsolin to protect it

from cleavage and, in a separate context, mediates mTORC1-dependent m6A methylation to impede autophagy (Cuéllar *et al.*, 2019, 2022; Ghozlan *et al.*, 2022). Therefore, it is formally possible that TRiC sequesters proteins required for mitochondrial function and this activity is compromised when MSTO1 is depleted**.**

4.4. MSTO1 is a novel TRiC assembly factor

I found that MSTO1 and TRiC protein levels are interdependent. Through co-immunoprecipitation and BN-PAGE, I also demonstrate that MSTO1 interacts with the fully assembled TRiC. This relationship between MSTO1 and TRiC is interesting, as baed on the OpenCell predictions and my MSTO1-FLAG-AID Co-IP, MSTO1 only interacts with about 4% of TRiC at one time. Using BN-PAGE to visualize TRiC assembly intermediate scaffolds in MSTO1-depleted cells, I found that the assembly scaffolds CCT2-CCT4 and CCT5-CCT7 accumulate in the absence of MSTO1, suggesting MSTO1 assists in early assembly of TRiC. This is consistent with Betancourt Moreira et al., which found that TRiC assembly is not thermodynamically favorable; therefore, other factors must be regulating assembly. Notably, depletion of TRiC through knockdown of individual CCT subunits leads to accumulation of CCT2–CCT4 and CCT5–CCT7 assembly intermediates. Since our data show that CCT1 knockdown also reduces MSTO1 levels, it is likely that depletion of other CCT subunits similarly lowers MSTO1 protein levels. Therefore, we speculate that MSTO1 promotes assembly of the CCT2-CCT4 and CCT5-CCT7 intermediate scaffolds into the fully assembled TRiC. In the absence of MSTO1, these intermediate scaffolds are either assembling too slow or cannot be assembled without MSTO1, leading to intermediate scaffold accumulation.

It is unclear how an assembly factor is affecting the relationship between TRiC and the mitochondria. An open question is how MSTO1 and TRiC are connected to mitochondrial function. MSTO1 localization has only been visualized in overexpression systems. In MSTO1-overexpressing HeLa cells, MSTO1 forms cytoplasmic puncta. Using selective detergents to permeabilize different cellular membranes, Gel et al. found that some MSTO1 remained on the mitochondria after all the cytoplasmic components were released from the cell. This paper concluded that MSTO1 interacts transiently with the mitochondrial outer membrane. While this was done in an overexpression system, it leaves open the possibility that MSTO1 may direct TRiC complex assembly specifically near the mitochondria.

Interestingly, my results suggest that MSTO1 only interacts with 4 percent of TRiC, yet more than 40% of TRiC is lost following MSTO1 depletion. MSTO1-depleted cells have residual levels of MSTO1 protein, therefore TRiC assembly may still be occurring in MSTO1-depleted cells but at a rate slower than TRiC degradation leading to the overall 40% decrease. Another possible explanation is TRiC assembly in MSTO1-depleted cells leads to the formation of aberrant off-pathway TRiC complexes which have been documented to occur when subunits are expressed at different levels. These aberrant TRiC complexes are often not fully functional leading to degradation which may explain the 40% overall decrease in TRiC abundance.

Chapter 5. Future Directions

5.1. Determining if MSTO1 regulates mtDNA in development

To determine whether MSTO1 is required for mtDNA maintenance during development, I would compare the effects of MSTO1 loss of function in *Xenopus tropicalis* using both MO knockdown and CRISPR-Cas9 knockout approaches. Whole-embryo MSTO1 loss-of-function experiments would first be performed to assess developmental phenotypes, with particular attention to stages between 1- and 2-days post-fertilization, when defects in motor behavior and tail size become apparent in my first exploratory study.

MSTO1 patients present with both ataxia and muscle myopathy. Ataxia is a neuronal phenotype that often leads to muscle weakness. However, it is unclear if the muscle weakness observed in patients is independent of ataxia. I observed similar phenotypes to MSTO1 patients when embryos were injected with MSTO1-MO, demonstrating that this would be a valuable model. To tease out which phenotypes are neuronal or muscular, I would use tissue-specific MSTO1-MO injections and MSTO1 CRISPR-mediated knockouts in neuronal or muscle lineages. I expect to observe neuronal defects, and my prediction is that these are caused by depletion of mtDNA, as seen in patients with mtDNA-depletion syndromes. It is also possible that we would observe defects in muscle development or tissue formation as this tissue has high ATP-demands. This could also correlate with mtDNA depletion but may result from other mitochondrial defects.

In both whole-embryo and tissue-specific loss-of-function experiments, I would also visualize mitochondria and mtDNA for imaging with fluorescence microscopy. *Xenopus tropicalis* tadpoles are

translucent at 3 days post-fertilization, providing an ideal system for live imaging of mtDNA nucleoids and mitochondrial morphology using picogreen and mitotracker, respectively. If MSTO1 is required for mtDNA maintenance during development, I would expect MSTO1-deficient embryos to have a decrease in mtDNA nucleoids number compared to controls and this may or may not be accompanied by a short mitochondrial phenotype.

5.2. Defining proteome changes in MSTO1-depleted cells

My data indicate that TRiC and mitochondria are connected but how is not known. I hypothesize that either loss of TRiC affects less abundant substrates that are involved in mitochondrial-related processes or TRiC folds an unidentified outer-mitochondrial membrane protein. To test both, I need to identify proteins with changing levels following MSTO1 depletion. Since TRiC folds about 10 percent of all cytosolic proteins, systematically choosing known TRiC substrates to test using Western blotting would be almost impossible. Therefore, I would compare the proteome of MSTO1-FLAG-AID cells treated with either auxin or vehicle for 6 days using mass spectrometry (MS). Volcano plots comparing the two experimental groups would allow identification of statistically significant differences between these populations and I would confirm the changes by Western blotting. I would then take the promising hits and assess if the hit is a substrate of TRiC. To do this, I would determine if a knockdown of TRiC leads to a decrease in protein levels of the hit. To determine if loss of the hit also leads to mitochondrial morphology changes, I would knockdown the hit and use live-cell imaging to visualize the mitochondria. Lastly, I would assess if the hits were interactors of MSTO1 using FLAG-coated beads to immunoprecipitated MSTO1-FLAG and western blotting to detect if the hit was pulled down with MSTO1.

MSTO1-depleted and shCCT1 cells behave differently in cell culture, even though both cells have a similar decrease in MSTO1 and CCT1. Cells with knockdowns of CCT1 are much more prone to cell death and are hard to grow in culture, while MSTO1-depleted cells can grow for weeks with minimal cell death, suggesting there may be differences in the proteomes of each cell line. To assess this, shRFP and shCCT1 cells will be analyzed by MS alongside MSTO1-depleted and vehicle controls.

5.3. Further characterizing MSTO1 as a TRiC assembly factor

My current work identifies MSTO1 as a TRiC assembly factor, but future studies are required to fully characterize this function of MSTO1. To validate that MSTO1 is interacting with the full TRiC

complex, I would use a BN-PAGE antibody shift assay. If MSTO1 is interacting with fully assembled TRiC, then the addition of the CCT1 or FLAG antibody should shift the molecular weight of both TRiC and MSTO1. If MSTO1 does not increase in molecular weight when the anti-CCT1 antibody is added, then I would conclude that MSTO1 is not interacting with fully assembled TRiC. If this is the case, MSTO1 could be interacting with another large complex. To determine what MSTO1 is interacting with, I would immunoprecipitated MSTO1-FLAG following treatment of cells with cross-linking agents and then use MS to identify MSTO1 interactors.

I discovered that MSTO1 is an assembly factor for TRiC, but the molecular mechanisms are still unclear. After 3 days of auxin treatment, MSTO1-depleted cells have a clear accumulation of CCT2 and CCT7 assembly intermediates. To determine when and how fast assembly intermediates begin to accumulate I would assess how early this accumulation occurs after MSTO1-depletion. To do this, I would use BN-PAGE to quantify TRiC assembly intermediate scaffolds in MSTO1-FLAG-AID cells treated with auxin at 8, 16, 24, 48, and 36 hours. I would also test later timepoints (3 and 6 days of auxin) to determine if the phenotype is consistent up until the time mitochondrial changes occur.

To determine if MSTO1 facilitates TRiC assembly, I would determine if changes in MSTO1 expression affects the kinetics of assembly of purified TRiC subunits. All TRiC subunits have been purified from insect cells as well as mammalian suspension cells. MSTO1 has not been purified. We attempted to purify MSTO1 but found that the StrepTag was not accessible following overexpression as MSTO1-TwinStrep did not bind to the beads. To circumvent the need for pure protein, I would use crude lysates from MSTO1-depleted, MSTO1-overexpressing, or control cells and add individual purified TRiC subunits. Assembly efficiency would be assessed by BN-PAGE which allows visualization of both fully assembled TRiC complexes and intermediate species. If MSTO1 acts as an assembly-promoting factor, I would expect MSTO1-enriched lysates to enhance the formation or stability of fully assembled TRiC complexes, whereas MSTO1-depleted lysates would reduce assembly efficiency or increase accumulation of aberrant assemblies.

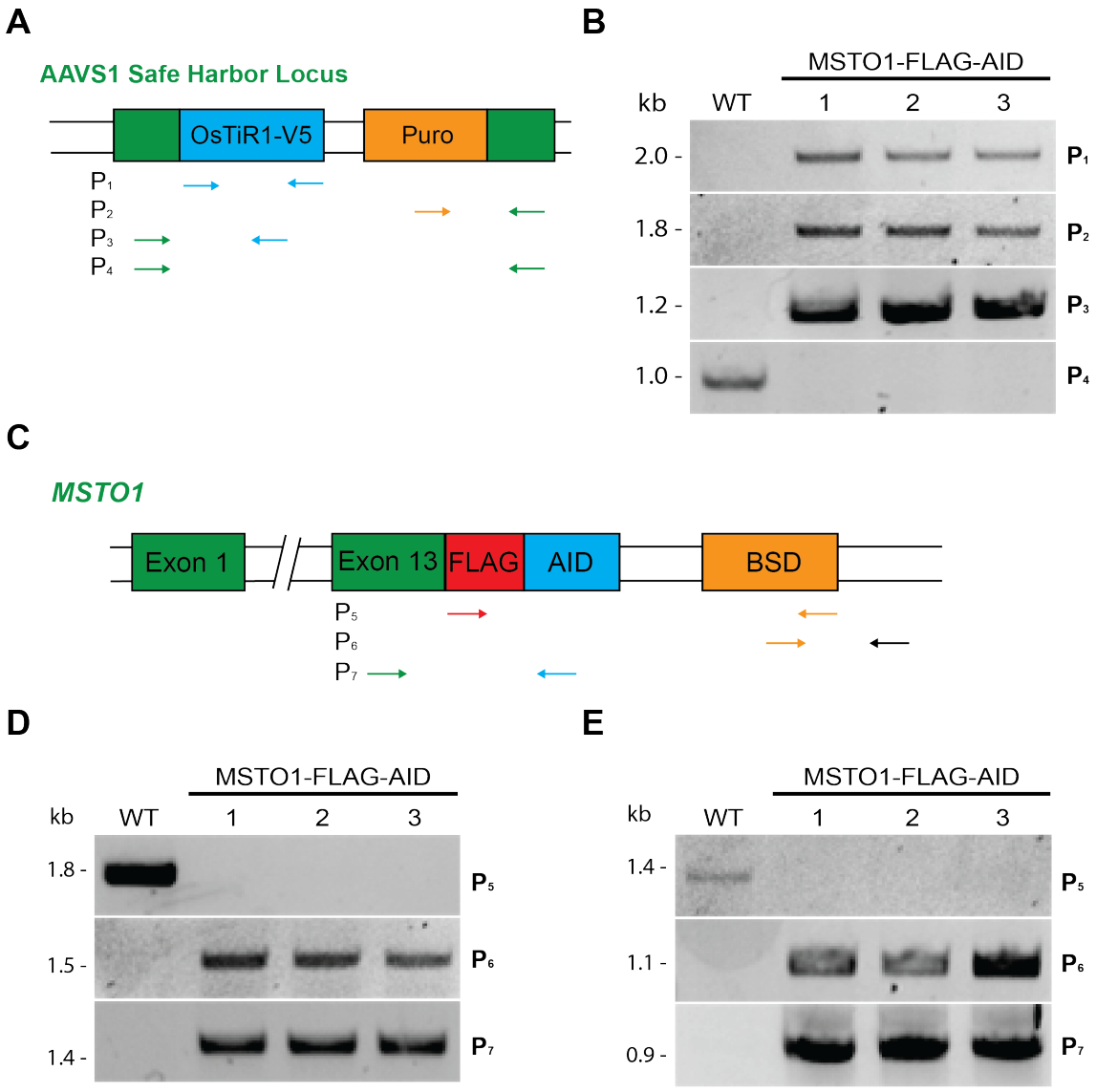

Figure 6.1. Confirming OsTiR1-V5 and MSTO1 C-terminus FLAG-AID tag insertions. (A) Schematic of PCR genotyping strategy used to verify insertion of OsTiR1-V5 (blue) and the puromycin resistance cassette (puro; orange) into the AAVS1 safe harbor locus (green). Arrows indicate primer pairs used for PCR amplification. Primer pair P_1 distinguishes wild-type and modified alleles; absence of wild-type amplification indicates homozygous insertion. Primer pairs P_2 and P_3 confirm correct integration at the AAVS1 locus, while P_4 verifies the presence of full-length OsTiR1-V5 construct. **(B)** PCR genotyping results confirming homozygous insertion of OsTiR1-V5 at the AAVS1 safe harbor locus in three clonal populations. **(C)** Schematic of PCR genotyping strategy used to verify insertion of FLAG-AID tag (red/blue) and the blasticidin resistance cassette (BSD; orange) immediately downstream of the final coding exon of *MSTO1* (green). Arrows indicate primer pairs used for PCR amplification. Primer pair P_5 distinguishes wild-type and modified alleles; absence of wild-type amplification indicates homozygous insertion. Primer pairs P_6 and P_7 confirm correct integration at the correct *MSTO1* locus. **(D)** PCR genotyping results confirming homozygous insertion of the FLAG-AID tag at the last coding exon of *MSTO1* in three clonal populations. **(E)** PCR genotyping results indicating homozygous insertion of the FLAG-AID tag at the *MSTO2P* locus in three clonal populations.

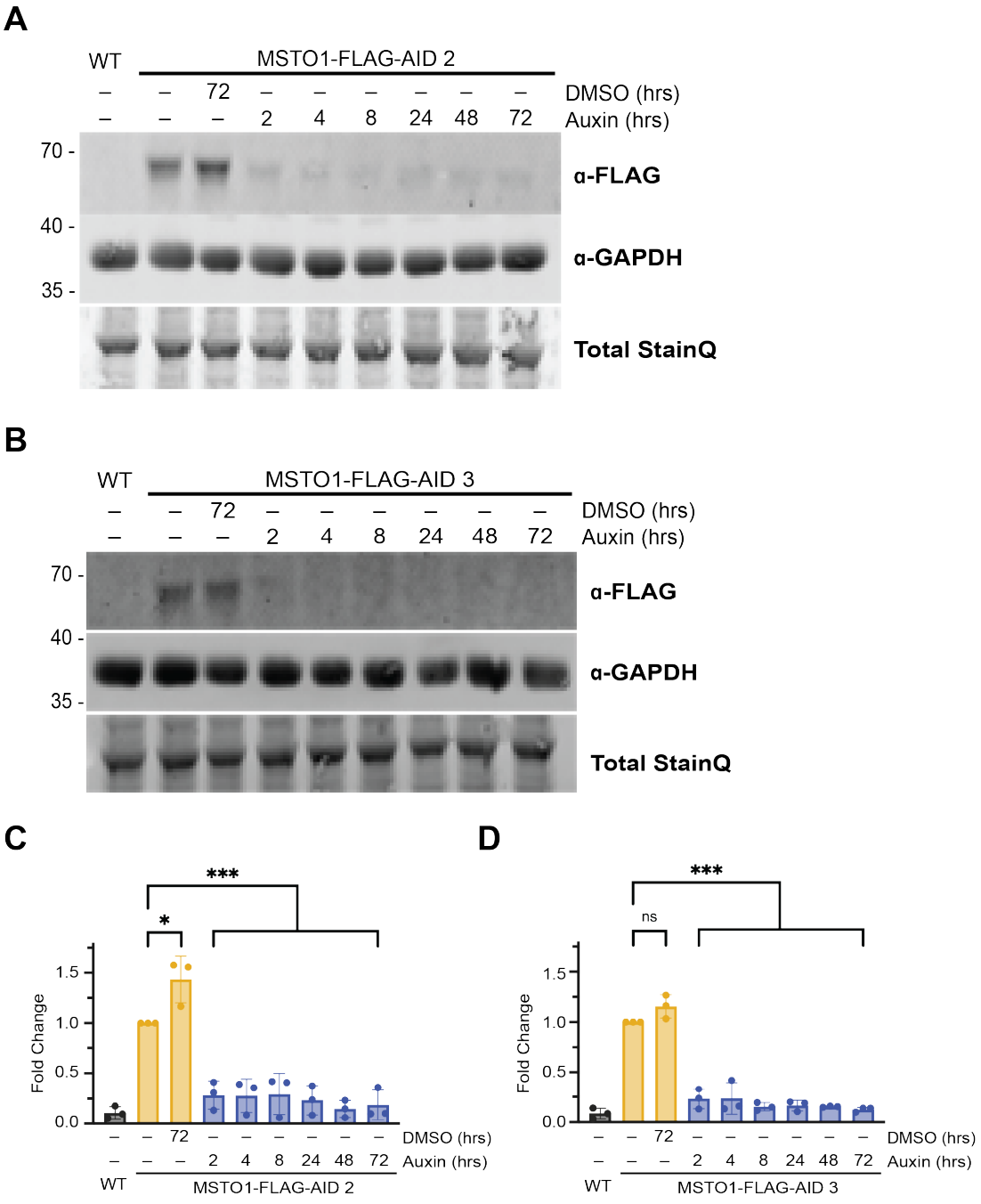

Figure 6.2. MSTO1 is depleted after 2 hours of auxin treatment in MSTO1-AID-FLAG clonal populations 2 and 3. (A-D) MSTO1-FLAG-AID clonal 2 (A) and clonal 3 (B) cells were treated with 20 μM auxin in increments between 2 and 72 hrs. Whole-cell lysates prepared from MSTO1-FLAG-AID cell lines subject to SDS–PAGE and immunoblotting with anti-FLAG, and anti-GADPH. Staining of total protein with Total StainQ was used as loading control. **(C-D)** Average fold change of clonal 2 (C) and clonal 3 (D) of MSTO1-FLAG-AID protein expression relative to WT HCT116 cells from three independent experiments are shown. The graph shows mean and standard deviation from 3 independent experiments, ns: not significant, *P<-.05, ***P < 0.001, ordinary one-way Anova with multiple comparisons.

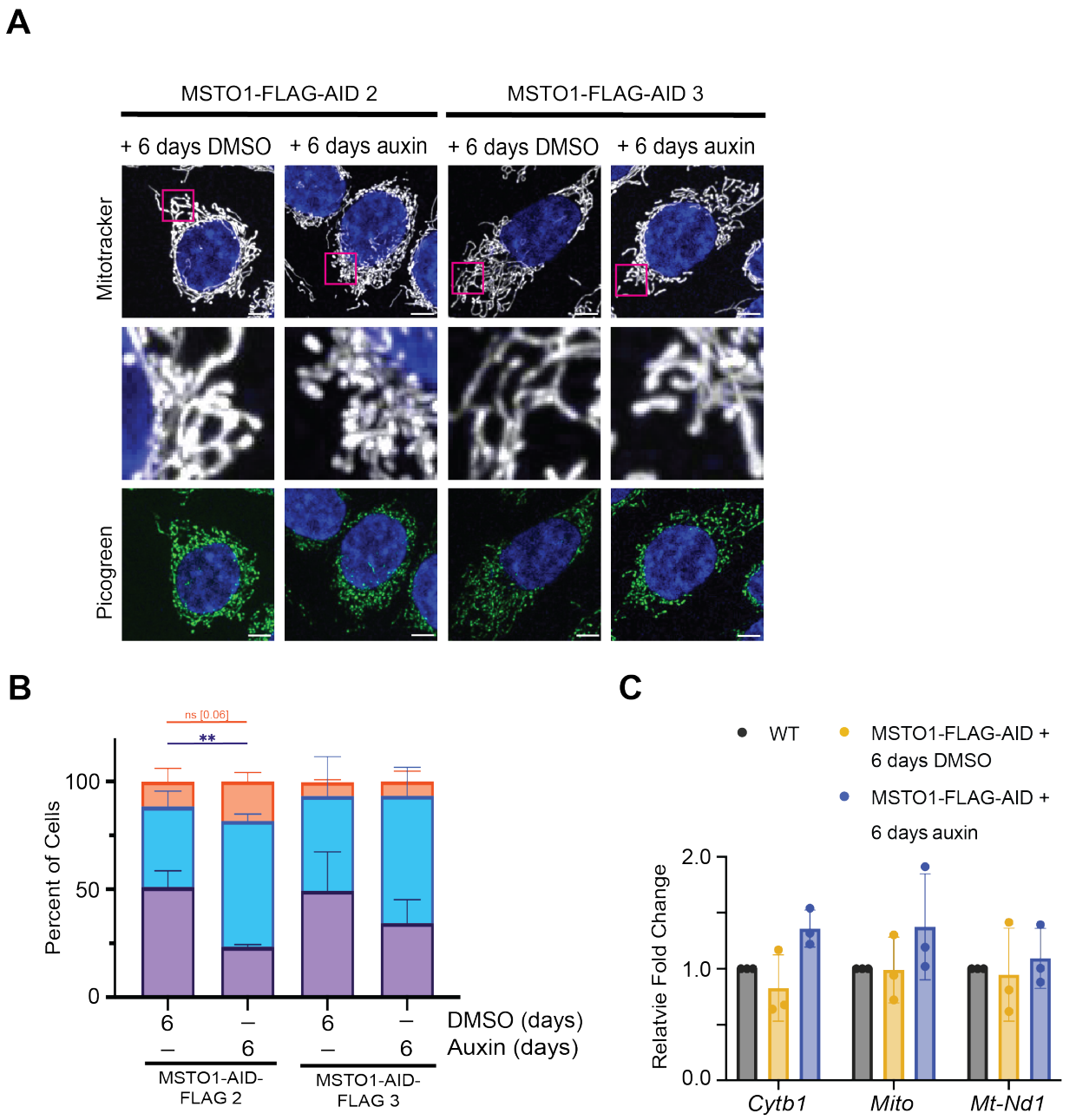

Figure 6.3. MSTO1-depleted cells have short mitochondria in MSTO1-AID-FLAG clonal populations 2 and 3. (A) Representative live cell images of WT, WT+OsTiR1-V5, and MSTO1-FLAG-AID clonal populations 2 and 3 treated with auxin or vehicle for 6 days. Mitochondria were labeled with Mitotracker Red CMXRos, mtDNA were labeled with Quant-iT™ PicoGreen® dsDNA Reagent, and nuclei were labeled with NucBlue. All were visualized by fluorescence microscopy. Scale bar is 5 μM. **(B)** Quantification of mitochondrial morphology for cell lines described in (A). The graph shows mean and standard deviation from 3 independent experiments. **P < 0.01, ordinary two-way Anova with multiple comparisons. **(C)** Genomic DNA samples were prepared from MSTO1-AID-FLAG clonal 2 cells treated with auxin or vehicle for 6 days. MtDNA was quantified relative to *GAPDH*, a nuclear housekeeping gene, by qPCR.

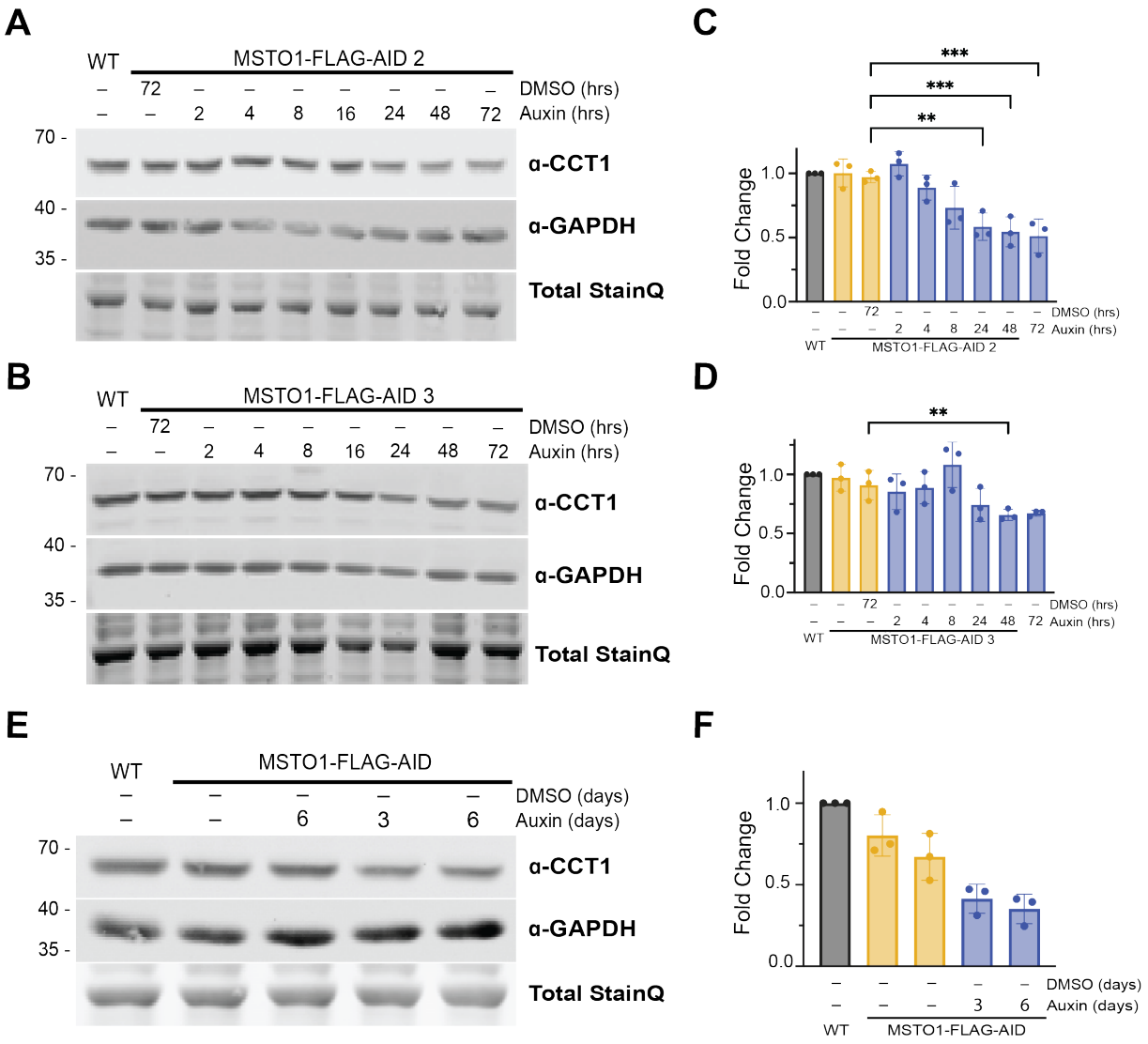

Figure 6.4. TRIC levels are significantly reduced before mitochondrial morphology changes in MSTO1-AID-FLAG clonal populations 2 and 3. (A-B) MSTO1-FLAG-AID clonals 2 and 3 cells were treated with 20 μM auxin for indicated times. Whole-cell lysates prepared from MSTO1-FLAG-AID clonals 2 and 3 cell lines subject to SDS–PAGE and immunoblotting with anti-CCT1, and anti-GADPH. Staining of total protein with Total StainQ was used as loading control. **(C-D)** Quantification of Western blots from (A-B). Average fold change of CCT1 protein expression relative to WT HCT116 cells from three independent experiments are shown. The graph shows mean and standard deviation from 3 independent experiments, **P < 0.01, ***P < 0.001, ordinary one-way Anova with multiple comparisons. **(E)** MSTO1-FLAG-AID clonal 2 cells were treated with 20 μM auxin for indicated times. Whole-cell lysates prepared from MSTO1-FLAG-AID clonal 2 cell lines subject to SDS–PAGE and immunoblotting with anti-CCT1, and anti-GADPH. Staining of total protein with Total StainQ was used as loading control. **(C-D)** Quantification of Western blots from (E). Average fold change of CCT1 protein expression relative to WT HCT116 cells from three independent experiments are shown. The graph shows mean and standard deviation from 3 independent experiments.

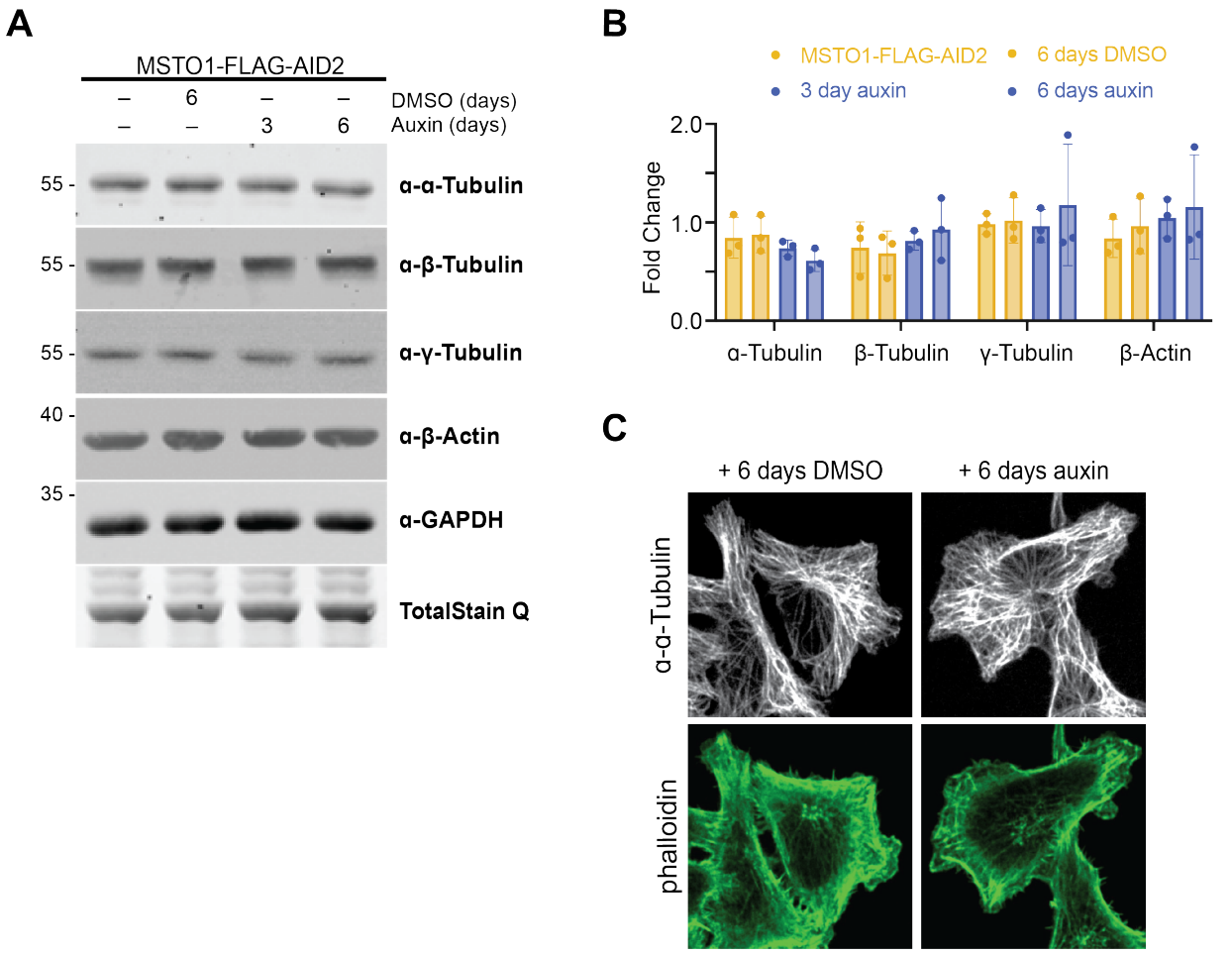

Figure 6.5. MSTO1-depleted cells have no changes in tubulin and actin protein expression or cytoskeletal networks. (A) MSTO1-FLAG-AID clonal 2 cells were treated with 20 μM auxin or vechicle for 3 or 6 days. Whole-cell lysates prepared from MSTO1-FLAG-AID clonal 2 cell lines subject to SDS–PAGE and immunoblotting with anti-α-tubulin, anti-β-tubulin, anti-γ-tubulin, anti-β-actin, and anti-GADPH. Staining of total protein with Total StainQ was used as loading control. **(F)** Quantification of Western Blots from (A). Average fold change of -tubulin, β-tubulin, γ-tubulin, β-actin protein expression relative to WT HCT116 cells from three independent experiments are shown. The graph shows mean and standard deviation from 3 independent experiments. **(C)** Representative live cell images of MSTO1-FLAG-AID cells treated with 20 μM auxin or vehicle for 3 or 6 days. Microtubules were immunostained with anti-α-tubulin and actin was immunostained with phalloidin. All were visualized by fluorescence microscopy.

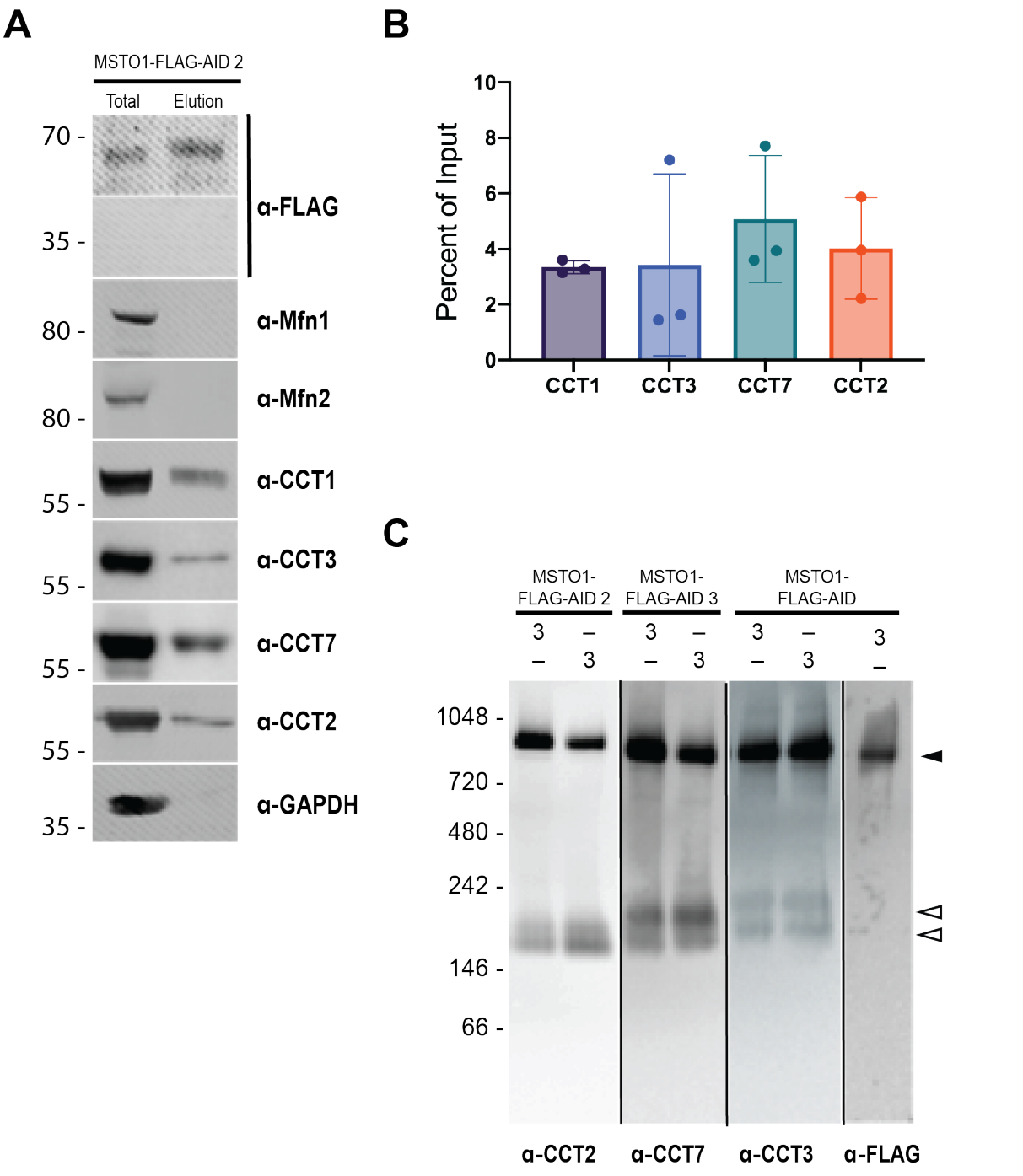

Figure 6.6. MSTO1 interacts with TRiC and is a novel assembly factor in MSTO1-FLAG-AID clonal 2 cells. (A) Co-immunoprecipitation (Co-IP) pulling on mcherry-FLAG or MSTO1-FLAG-AID clonal 2 with FLAG-coated magnetic beads. Co-IP Total (0.66%) and Elution (6.6%) subject to SDS–PAGE and immunoblotting with anti-FLAG, anti-Mfn1, anti-Mfn2, anti-CCT1, anti-CCT3, anti-CCT7, anti-CCT2, or anti-GADPH. **(B)** Quantification of fraction of CCT1, CCT3, CCT7, and CCT2 protein levels pulled down in elution compared to total protein levels from Co-IP from (A). **(C)** Whole-cell lysates prepared from MSTO1-FLAG-AID clonal 2 cells treated with auxin or vehicle for 3 days were subject to separation by BN-PAGE followed by immunoblotting with anti-CCT1, anti-CCT3, anti-CCT7, anti-CCT2, or anti-FLAG. Open arrowhead indicates ~146 kDa intermediate scaffolds and closed arrowhead indicate fully assemble TRiC at ~720 kDa.

Chapter 7. References

Amari, L, and Germain, M (2021). Mitochondrial Extracellular Vesicles – Origins and Roles. Front Mol Neurosci 14.

Anderson, AP, Luo, X, Russell, W, and Yin, YW (2020). Oxidative damage diminishes mitochondrial DNA polymerase replication fidelity. Nucleic Acids Res 48, 817–829.

Anderson, S, Bankier, AT, Barrell, BG, de Bruijn, MH, Coulson, AR, Drouin, J, Eperon, IC, Nierlich, DP, Roe, BA, Sanger, F, *et al.* (1981). Sequence and organization of the human mitochondrial genome. Nature 290, 457–465.

Antonny, B, Burd, C, De Camilli, P, Chen, E, Daumke, O, Faelber, K, Ford, M, Frolov, VA, Frost, A, Hinshaw, JE, *et al.* (2016). Membrane fission by dynamin: what we know and what we need to know. EMBO J 35, 2270–2284.

Archibald, JM, Blouin, C, and Doolittle, WF (2001). Gene duplication and the evolution of group II chaperonins: implications for structure and function. J Struct Biol 135, 157–169.

Ardicli, D, Sarkozy, A, Zaharieva, I, Deshpande, C, Bodi, I, Siddiqui, A, U-King-Im, JM, Selfe, A, Phadke, R, Jungbluth, H, *et al.* (2019). A novel case of MSTO1 gene related congenital muscular dystrophy with progressive neurological involvement. Neuromuscul Disord NMD 29, 448–455.

Aryaman, J, Bowles, C, Jones, NS, and Johnston, IG (2019). Mitochondrial Network State Scales mtDNA Genetic Dynamics. Genetics 212, 1429–1443.

Baloh, RH, Schmidt, RE, Pestronk, A, and Milbrandt, J (2007). Altered axonal mitochondrial transport in the pathogenesis of Charcot-Marie-Tooth disease from mitofusin 2 mutations. J Neurosci Off J Soc Neurosci 27, 422–430.

Ban-Ishihara, R, Ishihara, T, Sasaki, N, Mihara, K, and Ishihara, N (2013). Dynamics of nucleoid structure regulated by mitochondrial fission contributes to cristae reformation and release of cytochrome *c.* Proc Natl Acad Sci 110, 11863–11868.

Betancourt Moreira, K, Collier, MP, Leitner, A, Li, KH, Lachapel, ILS, McCarthy, F, Opoku-Nsiah, KA, Morales-Polanco, F, Barbosa, N, Gestaut, D, *et al.* (2023). A hierarchical assembly pathway directs the unique subunit arrangement of TRiC/CCT. Mol Cell 83, 3123-3139.e8.

Boland, ML, Chourasia, AH, and Macleod, KF (2013). Mitochondrial dysfunction in cancer. Front Oncol 3, 292.

Calkins, MJ, Manczak, M, Mao, P, Shirendeb, U, and Reddy, PH (2011). Impaired mitochondrial biogenesis, defective axonal transport of mitochondria, abnormal mitochondrial dynamics and synaptic degeneration in a mouse model of Alzheimer's disease. Hum Mol Genet 20, 4515–4529.

Canty, JT, Hensley, A, Aslan, M, Jack, A, and Yildiz, A (2023). TRAK adaptors regulate the recruitment and activation of dynein and kinesin in mitochondrial transport. Nat Commun 14, 1376.

Chapman, J, Ng, YS, and Nicholls, TJ (2020). The Maintenance of Mitochondrial DNA Integrity and Dynamics by Mitochondrial Membranes. Life Basel Switz 10, E164.

Chen, H, Detmer, SA, Ewald, AJ, Griffin, EE, Fraser, SE, and Chan, DC (2003a). Mitofusins Mfn1 and Mfn2 coordinately regulate mitochondrial fusion and are essential for embryonic development. J Cell Biol 160, 189–200.

Chen, H, Detmer, SA, Ewald, AJ, Griffin, EE, Fraser, SE, and Chan, DC (2003b). Mitofusins Mfn1 and Mfn2 coordinately regulate mitochondrial fusion and are essential for embryonic development. J Cell Biol 160, 189–200.

Chen, H, Vermulst, M, Wang, YE, Chomyn, A, Prolla, TA, McCaffery, JM, and Chan, DC (2010). Mitochondrial fusion is required for mtDNA stability in skeletal muscle and tolerance of mtDNA mutations. Cell 141, 280–289.

Chen, J, Xiao, J, Chen, G, Xu, Q, Wu, X, Tian, L, Huang, Z, Xin, C, Zhao, Y, Guo, Z, *et al.* (2022). Indentification of novel MSTO1 compound heterozygous mutations in a Chinese family with recessive cerebellar atrophy and ataxia. Front Neurol 13, 988519.

Chen, Y, Liu, Y, and Dorn, GW (2011). Mitochondrial fusion is essential for organelle function and cardiac homeostasis. Circ Res 109, 1327–1331.

Chen, Y, Shi, H, Dong, Y, and Cui, W (2025). LncRNA MSTO2P affects the proliferation, invasion and migration of non-small cell lung cancer by regulating the Wnt/β-catenin pathway. Discov Oncol 16, 150.

Cho, NH, Cheveralls, KC, Brunner, A-D, Kim, K, Michaelis, AC, Raghavan, P, Kobayashi, H, Savy, L, Li, JY, Canaj, H, *et al.* (2022). OpenCell: Endogenous tagging for the cartography of human cellular organization. Science 375, eabi6983.

Collier, MP, Moreira, KB, Li, KH, Chen, Y-C, Itzhak, D, Samant, R, Leitner, A, Burlingame, A, and Frydman, J (2021). Native mass spectrometry analyses of chaperonin complex TRiC/CCT reveal subunit N-terminal processing and re-association patterns. Sci Rep 11, 13084.

Cong, Y, Baker, ML, Jakana, J, Woolford, D, Miller, EJ, Reissmann, S, Kumar, RN, Redding-Johanson, AM, Batth, TS, Mukhopadhyay, A, *et al.* (2010). 4.0-Å resolution cryo-EM structure of the mammalian chaperonin TRiC/CCT reveals its unique subunit arrangement. Proc Natl Acad Sci 107, 4967–4972.

Cuéllar, J, Ludlam, WG, Tensmeyer, NC, Aoba, T, Dhavale, M, Santiago, C, Bueno-Carrasco, MT, Mann, MJ, Plimpton, RL, Makaju, A, *et al.* (2019). Structural and functional analysis of the role of the chaperonin CCT in mTOR complex assembly. Nat Commun 10, 2865.

Cuéllar, J, Vallin, J, Svanström, A, Maestro-López, M, Bueno-Carrasco, MT, Ludlam, WG, Willardson, BM, Valpuesta, JM, and Grantham, J (2022). The Molecular Chaperone CCT Sequesters Gelsolin and Protects it from Cleavage by Caspase-3. J Mol Biol 434, 167399.

Detmer, SA, Vande Velde, C, Cleveland, DW, and Chan, DC (2008). Hindlimb gait defects due to motor axon loss and reduced distal muscles in a transgenic mouse model of Charcot-Marie-Tooth type 2A. Hum Mol Genet 17, 367–375.

Ding, Y, Gao, H, Zhao, L, Wang, X, and Zheng, M (2015). Mitofusin 2-Deficiency Suppresses Cell Proliferation through Disturbance of Autophagy. PLoS ONE 10, e0121328.

Dominguez, R, and Holmes, KC (2011). Actin Structure and Function. Annu Rev Biophys 40, 169–186.

Donkervoort, S, Yun, P, Gauquelin, L, Chao, KR, Hu, Y, Al Khatib, I, Töpf, A, Mohassel, P, Cummings, BB, Kaur, R, *et al.* (2019). MSTO1 mutations cause mtDNA depletion, manifesting as muscular dystrophy with cerebellar involvement. Acta Neuropathol (Berl) 138, 1013–1031.

Drum, BML, Yuan, C, Li, L, Liu, Q, Wordeman, L, and Santana, LF (2016). Oxidative stress decreases microtubule growth and stability in ventricular myocytes. J Mol Cell Cardiol 93, 32–43.

Dutkowska, A, Domańska-Senderowska, D, Czarnecka-Chrebelska, KH, Pikus, E, Zielińska, A, Biskup, L, Kołodziejska, A, Madura, P, Możdżan, M, Załuska, U, *et al.* (2024). Mitochondrial Dynamics in Non-Small Cell Lung Cancer. Cancers 16, 2823.

El-Hattab, AW, and Scaglia, F (2013). Mitochondrial DNA Depletion Syndromes: Review and Updates of Genetic Basis, Manifestations, and Therapeutic Options. Neurotherapeutics 10, 186–198.

Engelhart, EA, and Hoppins, S (2019). A catalytic domain variant of mitofusin requiring a wildtype paralog for function uncouples mitochondrial outer-membrane tethering and fusion. J Biol Chem 294, 8001–8014.

Eura, Y, Ishihara, N, Yokota, S, and Mihara, K (2003). Two mitofusin proteins, mammalian homologues of FZO, with distinct functions are both required for mitochondrial fusion. J Biochem (Tokyo) 134, 333–344.

Fan, X, Hussien, R, and Brooks, GA (2010). H2O2-induced mitochondrial fragmentation in C2C12 myocytes. Free Radic Biol Med 49, 1646–1654.

Feng, S-T, Wang, Z-Z, Yuan, Y-H, Wang, X-L, Sun, H-M, Chen, N-H, and Zhang, Y (2020). Dynamin-related protein 1: A protein critical for mitochondrial fission, mitophagy, and neuronal death in Parkinson's disease. Pharmacol Res 151, 104553.

Ferguson, SM, and De Camilli, P (2012). Dynamin, a membrane-remodelling GTPase. Nat Rev Mol Cell Biol 13, 75–88.

Fernández Casafuz, AB, De Rossi, MC, and Bruno, L (2023). Mitochondrial cellular organization and shape fluctuations are differentially modulated by cytoskeletal networks. Sci Rep 13, 4065.

Filadi, R, Pendin, D, and Pizzo, P (2018). Mitofusin 2: from functions to disease. Cell Death Dis 9, 330.

Forte, M, Schirone, L, Ameri, P, Basso, C, Catalucci, D, Modica, J, Chimenti, C, Crotti, L, Frati, G, Rubattu, S, *et al.* (2021). The role of mitochondrial dynamics in cardiovascular diseases. Br J Pharmacol 178, 2060–2076.

Gal, A, Balicza, P, Weaver, D, Naghdi, S, Joseph, SK, Várnai, P, Gyuris, T, Horváth, A, Nagy, L, Seifert, EL, *et al.* (2017). MSTO1 is a cytoplasmic pro-mitochondrial fusion protein, whose mutation induces myopathy and ataxia in humans. EMBO Mol Med 9, 967–984.

Gál, A, Santos, JH, Molnár, MJ, and Hajnóczky, G (2023a). Answer to Gerber et al. "Autosomal recessive pathogenic MSTO1 variants in hereditary optic atrophy." EMBO Mol Med 15, e16251.

Gál, A, Santos, JH, Molnár, MJ, and Hajnóczky, G (2023b). Answer to Gerber et al. "Autosomal recessive pathogenic MSTO1 variants in hereditary optic atrophy." EMBO Mol Med 15, e16251.

Gatti, P, Schiavon, C, Cicero, J, Manor, U, and Germain, M (2025). Mitochondria- and ER-associated actin are required for mitochondrial fusion. Nat Commun 16, 451.

Gekko, H, Nomura, R, Kuzuhara, D, Kaneyasu, M, Koseki, G, Adhikari, D, Mio, Y, Carroll, J, Kono, T, Funahashi, H, *et al.* (2025). Redistribution of fragmented mitochondria ensure symmetric organelle partitioning and faithful chromosome segregation in mitotic mouse zygotes. eLife 13.

Gerber, S, Lessard, L, Rouzier, C, Ait-el-Mkadem Saadi, S, Ameli, R, Thobois, S, Abouaf, L, Bouhour, F, Kaplan, J, Putoux, A, *et al.* (2023). Autosomal recessive pathogenic MSTO1 variants in hereditary optic atrophy. EMBO Mol Med 15, e16090.

Ghozlan, H, Cox, A, Nierenberg, D, King, S, and Khaled, AR (2022). The TRiCky Business of Protein Folding in Health and Disease. Front Cell Dev Biol 10, 906530.

Gomes, LC, Di Benedetto, G, and Scorrano, L (2011). During autophagy mitochondria elongate, are spared from degradation and sustain cell viability. Nat Cell Biol 13, 589–598.

Goyal, G, Fell, B, Sarin, A, Youle, RJ, and Sriram, V (2007). Role of Mitochondrial Remodeling in Programmed Cell Death in Drosophila melanogaster. Dev Cell 12, 807–816.

Gu, M, and Wang, X (2022). Pseudogene MSTO2P Interacts with miR-128-3p to Regulate Coptisine Sensitivity of Non-Small-Cell Lung Cancer (NSCLC) through TGF-β Signaling and VEGFC. J Oncol 2022, 9864411.

Guo, M, and Zhang, X (2022). LncRNA MSTO2P promotes colorectal cancer progression through epigenetically silencing CDKN1A mediated by EZH2. World J Surg Oncol 20, 95.

Gurvitz, A, Hartig, A, Ruis, H, Hamilton, B, and de Couet, HG (2002). Preliminary characterisation of DML1, an essential Saccharomyces cerevisiae gene related to misato of Drosophila melanogaster. FEMS Yeast Res 2, 123–135.

Gustafsson, CM, Falkenberg, M, and Larsson, N-G (2016). Maintenance and Expression of Mammalian Mitochondrial DNA. Annu Rev Biochem 85, 133–160.

Hahn, A, and Zuryn, S (2019). Mitochondrial Genome (mtDNA) Mutations that Generate Reactive Oxygen Species. Antioxidants 8, 392.

Hatch, AL, Gurel, PS, and Higgs, HN (2014). Novel roles for actin in mitochondrial fission. J Cell Sci 127, 4549–4560.

Heymann, JAW, and Hinshaw, JE (2009). Dynamins at a glance. J Cell Sci 122, 3427–3431.

Hoffmann, HP, and Avers, CJ (1973). Mitochondrion of yeast: ultrastructural evidence for one giant, branched organelle per cell. Science 181, 749–751.

Hoppins, S, Collins, SR, Cassidy-Stone, A, Hummel, E, DeVay, RM, Lackner, LL, Westermann, B, Schuldiner, M, Weissman, JS, and Nunnari, J (2011a). A mitochondrial-focused genetic interaction map reveals a scaffold-like complex required for inner membrane organization in mitochondria. J Cell Biol 195, 323–340.

Hoppins, S, Edlich, F, Cleland, MM, Banerjee, S, McCaffery, JM, Youle, RJ, and Nunnari, J (2011b). The soluble form of Bax regulates mitochondrial fusion via MFN2 homotypic complexes. Mol Cell 41, 150–160.

Hung, C (2021). Importance of retrograde axonal transport in mitochondrial health and distribution. Cell Death Discov 7, 106.

Hurwitz, SM, Zagotta, WN, Gordon, SE, and Hoppins, S (2026). Time-resolved tmFRET reveals GTP-coupled conformational changes in Mfn1. J Cell Biol 225, e202511077.

Ishihara, N, Eura, Y, and Mihara, K (2004). Mitofusin 1 and 2 play distinct roles in mitochondrial fusion reactions via GTPase activity. J Cell Sci 117, 6535–6546.

Iwama, K, Takaori, T, Fukushima, A, Tohyama, J, Ishiyama, A, Ohba, C, Mitsuhashi, S, Miyatake, S, Takata, A, Miyake, N, *et al.* (2018). Novel recessive mutations in MSTO1 cause cerebellar atrophy with pigmentary retinopathy. J Hum Genet 63, 263–270.

Jakubke, C, Roussou, R, Maiser, A, Schug, C, Thoma, F, Bunk, D, Hörl, D, Leonhardt, H, Walter, P, Klecker, T, *et al.* (2021). Cristae-dependent quality control of the mitochondrial genome. Sci Adv 7, eabi8886.

Jimah, JR, and Hinshaw, JE (2019). Structural Insights into the Mechanism of Dynamin Superfamily Proteins. Trends Cell Biol 29, 257–273.

Joachimiak, LA, Walzthoeni, T, Liu, C, Aebersold, R, and Frydman, J (2014). The structural basis of substrate recognition by the eukaryotic chaperonin TRiC/CCT. Cell 159, 1042–1055.

Kakanj, P, Bonse, M, Kshirsagar, A, Gökmen, A, Gaedke, F, Sen, A, Mollá, B, Vogelsang, E, Schauss, A, Wodarz, A, *et al.* (2025). Retromer promotes the lysosomal turnover of mtDNA. Sci Adv 11, eadr6415.

Karbowski, M, and Youle, RJ (2003). Dynamics of mitochondrial morphology in healthy cells and during apoptosis. Cell Death Differ 10, 870–880.

Kelly, JJ, Tranter, D, Pardon, E, Chi, G, Kramer, H, Happonen, L, Knee, KM, Janz, JM, Steyaert, J, Bulawa, C, *et al.* (2022). Snapshots of actin and tubulin folding inside the TRiC chaperonin. Nat Struct Mol Biol 29, 420–429.

Kiefel, BR, Gilson, PR, and Beech, PL (2004). Diverse Eukaryotes have Retained Mitochondrial Homologues of the Bacterial Division Protein FtsZ. Protist 155, 105–115.

Kim, H, Park, J, and Roh, S-H (2024). The structural basis of eukaryotic chaperonin TRiC/CCT: Action and folding. Mol Cells 47, 100012.

Kim, Y, and Chang, S (2006). Ever-expanding network of dynamin-interacting proteins. Mol Neurobiol 34, 129–135.

Kimura, M, and Okano, Y (2007). Human Misato regulates mitochondrial distribution and morphology. Exp Cell Res 313, 1393–1404.

Kizmaz, B, Nutz, A, Egeler, A, and Herrmann, JM (2024). Protein insertion into the inner membrane of mitochondria: routes and mechanisms. FEBS Open Bio 14, 1627–1639.

Knezevic, I, Predescu, D, Bardita, C, Wang, M, Sharma, T, Keith, B, Neamu, R, Malik, AB, and Predescu, S (2011). Regulation of dynamin-2 assembly–disassembly and function through the SH3A domain of intersectin-1s. J Cell Mol Med 15, 2364–2376.

König, T, Nolte, H, Aaltonen, MJ, Tatsuta, T, Krols, M, Stroh, T, Langer, T, and McBride, HM (2021). MIROs and DRP1 drive mitochondrial-derived vesicle biogenesis and promote quality control. Nat Cell Biol 23, 1271–1286.

Korobova, F, Ramabhadran, V, and Higgs, HN (2013). An Actin-Dependent Step in Mitochondrial Fission Mediated by the ER-Associated Formin INF2. Science 339, 464–467.

Kraft, F, Rodriguez-Aliaga, P, Yuan, W, Franken, L, Zajt, K, Hasan, D, Lee, T-T, Flex, E, Hentschel, A, Innes, AM, *et al.* (2024). Brain malformations and seizures by impaired chaperonin function of TRiC. Science 386, 516–525.

Kukat, C, Wurm, CA, Spåhr, H, Falkenberg, M, Larsson, N-G, and Jakobs, S (2011). Super-resolution microscopy reveals that mammalian mitochondrial nucleoids have a uniform size and frequently contain a single copy of mtDNA. Proc Natl Acad Sci U S A 108, 13534–13539.

Kumar, S, Pan, CC, Shah, N, Wheeler, SE, Hoyt, KR, Hempel, N, Mythreye, K, and Lee, NY (2016). Activation of mitofusin2 by Smad2-RIN1 complex during mitochondrial fusion. Mol Cell 62, 520–531.

Kuryshev, VYu, Vorobyov, E, Zink, D, Schmitz, J, Rozhdestvensky, TS, Münstermann, E, Ernst, U, Wellenreuther, R, Moosmayer, P, Bechtel, S, *et al.* (2006). An anthropoid-specific segmental duplication on human chromosome 1q22. Genomics 88, 143–151.

Larrea, D, Pera, M, Gonnelli, A, Quintana-Cabrera, R, Akman, HO, Guardia-Laguarta, C, Velasco, KR, Area-Gomez, E, Dal Bello, F, De Stefani, D, *et al.* (2019). MFN2 mutations in Charcot-Marie-Tooth disease alter mitochondria-associated ER membrane function but do not impair bioenergetics. Hum Mol Genet 28, 1782–1800.

Lee, SR, and Han, J (2017). Mitochondrial Nucleoid: Shield and Switch of the Mitochondrial Genome. Oxid Med Cell Longev 2017, 8060949.

Lee-Glover, LP, Picard, M, and Shutt, TE (2025). Mitochondria – the CEO of the cell. J Cell Sci 138, jcs263403.

Leitner, A, Joachimiak, LA, Bracher, A, Mönkemeyer, L, Walzthoeni, T, Chen, B, Pechmann, S, Holmes, S, Cong, Y, Ma, B, *et al.* (2012). The Molecular Architecture of the Eukaryotic Chaperonin TRiC/CCT. Structure 20, 814–825.

Lewis, MR, and Lewis, WH (1915). Mitochondria (and other cytoplasmic structures) in tissue cultures - Lewis - 1915 - American Journal of Anatomy - Wiley Online Library. 17, 339–401.

Lewis, SC, Uchiyama, LF, and Nunnari, J (2016). ER-mitochondria contacts couple mtDNA synthesis with mitochondrial division in human cells. Science 353, aaf5549.

Lhuissier, C, Wagner, BE, Vincent, A, Garraux, G, Hougrand, O, Van Coster, R, Benoit, V, Karadurmus, D, Lenaers, G, Gueguen, N, *et al.* (2022). Case report: Thirty-year progression of an EMPF1 encephalopathy due to defective mitochondrial and peroxisomal fission caused by a novel de novo heterozygous DNM1L variant. Front Neurol 13.

Li, H, Zhu, H, Zhou, Y, Wang, H, Niu, Z, Shen, Y, and Lv, L (2017). Long non-coding RNA MSTO2P promotes the proliferation and colony formation in gastric cancer by indirectly regulating miR-335 expression. Tumour Biol J Int Soc Oncodevelopmental Biol Med 39, 1010428317705506.

Li, K, Jin, R, and Wu, X (2020). Whole-exome sequencing identifies rare compound heterozygous mutations in the MSTO1 gene associated with cerebellar ataxia and myopathy. Eur J Med Genet 63, 103623.

Li, S, and Sheng, Z-H (2022). Energy matters: presynaptic metabolism and the maintenance of synaptic transmission | Nature Reviews Neuroscience. 23.

Li, Y-J, Cao, Y-L, Feng, J-X, Qi, Y, Meng, S, Yang, J-F, Zhong, Y-T, Kang, S, Chen, X, Lan, L, *et al.* (2019). Structural insights of human mitofusin-2 into mitochondrial fusion and CMT2A onset. Nat Commun 10, 4914.

Liu, H, Xie, J, Zhen, C, Zeng, L, Fan, H, Zhuang, H, and Feng, D Nucleoid-phagy: a novel safeguard against mitochondrial DNA-Induced inflammation. Autophagy 20, 2821–2823.

Liu, L, Su, R, Huang, P, Li, X, Xiong, J, Xiao, Y, Mao, D, and Liu, L (2022). Case Report: Evidences of myasthenia and cerebellar atrophy in a chinese patient with novel compound heterozygous MSTO1 variants. Front Genet 13, 947886.

Liu, X, Lin, C-Y, Lei, M, Yan, S, Zhou, T, and Erikson, RL (2005). CCT chaperonin complex is required for the biogenesis of functional Plk1. Mol Cell Biol 25, 4993–5010.

Losón, OC, Song, Z, Chen, H, and Chan, DC (2013). Fis1, Mff, MiD49, and MiD51 mediate Drp1 recruitment in mitochondrial fission. Mol Biol Cell 24, 659–667.

Margolin, W (2005). FTSZ AND THE DIVISION OF PROKARYOTIC CELLS AND ORGANELLES. Nat Rev Mol Cell Biol 6, 862–871.

Melkov, A, and Abdu, U (2017). Regulation of long-distance transport of mitochondria along microtubules. Cell Mol Life Sci CMLS 75, 163–176.

Miklos, GLG, Yamamoto, M-T, Burns, RG, and Maleszka, R (1997a). An essential cell division gene of Drosophila, absent from Saccharomyces, encodes an unusual protein with tubulin-like and myosin-like peptide motifs. Proc Natl Acad Sci U S A 94, 5189–5194.

Miklos, GLG, Yamamoto, M-T, Burns, RG, and Maleszka, R (1997b). An essential cell division gene of Drosophila, absent from Saccharomyces, encodes an unusual protein with tubulin-like and myosin-like peptide motifs. Proc Natl Acad Sci U S A 94, 5189–5194.

Min, S, Yoon, W, Cho, H, and Chung, J (2017). Misato underlies visceral myopathy in Drosophila. Sci Rep 7, 17700.

Mitra, K, Wunder, C, Roysam, B, Lin, G, and Lippincott-Schwartz, J (2009). A hyperfused mitochondrial state achieved at G1-S regulates cyclin E buildup and entry into S phase. Proc Natl Acad Sci U S A 106, 11960–11965.

Mooren, OL, Galletta, BJ, and Cooper, JA (2012). Roles for actin assembly in endocytosis. Annu Rev Biochem 81, 661–686.

Mottier-Pavie, V, Cenci, G, Vernì, F, Gatti, M, and Bonaccorsi, S (2011). Phenotypic analysis of misato function reveals roles of noncentrosomal microtubules in Drosophila spindle formation. J Cell Sci 124, 706–717.

Murrell, M, Oakes, PW, Lenz, M, and Gardel, ML (2015). Forcing cells into shape: the mechanics of actomyosin contractility. Nat Rev Mol Cell Biol 16, 486–498.

Nasca, A, Di Meo, I, Fellig, Y, Saada, A, Elpeleg, O, Ghezzi, D, and Edvardson, S (2021a). A novel homozygous MSTO1 mutation in Ashkenazi Jewish siblings with ataxia and myopathy. J Hum Genet.

Nasca, A, Di Meo, I, Fellig, Y, Saada, A, Elpeleg, O, Ghezzi, D, and Edvardson, S (2021b). A novel homozygous MSTO1 mutation in Ashkenazi Jewish siblings with ataxia and myopathy. J Hum Genet.

Nasca, A, Scotton, C, Zaharieva, I, Neri, M, Selvatici, R, Magnusson, OT, Gal, A, Weaver, D, Rossi, R, Armaroli, A, *et al.* (2017a). Recessive mutations in MSTO1 cause mitochondrial dynamics impairment, leading to myopathy and ataxia. Hum Mutat 38, 970–977.

Nasca, A, Scotton, C, Zaharieva, I, Neri, M, Selvatici, R, Magnusson, OT, Gal, A, Weaver, D, Rossi, R, Armaroli, A, *et al.* (2017b). Recessive mutations in *MSTO1* cause mitochondrial dynamics impairment, leading to myopathy and ataxia. Hum Mutat 38, 970–977.

Ni, H-M, Williams, JA, and Ding, W-X (2015). Mitochondrial dynamics and mitochondrial quality control. Redox Biol 4, 6–13.

Nogales, E, Downing, KH, Amos, LA, and Löwe, J (1998). Tubulin and FtsZ form a distinct family of GTPases. Nat Struct Biol 5, 451–458.

Nogueira, C, Almeida, LS, Nesti, C, Pezzini, I, Videira, A, Vilarinho, L, and Santorelli, FM (2014). Syndromes associated with mitochondrial DNA depletion. Ital J Pediatr 40, 34.

Obinata, H, Watanabe, T, Takahashi, H, Shimo, S, Oda, T, Sugimoto, A, and Niwa, S (2025). SLC-25A46 regulates mitochondrial fusion through the mitofusin protein FZO-1 and is essential for maintaining neuronal morphology. J Cell Sci 138, jcs263571.

Osellame, LD, Singh, AP, Stroud, DA, Palmer, CS, Stojanovski, D, Ramachandran, R, and Ryan, MT (2016). Cooperative and independent roles of the Drp1 adaptors Mff, MiD49 and MiD51 in mitochondrial fission. J Cell Sci 129, 2170–2181.

Palmer, CS, Elgass, KD, Parton, RG, Osellame, LD, Stojanovski, D, and Ryan, MT (2013). Adaptor Proteins MiD49 and MiD51 Can Act Independently of Mff and Fis1 in Drp1 Recruitment and Are Specific for Mitochondrial Fission. J Biol Chem 288, 27584–27593.

Palumbo, V, Pellacani, C, Heesom, KJ, Rogala, KB, Deane, CM, Mottier-Pavie, V, Gatti, M, Bonaccorsi, S, and Wakefield, JG (2015). Misato Controls Mitotic Microtubule Generation by Stabilizing the Tubulin Chaperone Protein-1 Complex. Curr Biol 25, 1777–1783.

Papanicolaou, KN, Khairallah, RJ, Ngoh, GA, Chikando, A, Luptak, I, O'Shea, KM, Riley, DD, Lugus, JJ, Colucci, WS, Lederer, WJ, *et al.* (2011). Mitofusin-2 maintains mitochondrial structure and contributes to stress-induced permeability transition in cardiac myocytes. Mol Cell Biol 31, 1309–1328.

Paraiso, KD, Blitz, IL, Zhou, JJ, and Cho, KWY (2019). Morpholinos do not elicit an innate immune response during early Xenopus embryogenesis. Dev Cell 49, 643-650.e3.

Pavluch, V, Špaček, T, Engstová, H, Dlasková, A, and Ježek, P (2023). Possible frequent multiple mitochondrial DNA copies in a single nucleoid in HeLa cells. Sci Rep 13, 5788.

Prudent, J, and McBride, HM (2016). Mitochondrial Dynamics: ER Actin Tightens the Drp1 Noose. Curr Biol 26, R207–R209.

Radmard, S, Zesiewicz, TA, and Kuo, S-H (2023). Evaluation of Cerebellar Ataxic Patients. Neurol Clin 41, 21–44.

Reissmann, S, Joachimiak, LA, Chen, B, Meyer, AS, Nguyen, A, and Frydman, J (2012). A Gradient of ATP Affinities Generates an Asymmetric Power Stroke Driving the Chaperonin TRIC/CCT Folding Cycle. Cell Rep 2, 866–877.

Robertson, GL, Riffle, S, Patel, M, Bodnya, C, Marshall, A, Beasley, HK, Garza-Lopez, E, Shao, J, Vue, Z, Hinton, A, *et al.* (2023). DRP1 mutations associated with EMPF1 encephalopathy alter mitochondrial membrane potential and metabolic programs. J Cell Sci 136, jcs260370.

Rojo, M, Legros, F, Chateau, D, and Lombès, A (2002). Membrane topology and mitochondrial targeting of mitofusins, ubiquitous mammalian homologs of the transmembrane GTPase Fzo. J Cell Sci 115, 1663–1674.

Ross, JA, Chen, Y, Müller, J, Barylko, B, Wang, L, Banks, HB, Albanesi, JP, and Jameson, DM (2011). Dimeric Endophilin A2 Stimulates Assembly and GTPase Activity of Dynamin 2. Biophys J 100, 729–737.

Rüßmann, F, Stemp, MJ, Mönkemeyer, L, Etchells, SA, Bracher, A, and Hartl, FU (2012). Folding of large multidomain proteins by partial encapsulation in the chaperonin TRiC/CCT. Proc Natl Acad Sci U S A 109, 21208–21215.

Santel, A, and Fuller, MT (2001). Control of mitochondrial morphology by a human mitofusin. J Cell Sci 114, 867–874.

Schägger, H, and von Jagow, G (1991). Blue native electrophoresis for isolation of membrane protein complexes in enzymatically active form. Anal Biochem 199, 223–231.

Schaks, M, Giannone, G, and Rottner, K (2019). Actin dynamics in cell migration. Essays Biochem 63, 483–495.

Schultz-Rogers, L, Ferrer, A, Dsouza, NR, Zimmermann, MT, Smith, BE, Klee, EW, and Dhamija, R (2019). Novel biallelic variants in MSTO1 associated with mitochondrial myopathy. Cold Spring Harb Mol Case Stud 5, a004309.

Schwarz, TL (2013). Mitochondrial trafficking in neurons. Cold Spring Harb Perspect Biol 5, a011304.

Sebastián, D, Sorianello, E, Segalés, J, Irazoki, A, Ruiz-Bonilla, V, Sala, D, Planet, E, Berenguer-Llergo, A, Muñoz, JP, Sánchez-Feutrie, M, *et al.* (2016). Mfn2 deficiency links age-related sarcopenia and impaired autophagy to activation of an adaptive mitophagy pathway. EMBO J 35, 1677–1693.

Sen, A, Kallabis, S, Gaedke, F, Jüngst, C, Boix, J, Nüchel, J, Maliphol, K, Hofmann, J, Schauss, AC, Krüger, M, *et al.* (2022). Mitochondrial membrane proteins and VPS35 orchestrate selective removal of mtDNA. Nat Commun 13, 6704.

Sergeeva, OA, Chen, B, Haase-Pettingell, C, Ludtke, SJ, Chiu, W, and King, JA (2013). Human CCT4 and CCT5 chaperonin subunits expressed in Escherichia coli form biologically active homo-oligomers. J Biol Chem 288, 17734–17744.

Sergeeva, OA, Haase-Pettingell, C, and King, JA (2019). Co-expression of CCT subunits hints at TRiC assembly. Cell Stress Chaperones 24, 1055–1065.

Sharma, G, Zaman, M, Sabouny, R, Joel, M, Martens, K, Martino, D, de Koning, APJ, Pfeffer, G, and Shutt, TE (2021). Characterization of a novel variant in the HR1 domain of MFN2 in a patient with ataxia, optic atrophy and sensorineural hearing loss. F1000Research 10, 606.

Sheffer, R, Douiev, L, Edvardson, S, Shaag, A, Tamimi, K, Soiferman, D, Meiner, V, and Saada, A (2016). Postnatal microcephaly and pain insensitivity due to a de novo heterozygous DNM1L mutation causing impaired mitochondrial fission and function. Am J Med Genet A 170, 1603–1607.

Shen, Q, Yamano, K, Head, BP, Kawajiri, S, Cheung, JTM, Wang, C, Cho, J-H, Hattori, N, Youle, RJ, and van der Bliek, AM (2014). Mutations in Fis1 disrupt orderly disposal of defective mitochondria. Mol Biol Cell 25, 145–159.

Shi, C, Huang, C-M, Wang, B, Sun, T-F, Zhu, A-X, and Zhu, Y-C (2020). Pseudogene MSTO2P enhances hypoxia-induced osteosarcoma malignancy by upregulating PD-L1. Biochem Biophys Res Commun 530, 673–679.

Shi, P, Zhang, Y, and Wu, C (2025). Actin in mitochondrial regulation and mechanometabolic crosstalk. Curr Opin Cell Biol 95, 102539.

Silva Ramos, E, Motori, E, Brüser, C, Kühl, I, Yeroslaviz, A, Ruzzenente, B, Kauppila, JHK, Busch, JD, Hultenby, K, Habermann, BH, *et al.* (2019). Mitochondrial fusion is required for regulation of mitochondrial DNA replication. PLoS Genet 15, e1008085.

Sloat, SR, and Hoppins, S (2023). A dominant negative mitofusin causes mitochondrial perinuclear clusters because of aberrant tethering. Life Sci Alliance 6, e202101305.

Sloat, SR, Whitley, BN, Engelhart, EA, and Hoppins, S (2019). Identification of a mitofusin specificity region that confers unique activities to Mfn1 and Mfn2. Mol Biol Cell 30, 2309–2319.

Soulet, F, Yarar, D, Leonard, M, and Schmid, SL (2005). SNX9 Regulates Dynamin Assembly and Is Required for Efficient Clathrin-mediated Endocytosis. Mol Biol Cell 16, 2058–2067.

Srivastava, S (2017). The Mitochondrial Basis of Aging and Age-Related Disorders. Genes 8, 398.

Stevens, BJ Mitochondrial Structure. In: The Molecular Biology of the Yeast *Saccharomyces:* Life Cycle and Inheritance, Cold Spring Harbor, New York: Cold Spring Harbor Laboratory Press, 471–504.

Stevens, BJ, and White, JG (1979). [61] Computer reconstruction of mitochondria from yeast. In: Methods in Enzymology, Academic Press, 718–728.

Sugiura, A, McLelland, G-L, Fon, EA, and McBride, HM (2014). A new pathway for mitochondrial quality control: mitochondrial-derived vesicles. EMBO J 33, 2142–2156.

TerBush, AD, Yoshida, Y, and Osteryoung, KW (2013a). FtsZ in chloroplast division: structure, function and evolution. Curr Opin Cell Biol 25, 461–470.

TerBush, AD, Yoshida, Y, and Osteryoung, KW (2013b). FtsZ in chloroplast division: structure, function and evolution. Curr Opin Cell Biol 25, 461–470.

The UniProt Consortium (2025). UniProt: the Universal Protein Knowledgebase in 2025. Nucleic Acids Res 53, D609–D617.

Timmis, JN, Ayliffe, MA, Huang, CY, and Martin, W (2004). Endosymbiotic gene transfer: organelle genomes forge eukaryotic chromosomes. Nat Rev Genet 5, 123–135.

Ursic, D, and Culbertson, MR (1991). The yeast homolog to mouse Tcp-1 affects microtubule-mediated processes. Mol Cell Biol 11, 2629–2640.

Wang, L-J, Sun, G-Z, and Chen, Y-F (2019). LncRNA MSTO2P promotes proliferation and autophagy of lung cancer cells by up-regulating EZH2 expression. Eur Rev Med Pharmacol Sci 23, 3375–3382.

Wang, Y, Troughton, LD, Xu, F, Chatterjee, A, Ding, C, Zhao, H, Pulido Cifuentes, L, Wagner, RB, Wang, T, Tan, S, *et al.* (2023). Atypical peripheral actin band formation via overactivation of RhoA and nonmuscle myosin II in mitofusin 2-deficient cells. eLife 12, e88828.

Wei, Y, Chang, Z, Wu, C, Zhu, Y, Li, K, and Xu, Y (2017). Identification of potential cancer-related pseudogenes in lung adenocarcinoma based on ceRNA hypothesis. Oncotarget 8, 59036–59047.

Wei, Y, and Qian, M (2021). Case Report: A Novel de novo Mutation in DNM1L Presenting With Developmental Delay, Ataxia, and Peripheral Neuropathy. Front Pediatr 9, 604105.

Whitworth, AJ, and Pallanck, LJ (2009). The PINK1/Parkin pathway: a mitochondrial quality control system? J Bioenerg Biomembr 41, 499–503.

Wu, Y, Tu, G, Yuan, Y, Liu, J, Jiang, Q, Liu, Y, Wu, Q, Wu, L, and Chen, Y (2025). The Molecular Chaperone TCP1 Affects Carcinogenicity and Is a Potential Therapeutic Target for Acute Myeloid Leukemia. Pharmaceutics 17.

Xing, H, Rosenkranz, RRE, Rodriguez-Aliaga, P, Lee, T-T, Majtner, T, Böhm, S, Turoňová, B, Frydman, J, and Beck, M (2025). In situ analysis reveals the TRiC duty cycle and PDCD5 as an open-state cofactor. Nature 637, 983–990.

Yamada, H, Abe, T, Satoh, A, Okazaki, N, Tago, S, Kobayashi, K, Yoshida, Y, Oda, Y, Watanabe, M, Tomizawa, K, *et al.* (2013). Stabilization of Actin Bundles by a Dynamin 1/Cortactin Ring Complex Is Necessary for Growth Cone Filopodia. J Neurosci 33, 4514–4526.

Yamano, K, Fogel, AI, Wang, C, van der Bliek, AM, and Youle, RJ Mitochondrial Rab GAPs govern autophagosome biogenesis during mitophagy. eLife 3, e01612.

Yan, L, Yue, C, Xu, Y, Jiang, X, Zhang, L, and Wu, J (2020). Prognostic Value and Molecular Regulatory Mechanism of MSTO2P in Hepatocellular Carcinoma: A Comprehensive Study Based on Bioinformatics, Clinical Analysis and in vitro Validation. OncoTargets Ther 13, 2583–2598.

Yu, J, Luo, Y, Lin, J, Li, Z, Fang, Z, He, H, Yan, C, and Song, Z (2025). Mitochondrial cristae remodeling: Mechanisms, functions, and pathology. Cell Insight 4, 100285.

Yu, R, Liu, T, Jin, S-B, Ankarcrona, M, Lendahl, U, Nistér, M, and Zhao, J (2021). MIEF1/2 orchestrate mitochondrial dynamics through direct engagement with both the fission and fusion machineries. BMC Biol 19, 229.

Yu, T, Jhun, BS, and Yoon, Y (2011). High-Glucose Stimulation Increases Reactive Oxygen Species Production Through the Calcium and Mitogen-Activated Protein Kinase-Mediated Activation of Mitochondrial Fission. Antioxid Redox Signal 14, 425–437.

Zeng, C, Han, S, Pan, Y, Huang, Z, Zhang, B, and Zhang, B (2024). Revisiting the chaperonin T-complex protein-1 ring complex in human health and disease: A proteostasis modulator and beyond. Clin Transl Med 14, e1592.

Zhang, Y, Liu, X, Bai, J, Tian, X, Zhao, X, Liu, W, Duan, X, Shang, W, Fan, H-Y, and Tong, C (2016). Mitoguardin Regulates Mitochondrial Fusion through MitoPLD and Is Required for Neuronal Homeostasis. Mol Cell 61, 111–124.

Zhang, Z, Li, T-E, Chen, M, Xu, D, Zhu, Y, Hu, B-Y, Lin, Z-F, Pan, J-J, Wang, X, Wu, C, *et al.* (2020). MFN1-dependent alteration of mitochondrial dynamics drives hepatocellular carcinoma metastasis by glucose metabolic reprogramming. Br J Cancer 122, 209–220.

Zhao, Q, Li, J, Tong, Y, Li, Y, Han, W, Li, Z, Wang, Y, Yin, Y, Fang, J, Jiang, W, *et al.* (2026). TRiC folds the giant ciliary protein IFT172 via a non-canonical open-state mechanism. 2026.03.28.714460.

Züchner, S, Mersiyanova, IV, Muglia, M, Bissar-Tadmouri, N, Rochelle, J, Dadali, EL, Zappia, M, Nelis, E, Patitucci, A, Senderek, J, *et al.* (2004). Mutations in the mitochondrial GTPase mitofusin 2 cause Charcot-Marie-Tooth neuropathy type 2A. Nat Genet 36, 449–451.

Msto1 Endonuclease-mediated Allele Detail MGI Mouse (MGI:6257438). Mouse Genome Informatics. Available at: http://www.informatics.jax.org/allele/MGI:6257438. Accessed October 11, 2022.